

Throughout this exploration of *Unit Operations*, students require an understanding of what defines the equilibrium condition for a system with multiple components and, in most cases, across multiple phases. A background understanding in Chemical Engineering Thermodynamics provides the fundamental definition for the equilibrium, by combining mathematical representations of the First and Second Laws of Thermodynamics for a closed system with N distinguishable phases. As the system is closed, the differential energy balance arising from the First Law reduces to $dU^t = dQ + dW$, where dU^t represents the incremental change in the total internal energy of the system; dQ represents the incremental change in heat flow across the system boundary, where a positive value indicates heat flowing into the system; and dW represents mechanical or shaft work done on or by the system, where a positive value indicates work is being done *on* the system. In the context of the Second Law, Clausius' 1865 inequality ($dQ \leq TdS$) can be substituted for the definition of incremental heat flow, where T represents the system temperature and dS represents the incremental change in system entropy.

The resulting inequality provides an explicit context for the equilibrium of a system:

$$(Equation 1.1) \mathbf{dG}_{T,P}^t = dU^t + PdV^t - TdS^t \leq \mathbf{0}$$

where $dG_{T,P}^t$ represents the differential Gibbs free energy of a system at constant temperature and pressure (as denoted by the subscript), and the superscripts in each variable indicate extensive values are to be considered. Thus, the equilibrium conditions for a system are considered to be those that produce a global minimum in Gibbs free energy, which is defined without constraint below:

$$(Equation 1.2) \mathbf{dG} = VdP - SdT + \sum_i \mu_i dn_i$$

where the final term accounts for the chemical potential (μ_i) of the i^{th} component undergoing an incremental change in the amount (dn_i). Comparing equations 1.1 and 1.2 provides an illustration of Duhem's Theorem: "*for a closed system with known amounts of species, equilibrium is fully determined when any two independent variables are fixed.*" More importantly, equation 1.2 contextualises the three *driving forces* that must be resolved for a system to be considered at equilibrium:

- The **mechanical driving force**, whereby a pressure differential (dP) gives rise to the motion of fluids or deformation of solids, which is the subject of the subdiscipline of Fluid Mechanics;
- The **thermal driving force**, whereby a temperature difference (dT) gives rise to the transfer of heat across one or more phases, which is the subject of the subdiscipline of Heat Transfer; and
- The **chemical potential driving force**, whereby a difference in the distribution of a species (dn_i) across distinct phases gives rise to dissolution or diffusion, which is the subject of the subdiscipline of Mass Transfer.

As such, critically evaluating the definition of Gibbs free energy reveals that equilibrium is achieved when all three driving forces have been resolved. By way of example, consider a system with two components ("i" and "j") distributed across two phases (α and β), as shown in Figure 1.1 below. For the thermodynamic system comprising both phases to be considered at equilibrium, three conditions must be met: the temperature of both phases must be equal (that is, $T_\alpha = T_\beta$, where the thermal driving force is non-existent); the pressure across both phases must be equal (that is, $P_\alpha = P_\beta$, where the mechanical driving force is non-existent appreciating the hydrostatic pressure of the phases); and, quite critically, the chemical potential of each species is equal between species (that is, $\mu_i^\alpha = \mu_i^\beta$ and $\mu_j^\alpha = \mu_j^\beta$ for a binary system).

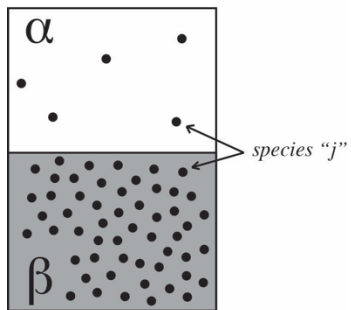


Figure 1.1. Equilibrium context in a binary (two-component) system containing lesser amounts of species "j" distributed, to different extents at equilibrium, within species "i" across two phases.

The third criterion is often misinterpreted to suggest that the absolute concentration of each species must be equal between the phases: however, as phases α and β must definitionally be distinct, equality in concentration would necessitate an *inequality* in chemical potential. That is, chemical potential represents the change in free energy from the addition or subtraction of an individual molecule to a given phase: thus, adding one molecule of component "i" to phase α must, by definition, differently affect the system chemical potential than adding one molecule of component "j" to the same phase. As such, equilibrium necessitates that the addition of a marginal molecule of component "i" to *either* phases α or β would engender the *same change in free energy*: that is, component "i" has achieved equality in chemical potential between both phases.

Anthropomorphising the chemical component momentarily, one molecule of component "i" would feel as *comfortable* in phase α as it would in phase β . It is precisely this reality that gives rise to the definition of the equilibrium solubility of a nominal component within a given phase: that is, *all components are soluble in all phases*, but it is simply a question of "how soluble" that enables the modern subdiscipline of mass transfer.

The subdiscipline of *Unit Operations* therefore considers those engineering designs that *intentionally* generate processes *not* at equilibrium, with the expectation that such systems should seek to achieve their thermodynamic equilibrium and, as a consequence, achieve an outcome that the engineer desires. For example, the unit operation of distillation recognises that a system of at least two components must be purified: the system experiences a series of stages that are sequentially farther from equilibrium, the result of which allow the engineer to "extract" one component from another.

To properly contextualise *Unit Operations*, the engineer must therefore have a working understanding of *both* thermodynamic equilibrium *and* the three driving forces (i.e. mechanical, thermal, and chemical potential) that distinguish a given system from its equilibrium condition. One important recognition herein is that non-equilibrium systems relax (i.e. change) toward their equilibrium condition at a *rate proportional to the degree to which they initially deviate from equilibrium*. That is, a system whose conditions are 50% outside (i.e. lesser or greater than) the equilibrium condition will relax toward equilibrium more rapidly (i.e. at a *greater rate*) than if the system were only 5% outside of the equilibrium condition. This can mathematically be expressed as the generalized rate (Γ) equation used throughout the engineering disciplines:

$$(Equation 1.3) \Gamma = R \cdot A_{action} \cdot \Delta G$$

where the rate at which a driving force relaxes (mechanical, thermal, or mass) is fundamentally defined by the a driving force of free energy (ΔG), the area across which that driving force acts (A_{action}), and a resistance of the material system to the driving force (R , which may correspond to viscosity, thermal conductivity, or diffusivity, respectively).

1.1 Distributing Components Between Phases

One key objective of the chemical engineer is to manage the creation and migration of a nominated species through processes of interest: fundamentally, there are two "tools" available that the engineer can exploit. If the target species has been created in nature, then the engineer must determine how to migrate that species from a typically dilute origin (e.g. < 1 mol%) to a highly concentrated serum that can be deployed for life-saving treatment. If the species does not occur naturally, then the engineer must determine how chemical reactions may be deployed to transform natural feedstock(s) in to the target species of interest. Foundational *Unit Operations* will focus on this first tool, or more specifically on those operations that have historically demonstrated sufficient capability so as to enable the engineer to accomplish the goal of purification. It is worth noting that "natural" feedstocks extend beyond those that are found in the untamed natural environments of the 20th century, but must now consider the by-products, waste streams, and recycled goods of 21st century industry.

For the engineer who wishes migrate a target species between two *phases*, Raoult's Law provides a governing basis for how a nominated component " i " will be distributed between two phases at equilibrium:

$$(Equation 1.4) \phi_i y_i P = \gamma_i x_i P_i^{sat}$$

where the left- and right-hand sides of the equation respectively govern the behaviour of the component in the vapour and liquid phases, respectively. In this formalism, y_i and x_i represent the mole fractions of the component in vapour and liquid phases, respectively, P is the total system pressure at equilibrium, and P_i^{sat} is the vapour pressure (also referred to as saturation pressure) of the component in the liquid phase. In most cases, Antoine-type relationships are deployed to calculate the vapour pressure, which itself varies only with system temperature.

Critically, ϕ_i is the fugacity coefficient of the component, which dictates the degree to which the component will behave non-ideally in its vapour phase. Similarly, γ_i is the activity coefficient of the component, which indicates its non-ideality in the liquid phase. If both the fugacity and activity coefficients have values of unity, the vapour and liquid phases are assumed to behave as an ideal gas and ideal solution, respectively. Both coefficients may be related back to the difference in the Gibbs energy of the ideal and real phases:

$$(Equation 1.5) \bar{G}_i - \bar{G}_i^{IDG} = \bar{G}_i^R = R T \ln \phi_i$$

$$(Equation 1.6) \bar{G}_i - \bar{G}_i^{ids} = \bar{G}_i^E = R T \ln \gamma_i$$

where the "bar" operator indicates a partial molar property, or the fraction of the thermodynamic property (Gibbs energy, in this case) that is attributable to the i^{th} component in the phase. Equation 1.5 illustrates that the *residual* Gibbs energy of the component -- which is defined as the difference between the real system and that of the ideal ("IDG") system -- is fundamentally defined as the product of the gas constant, system temperature, and the natural logarithm of the fugacity coefficient (ϕ_i). If the component can be assumed to have no molecular volume, and does not contribute to inter-molecular interactions, then it will behave *ideally*, whereby the fugacity

coefficient is equal to unity, and the natural logarithm term goes to zero along with the residual Gibbs energy of the vapour phase.

For the liquid phase (Equation 1.6), the difference between real and ideal solution ("ids") behaviour defines the *excess Gibbs energy* attributable to the i^{th} component, which can be expanded with a similar definition to the vapour phase. This excess Gibbs energy is similarly related to the natural logarithm of the *activity coefficient* (γ_i), which is similarly set to unity if the component is assumed to behave ideally in solution.

The prediction of activity and fugacity coefficients is a focus of advanced thermodynamics, and is heavily employed in both thermodynamic property tools and steady-state flow simulators. These tools, and the manual methods they replace, are key to the accurate deployment of Unit Operations knowledge. Closer inspection of Equation 1.4 reveals that property and flow calculations/simulations critically rely on four thermodynamic parameters:

- **Vapour pressure ($P_i^{sat} = f(T)$)**, which is often sourced from the Antoine relation and is a function of the system temperature;
- **System pressure (P)**, which typically relies on modifications to the Peng-Robinson (PR), Soave-Redlich-Kwong (SRK), or Cubic Plus Association (CPA) equations of state;
- **Activity coefficients (γ_i)**, which can deploy simple (Margules or van Laar) models for binary mixtures, or more elaborate (Wilson or UNIQUAC) models in complex and/or multi-component mixtures; and
- **Fugacity coefficients (ϕ_i)**, which follow similar predictive models to the above, but which must also consider the absolute pressure of the system.

1.2 Flash Calculations

As the engineer is typically seeking to manipulate the *composition* of a target component in one or more phases, they will typically modify the pressure and/or temperature of a system in order to seek the equilibrium condition that is most advantageous. However, thermodynamics places a boundary on the extent to which the engineer may transit material between phases at *each* pressure-temperature (PT) condition.

Notably, Raoult's Law constitutes equilibrium for a *closed, isolated system*: that is, if mass or energy are flowing through a system, then a more elaborate calculation basis is required. An example system is shown in Figure 1.2, where the "system" is characteristically defined by the boundary of the vessel walls (shown as an oval in the figure). As a feedstock at a molar flowrate F and molar compositions z_i (which can include any number of components) enters the vessel, it "flashes" to the equilibrium condition dictated by Raoult's Law for the vessel pressure and temperature: for reference, if the feedstock is already at the pressure and temperature of the vessel, then no flash will occur.

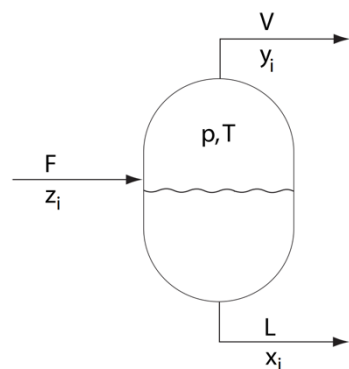


Figure 1.2. An example flash vessel operating at a singular pressure and temperature condition (p , T) with three flowing streams: (i) a feed at molar flowrate F with molar composition z_i ; (ii) a vapour product at molar flowrate V with molar composition y_i ; and (iii) a liquid product at molar flowrate L with molar composition x_i .

Molar balances can be applied across the entirety of the vessel ($F = V + L$) and across each component ($F \cdot z_i = V \cdot y_i + L \cdot x_i$). As the composition of the feedstock is often known, and the engineer determines (i) the feed molar flowrate and (ii) PT conditions of the vessel, there are two unknowns: the vapour product flowrate and the vapour composition, or the liquid product flowrate and the liquid composition. The traditional solution strategy behind such flash vessels is provided by the Rachford-Rice equation:

$$(Equation 1.7) \sum_i \frac{z_i K_i}{1 + \frac{V}{F} (K_i - 1)} = 1$$

where the vapour-liquid equilibrium ratio for each component is defined by $K_i = y_i/x_i$, which is a purely thermodynamic quantity. Note that the Riemann sum means the left-hand expression will produce *one term for every chemical component in the feedstock*. The equilibrium ratio can be determined by re-arranging Raoult's Law (Equation 1.4) as below, which allows the engineer flexibility in considering changes to operating pressure, temperature, and composition:

$$(Equation 1.8) K_i = \frac{y_i}{x_i} = \frac{\gamma_i P_i^{sat}}{\phi_i P}$$

For well-studied systems, such a system containing natural gas and it's 5+ components, previous studies of the equilibrium ratio may be available in the literature: DePriester Charts are one such historical example. In order to solve the Rachford-Rice equation for an N-component system, the engineer must first (i) know the feed composition z_i ; (ii) determine the equilibrium ratio of each component; and (iii) iterate on the value of $\frac{V}{F}$ until the left-hand expression is equal to unity, noting the same ratio will appear in each term of the left-hand side. The solution value for $\frac{V}{F}$ can then be used to solve the overall molar balance of the system and, in combination with the equilibrium constant for each component, the component molar balance for each species in the system.

It is important to note that process simulation tools, such as Aspen HYSYS, are actually quite simple in their construction: flash stages are addressed by deploying Equation 1.7; a large thermodynamic code base, including multiple cubic equations of state, enables calculation of Equation 1.8 over the range of necessary conditions; and flow between operations is addressed with steady-state correlations from fluid mechanics.

1.3 The Role of Equilibrium Stages

When an engineering system is designed with more than one flash vessel in sequence, whereby the products of either or both phases flow on to another flash vessel, the combined suite are considered to be "equilibrium stages." This concept is graphically represented in Figure 1.3, where four equilibrium stages are operated at difference pressure-temperature conditions. If species "j" is represented by the black circles -- constituting a "dilute" system in chemical terms -- then the mole fraction of "j" in *equilibrium* with phases α and β will vary with the pressure and temperature conditions.

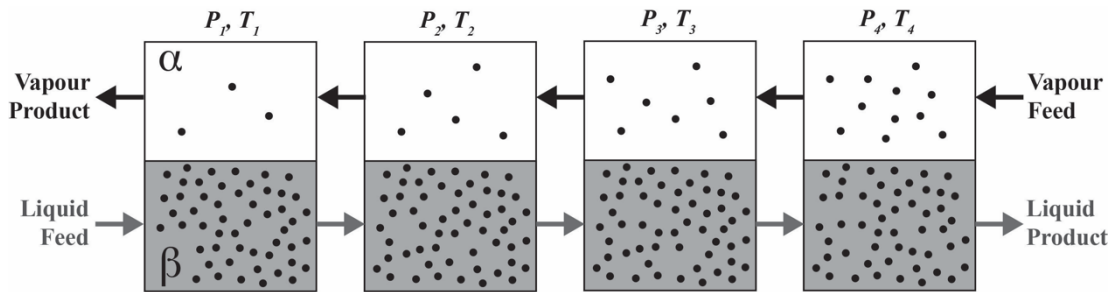


Figure 1.3. Illustration of four equilibrium stages, each operating at different pressure-temperature conditions, which control the migration of component "j" between phases α and β .

As such, *each* of the four equilibrium stages represented in Figure 1.3 is governed by Raoult's Law (Equation 1.4). Importantly, such a system could be designed to operate in batch mode, where by a single vessel could be exposed sequentially to each set of PT conditions (that is, from P_4, T_4 to P_1, T_1) to obtain the final equilibrium condition, or alternatively operated in a continuous mode where liquid and vapour are continually fed to one or more stages. Continuous mode operations are inherently more costly, as -- in this example -- three additional flash vessels would be required, alongside supporting infrastructure. However, a continuous operation in Figure 1.3 would enable the engineer to generate a continuous flow of vapour and/or liquid product streams of interest, which can be a critical dependency of additional operations. For example, if the operation were designed to "remove" the minority component "j" from phase α in Figure 1.3, the "vapour product" stream of the left-hand flash vessel (operating at P_1, T_1) might then be sent to a chemical reaction vessel: in that example, the importance of correctly operating these equilibrium stages would increase if the presence of "j" in the subsequent reaction vessel might result in a toxic byproduct.

The exploration of Unit Operations inherently requires the engineer to reflect on three questions, each of which underscore the importance of understanding thermodynamic equilibrium:

1. *What does thermodynamics dictate is the equilibrium condition for a given operation?*
2. *For an operation not at equilibrium, how long will it take to reach equilibrium?*
3. *If the time required is excessive (i.e. wasteful), how can the operation be modified to more efficiently reach equilibrium?*

Although the remaining topics in this curriculum may appear highly specific or nuanced, the purpose of each is to address these three fundamental, thermodynamic questions. The use property simulation tools, such as Aspen HYSYS, are an important -- but not exclusive -- aspect of Unit Operations, as they enable the engineer to rapidly iterate on different design and operating decisions (facilitating thermodynamic questions #2 and #3, above): however, it is important to appreciate that simulation tools, identical to the manual calculations they are meant to expedite, can invoke a multitude of assumptions. Critically, the engineer must decide whether the number and magnitude of assumptions are appropriate for a given solution.

As virtually all unit operations are designed around processes with flowing material, the simultaneous consideration of both momentum and heat/mass transfer is often required in modelling or analysis. To this end, the following section provides an overview of the key insights within the subdiscipline of Fluid Mechanics relevant to the unit operations being explored.

2.1 Hydrostatic Pressure

Of particular relevance to liquid- or solid-containing systems is the concept of hydrostatic equilibrium, whereby gravitational acceleration (i.e. from the mass of Earth's core) provides objects with a measurable weight that is proportional to their density. In the case of a fluid, this reality can be visualised by considering a column of fluid shown in Figure 2.1: a force balance applied across a differential thickness (dZ) illustrates that the pressure (p) is higher along the bottom edge of the slice.

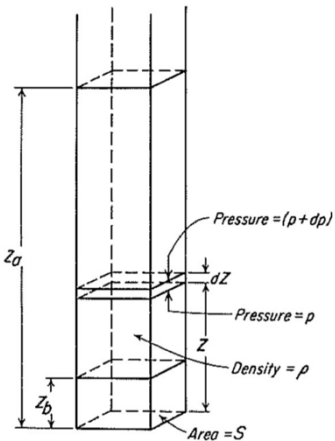


Figure 2.1. In a column of fluid (liquid, vapour, or supercritical), the pressure (p) within the column varies as a function of height (Z) and is proportional to its density (ρ), reproduced from McCabe, Smith and Harriott (7th Edition).

A force balance on the slice volume represented in Figure 2.1 reveals that the surface area (S) appears in all terms, and can be reduced out of the expression, leaving only the body force ($g \cdot \rho \cdot dZ$) and the difference in pressure on both faces (dp). Thus, the definition of pressure head, as exerted by a static fluid, can be equated to the difference in height:

$$(Equation 2.1) \quad p_b/\rho - p_a/\rho = g(Z_a - Z_b)$$

which assumes density does not vary with pressure. Where density does vary meaningfully with pressure, a relationship between the two must be employed. For example, employing the ideal gas equation of state allows a substitution of $\rho = (p \cdot M_w)/(RT)$ where molar volume is the product of molecular weight on density: this definition can be directly integrated at constant temperature to reveal the barometric equation:

$$(Equation 2.2) \quad \frac{p_b}{p_a} = \exp \left[\frac{-g M_w (Z_b - Z_a)}{RT} \right]$$

This approach may be taken with any definition of density -- from either alternative equations of state or through a more simplistic relationship, as may be appropriate in the case of liquids -- to practically estimate the "hydrostatic head" (that is, the pressure applied by fluids at rest) for a system. Of particular relevance to unit operations, hydrostatic head can be a useful and often inexpensive method of controlling pressure in fluid systems. For example, consider how a change in pressure (dP) in Equation 1.2 will affect the overall Gibbs energy of the i^{th} component: when multiple phases are present, this change in pressure intrinsically affects the equilibrium concentration of the i^{th} component in *each* phase. As such, unit operations where a large "liquid (hydrostatic) head" is present can generate a scenario where the equilibrium mole fraction is different at the top and bottom of the liquid phase: the engineer must be cognisant of this variation, in order to know where the product must be taken.

Although static fluids are rarely of interest to engineers, the scenario commonly emerges with manometers, an example of which is shown in Figure 2.2. The manometer is typically connected to a flowing channel of interest, such a cylindrical pipe containing high-pressure gas, and deploy a reduced form of the barometric equation in order to measure the pressure difference between two points: $(p_a - p_b) = gR_m(\rho_A - \rho_B)$. The working fluid of a manometer typically has a higher density (ρ_A) than the flowing field to which it is in contact (with density ρ_B , shown in Figure 2.2), ensuring the working fluid does not contact the flowing stream being assessed.

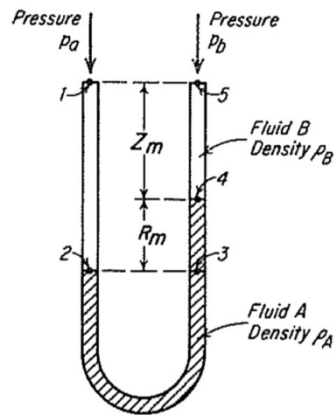
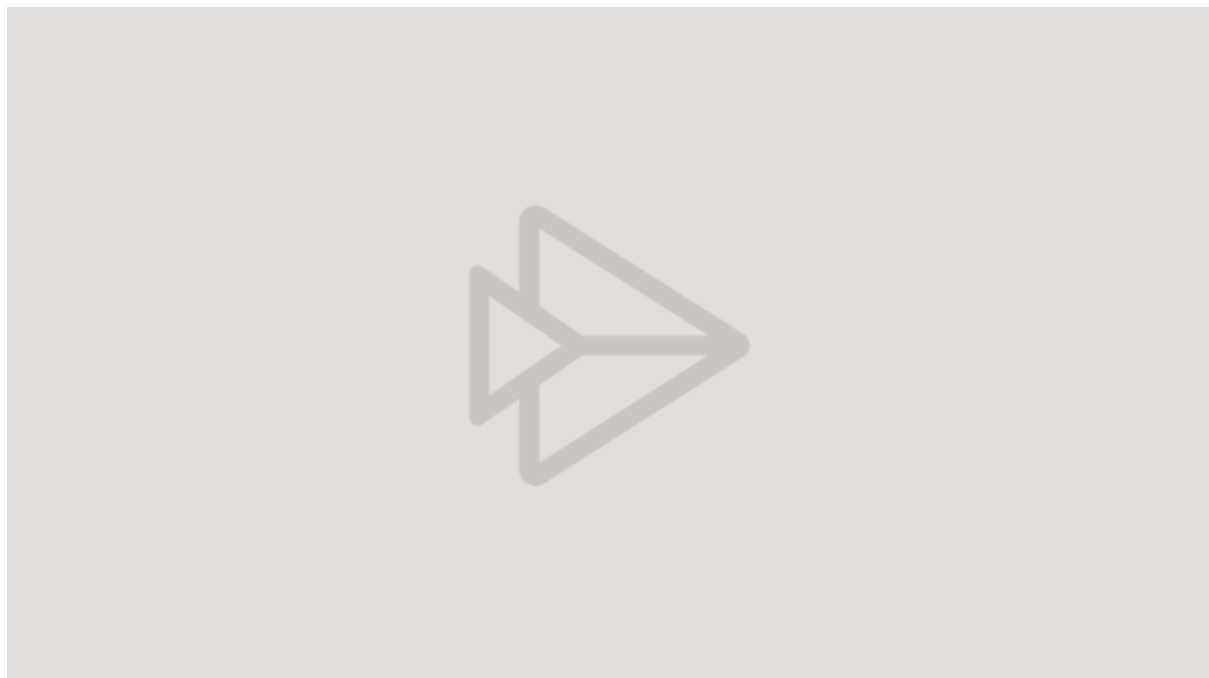


Figure 2.2. Diagram of a manometer, where a pressure difference (p_a and p_b) is reflected in the height difference (R_m) of the measurement fluid with density ρ_A , when exposed to a secondary flowing fluid with density ρ_B . Reproduced from McCabe, Smith and Harriott (7th Edition).

Manometers have historically been used to determine the speed of aircraft mid-flight, by relating the external pressure on the face of the aircraft to speed. Today, manometers are often used as a complement to orifice restrictions, which exemplify a simple thermodynamic operation in which a large pressure gradient is generated over a (relatively) small distance in the flow channel.



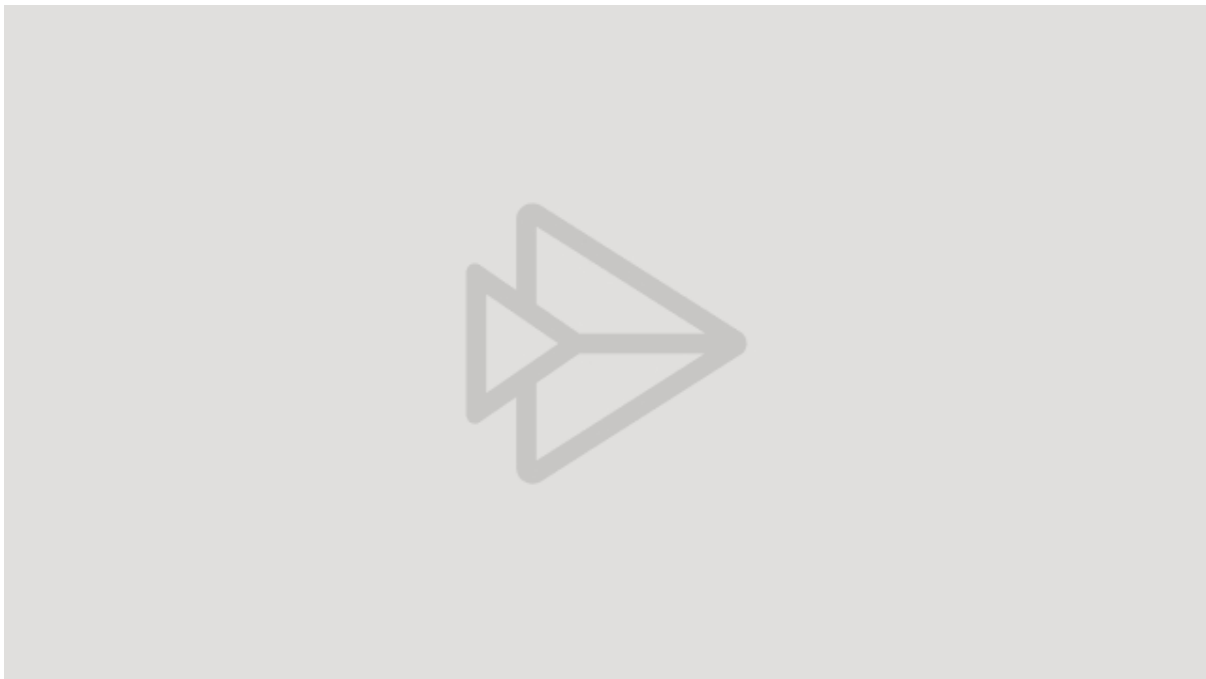
[Example 1 -- Use of a manometer, deploying Equations 2.1 and 2.2 \(video from Microsoft Stream\).](#)

2.2 Characterising Flow

Through observing turbulence in a transparent flow channel, Reynolds proposed a dimensionless quantity (termed the Reynolds Number, or Re) in 1883:

$$(Equation 2.3) Re = (\rho \cdot v \cdot D) / \mu$$

where ρ represents fluid density, μ represents fluid viscosity, v is the *average* velocity of the fluid stream (typically determined by the ratio of the volumetric flowrate and cross-sectional area of flow), and D is the *hydraulic diameter* of the flow (e.g. pipe diameter, in the case of a cylindrical pipe). Fundamentally, the Reynolds number represents the ratio of *inertial forces* to *viscous forces* in a system. Through observation, Reynolds proposed that laminar flow would dominate where $Re < 2100$ and turbulent flow would dominate where $Re > 4000$; the intermediary behaviour ($2100 < Re < 4000$) contained features of both laminar and turbulent flow, and was deemed a "transition" region. It's important to note that the definition and numerical boundaries of the Reynolds number are defined for well-defined, ducted flow: the engineer must use caution when considering such definitions in alternative geometries, such as the flash tank discussed in Figure 1.2.



Example 2 -- Calculating Reynolds number in lungs, using Equation 2.3 (video from Microsoft Stream).

2.3 Friction Loss

As fluid phases deform under a pressure gradient, the magnitude of the pressure gradient applied across them informs the extent to which they will flow. Incompressible flow simply assumes that the density of the fluid (ρ in Equation 2.4) changes negligibly with pressure, as is the case for the vast majority of liquids. The scenario *does not* apply in the vapour phase, where equations of state prescribe an exhaustive treatment of how the density (or molar volume) of gasses change in response to pressure. The simplest form of governing relationship for incompressible flow, derived from the conservation of energy across a volume through which fluid flows, was proposed by Bernoulli for laminar systems (that is, $Re < 2100$):

$$(Equation 2.4) P_1 + \frac{1}{2} \rho v_1^2 + \rho g z_1 + \eta W_p = P_2 + \frac{1}{2} \rho v_2^2 + \rho g z_2 + h_f$$

where a difference in pressure between P_1 and P_2 is translated into either an increase in kinetic energy of the fluids (e.g. $v_2 > v_1$) and/or an increase in the potential energy of the fluids (e.g. $z_2 > z_1$). The bolded terms in Equation 2.3 amend what is traditionally referenced as the Bernoulli equation, and include the addition of work from a pump (W_p) qualified by its efficiency (η , from 0 to 100%), and a generic frictional loss term (h_f). The description of potential energy follows that of fluid head, described in Equation 2.1, while the definition of kinetic energy follows that from Lord Kelvin in 1867. Numerous assumptions are required to deploy Equation 2.4, including that of laminar (non-turbulent, well-defined) flow and a constant cross-sectional area of flow: however, the relation provides a convenient conceptual basis to relate the applied force (i.e. pressure across an area) to the generation of fluid flow.

While pump efficiency and work are typically supplied by equipment vendors as experimentally-tested "pump curves," correct treatment of the frictional loss term is a chief concern for the engineer. Figure 2.3 provides an example assembly for incompressible flow, illustrating several key locations at which frictional pressure losses must be considered. First, the flow experiences a sudden contraction at the entrance header (left-hand side of Figure 2.3), as the cross-sectional area is reduced from the larger upstream value of S_a to a smaller downstream value of S_b . Second, flow experiences frictional loss from the wall for a straight section -- to be discussed below -- before encountering a valve, as one example obstruction. Finally, the flow experiences a frictional loss from rapid expansion, from the smaller upstream cross-sectional area of S_b to a larger downstream cross-sectional area of S_b . The mathematical treatment for each of these components is discussed in detail below.

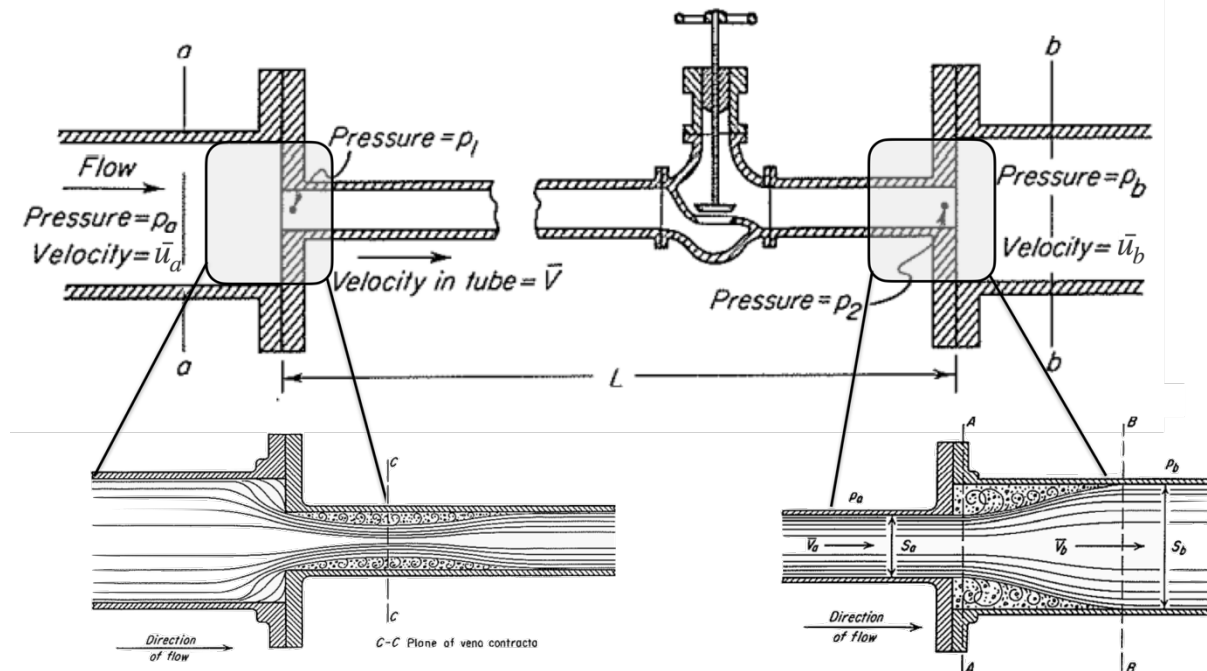


Figure 2.3. An example assembly demonstrating key concepts of friction loss for incompressible flow: sudden fluid contraction, fitting/valve loss, sudden fluid expansion, and steady-state flow loss. Modified from McCabe, Smith and Harriott (7th Edition).

The frictional loss term for sudden flow contraction, exemplified by the entrance header shown in Figure 2.3, is shown in Equation 2.5:

$$(Equation 2.5) h_{f_{contraction}} = K_c \frac{\bar{u}_b^2}{2}$$

which varies with the average fluid velocity *after* the contraction (\bar{u}_b) and is modified by a contraction loss coefficient (K_c). For laminar flow, this coefficient is taken to be less than 0.1, while turbulent flow requires a relationship with the ratio of cross-sectional areas: $K_c = 0.4(1 - \frac{S_b}{S_a})$. The frictional loss of sudden flow expansion, such as from the exit header in Figure 2.3, is shown in Equation 2.6:

$$(Equation 2.6) h_{f_{expansion}} = K_e \frac{\bar{u}_a^2}{2} = \left(1 - \frac{S_a}{S_b}\right)^2 \frac{\bar{u}_a^2}{2}$$

where a single definition of the expansion loss coefficient (K_e) is deployed, independent of whether or not the flow is laminar. Finally, the friction factor from *fittings, valves, and pipe/duct bends* follows Equation 2.7:

$$(Equation 2.7) h_{f_{fittings}} = K_f \frac{\bar{u}_a^2}{2}$$

where the loss coefficient (K_f) is determined from general lookup values, shown in Table 2.1. The table provides a useful first point of reference, where expanded versions are available in the literature, such as Perry's Handbook. In the example scenario from Figure 2.3, a single partially-open valve is shown; however, practical process operations are likely to have multiple fittings, valves, and pipe bends that require consideration from Equation 2.7.

Table 2.1. Friction loss coefficients (K_f) for fittings, valves, and pipe bends.

Fitting	K_f
Elbow, standard	
45°	0.35
90°	0.75
Elbows, welded	
90° bends, radius 2 x pipe diameter	0.19
90° bends, radius 4 x pipe diameter	0.16
90° bends, radius 6 x pipe diameter	0.21
Tee	
Straight through	0.4
Used as elbow	1.0
Return bend, 180°	1.5
Gate valve	
Half open	4.5
Wide open	0.17
Angle valve, wide open	2.0
Globe valve, wide open	6.0

Finally, the engineer must determine the appropriate friction loss term for flow through straight pipes/ducts, such as the portion of Figure 2.3 between the entrance gate and the valve. The general frictional loss contribution (h_f) for this scenario is defined in Equation 2.8, which requires knowledge of the Fanning friction factor (f), section length (L), inner diameter (D), and average fluid velocity (\bar{u}):

$$(Equation 2.8) h_f = 4f \frac{L}{D} \frac{\bar{u}^2}{2}$$

For cylindrical pipes, graphical methods like the Moody Diagram (Figure 2.4) provide for efficient lookup. To obtain an appropriate Fanning friction factor (f) from the Moody Diagram, the engineer must estimate the Reynolds number of the flowing system: as friction losses govern the translation of pressure difference to velocity via Equation 2.4, and velocity affects Reynolds number via Equation 2.3, deployment of the Moody Diagram can require an iterative solution approach.

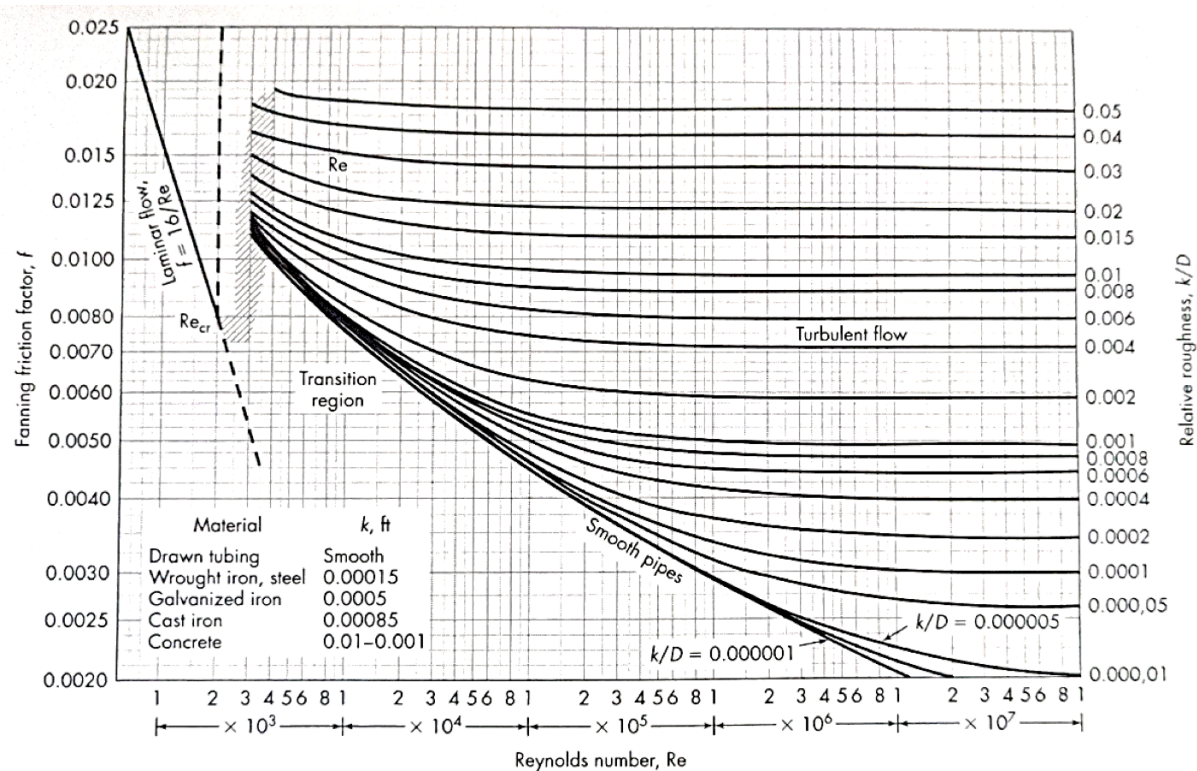


Figure 2.4. Moody Diagram for circular pipes, reproduced from McCabe, Smith and Harriott (7th Edition).

Further, the engineer must have some estimate, or must assume a reasonable value for, the *relative roughness* for turbulent flow, which is defined by the ratio of the internal surface roughness (k) on the internal pipe diameter (D). Internal surface roughness is typically considered to be the number (arithmetical) average of asperity size at the pipe wall, or the averaged difference between the highest and lowest point across each asperity. Three examples of asperity types and distribution are shown in Figure 2.5, which are exaggerated in dimension for illustrative purposes: the typical range of relative surface roughness in the Moody Diagram illustrates that, in most cases, the asperities are, at most, a few per cent of the pipe diameter.

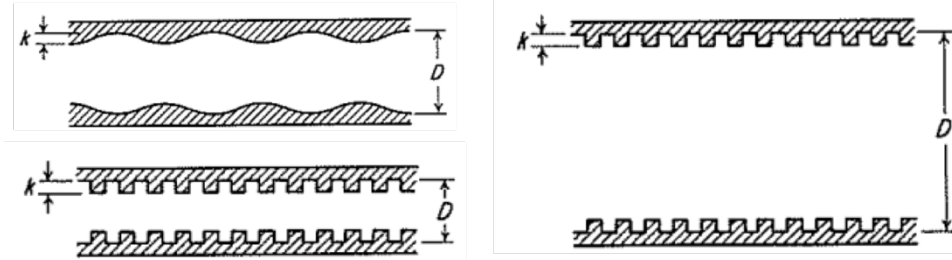


Figure 2.5. Illustration of surface roughness (k) in pipe flow of internal diameter (D), modified from McCabe, Smith and Harriott (7th Edition).

For the engineer designing an online prediction/management system, or who is rapidly iterating through design options, use of the Moody Diagram can be time consuming. Alternatively, Table 2.2 provides a suite of analytical relationships for cylindrical flow, where the friction factor is typically independent of Reynolds number above a value of 1,000,000.

Table 2.2. Analytical relationships for friction factor in ducted flow.

Scenario	Correlation
$Re < 2100$; smooth pipes	$f = \frac{16}{Re}$
$50,000 < Re < 1,000,000$; smooth pipes	$f = \frac{0.046}{Re^{0.2}}$
$3,000 < Re < 3,000,000$; smooth pipes	$f = 0.0014 + \frac{0.125}{Re^{0.32}}$
Turbulent flow; steel/rough pipes	$f = 0.026 \left(\frac{k}{D} \right)^{0.24}$

Upon comparison, each of the four friction losses identified above (Equations 2.5 through 2.8) contains the square of average velocity on two. Thus, the Bernoulli equation can be expanded, incorporating all potential frictional loss terms:

$$(Equation 2.9) \Delta P = \rho g (Z_a - Z_b) - \left(4f \frac{L}{D} + K_C + K_e + K_f \right) \cdot \frac{\rho \bar{u}^2}{2}$$

which is suitable for determining the average fluid velocity arising from the overall pressure difference applied to the flow network in Figure 2.3. More importantly, the model could be expanded to incorporate any additional number of contractions, expansions, fittings, valves, or bends through the right-hand term. While the expanded Bernoulli expression does not account for turbulent flow or multi-phase (e.g. vapour-liquid) flow, it provides an efficient method for single-phase systems at mild to moderate velocities: this can be useful for basic estimates, such as pump head requirements, or in assessing the order-of-magnitude accuracy of flow simulation tools. This section focusses on the characterisation of incompressible flow, for both laminar and turbulent conditions, which is the primary focus of the unit operations being studied. While some operations may deploy compressible fluids, they are typically not operated in high-pressure environments. However, it is expected that students have a basic working knowledge of compressible flow, from the perspectives of both fluid mechanics and thermodynamics.

3.1 Shear Stress

When flow is initiated, the amount of "pressure" or force applied to the wall of the container (e.g. the wall of a cylindrical pipeline) is referred to as the "shear stress." Common examples of this behaviour are shown in Figure 3.1, which relates the shear stress (τ) applied to the shear rate ($\dot{\gamma}$, also called velocity gradient) at the edge of the flowing field (e.g. at the pipe wall, for a cylindrical flow scenario). Importantly, the viscosity of the fluid dictates the *slope* of each curve: the fluid may have constant viscosity (curves A and B), demonstrate "shear thinning" behaviour (curve C), or demonstrate "shear thickening" behaviour (curve D). Common latex is an example of a shear thinning fluid, where the fluid becomes easier to deform as it experiences a higher shear rate (i.e. as the velocity gradient increases). Conversely, quicksand exemplifies a shear thickening fluid: the greater shear is applied (i.e. trying to escape), the more viscous the fluid phase will become.

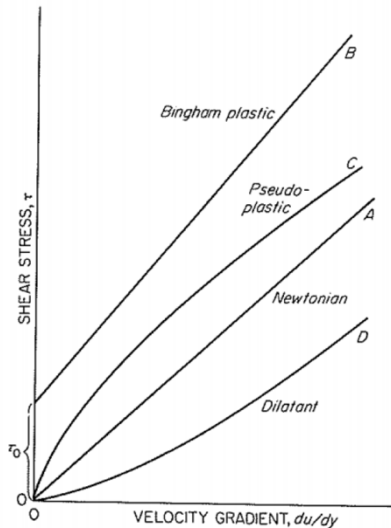


Figure 3.1. Shear stress (τ) as a function of the velocity gradient or shear rate ($\frac{du}{dy} = \dot{\gamma}$) for common fluid types: for a nominated shear rate, the tangent line to each curve represents the viscosity of the fluid. Reproduced from McCabe, Smith and Harriott (7th Edition).

Bingham plastics are special classes of fluids that behave like solids when minimal shear stress is applied: household tomato sauce or ketchup is one such example, where a meaningful pressure stress must be applied to the bottle before flow is observed. Once the so-called yield stress (τ_0) has been exceeded, the fluid will continuously deform under increasing shear stress. Predictions of fluid viscosity are not well-established, as the engineering property is an amalgam of thermodynamics and fluid mechanics: fluids with a high degree of intermolecular interaction, and when comprised of complex molecular structure(s), tend to give rise to a high degree of viscosity, but it is difficult to assess how these interactions and structures will evolve in the presence of a shear field. In most instances, experimental literature and/or laboratory measurements are best-placed to inform viscosity for engineering calculations: most predictive models are appropriate only for the specific phase and chemical species for which they were empirically regressed, where the use of extrapolation or ill-suited models can readily jeopardize the integrity of the calculation.

The velocity gradient, or shear rate, deployed in Figure 3.1 is defined as the slope of the velocity between the bulk fluid (e.g. the centre of a water pipe) and the wall. As a "no-slip" condition is applied at the wall, the flowing shear rate of a fluid is thus proportional to the average velocity of flow: however, it is important to note that velocity and shear rate are distinct quantities, with respective SI units of $\frac{m}{s}$ and $\frac{1}{s}$. This no-slip condition is visualised in Figure 3.2, where the local fluid velocity -- that is, the velocity that would be measured by placing the system under a powerful

microscope -- decreases as the wall is approached: this can be visualised by tracing the curve of the left-hand panel from top-right to bottom-left, where the fluid velocity reaches zero upon contact with the wall. Conversely, the right-hand panel illustrates the velocity *gradient* (i.e. the shear rate) over this same distance: the top of the ordinate (y-axis) is a reasonable distance from the wall and the fluid velocity does not fluctuate much in this region (leading to a near-zero *gradient* in fluid velocity). As the wall is approached, the value of the gradient ($\frac{du}{dy}$) increases monotonically until the wall is reached.

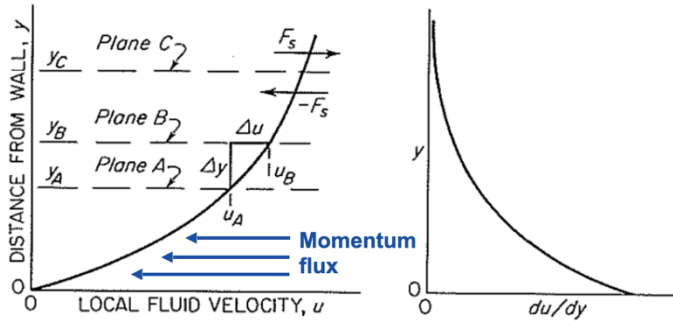


Figure 3.2. Illustration of no-slip condition as a flowing fluid approaches the wall. Modified from McCabe, Smith and Harriott (7th Edition).

When viscosity is appropriately measured, or can be reasonably estimated, the engineer must then consider how energy is transmitted through the flowing fluid. As discussed, the Bernoulli equation requires laminar flow: under this condition, the fluid flows in stratified "layers" in the direction of flow, which is visualised in Figure 3.2 with "planes" A through C. Conceptually, the phenomenon is similar to spreading a deck of playing cards across a table with one's hand, where each card (or "layer") acts as a singular body that experiences interfacial friction with those layers above and below it. Apart from a few operating scenarios that require its use, engineers tend to avoid systems in the laminar flow region: as the metaphorical playing cards operate as singular bodies, the transfer of mass or energy *between* playing cards is diffuse and can substantially increase the residence time of unit operations.

As turbulence increases beyond the laminar region, Reynolds observed the onset and growth of so-called "eddies" that could cross between each of the metaphorical playing cards, where the size and number of eddies increased directly with fluid velocity (and, consequently, the Reynolds number). The ability for eddies to cross between stratified fluid layers is precisely what makes turbulent flow so attractive to the engineer: in doing so, they improve the transfer of heat and/or mass between layers, replacing the diffusive transfer of laminar flow with convective transfer in turbulent flow. It is important to note that, in a turbulent system, there will be a *distribution* in the eddies present: as eddies can flow *against* or *normal* to the direction of flow, they exert *shear stress* on nearby fluid. Thus, the shear stress exerted by large eddies give way to smaller eddies, the shear stress of which give way to yet smaller eddies: this process is often referred to as the "energy cascade," and is pictured in Figure 3.3.

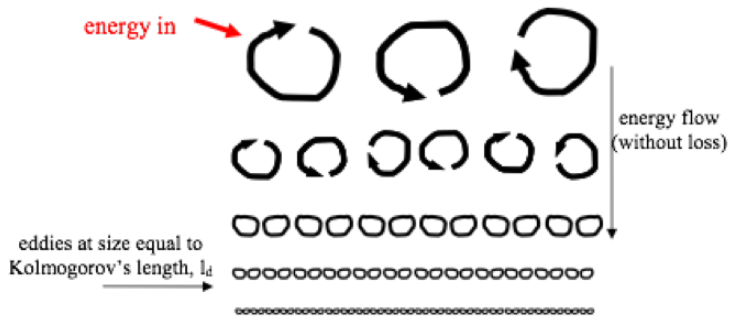


Figure 3.3. The energy cascade, where momentum (energy) is transferred from large (top) to small (bottom) eddies, reproduced from J. Boxall (2009).

In turbulent systems, measurement of absolute velocity will fluctuate around a mean (average) value, as shown in Figure 3.4. The magnitude and frequency of such fluctuations are the consequence of the large(r) eddies within the system. Put another way, these fluctuations are the physical manifestation of the combined eddies moving both *with* and *against* the primary direction of flow, as they "swirl" through the system.

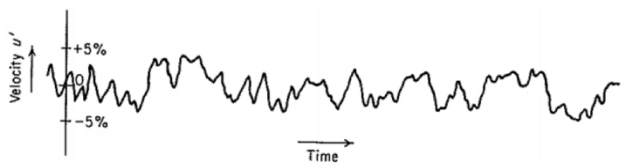


Figure 3.4. Variations in instantaneous velocity measured in time, where 0% corresponds to the numerical average. Reproduced from McCabe, Smith and Harriott (7th Edition).

A majority of the energy cascade takes places with near perfect efficiency, meaning new (smaller) eddies are generated without frictional loss: this portion of the cascade is referred to as the "inertial subrange." In 1941, Kolmogorov proposed a relation for the smallest eddy size that can be generated in a turbulent system, the length scale (l_D) of which is shown in Equation 3.1 and varies with the kinematic viscosity of the fluid (the Greek letter "nu," ν , defined by μ/ρ) and dissipation rate of turbulence kinetic energy (ϵ) in the system.

$$(Equation 3.1) \quad l_D = (\nu^3 / \epsilon)^{1/4}$$

where the dissipation of turbulence kinetic energy is similarly featured in the Reynolds-averaged Navier Stokes equations. Conceptually, this term may be thought of as the "destructive" or "consumptive" term when a general Chemical Engineering conservation equation is applied to momentum. Apart from very large or highly laminar systems, most practical engineering applications would consider the Kolmogorov length scale to be on the order of microns. Importantly, it is at *this* length scale of eddies that energy is finally dissipated (i.e. converted) to heat: the bottom two rows of eddies in Figure 3.3 are therefore referred to as the "viscous subrange" of the energy cascade, arising from the dependence of the Kolmogorov length scale on kinematic viscosity (Equation 3.1).

When a significant pressure differential is applied to flow an incompressible fluid, viscous dissipation can result in a measurable increase in fluid temperature: the significance of the effect increases with fluid viscosity and as the flow diameter decreases. Equation 3.2 can be used to estimate the degree of viscous heating expected:

$$(Equation 3.2) \Delta T = \frac{\Delta P}{\rho c_V}$$

The effect of viscous heating is mild when compared to magnitude Joule-Thomson expansion in compressed gasses, where a sudden pressure decrease of 100 bar can engender a 200 K decrease in temperature. For the example of a viscous hydrocarbon or polymer, an increase in temperature between 0.4 and 0.6 K for every MPa in differential pressure may be expected. This effect may be useful for engineers working with highly viscous fluids in flow, as an auxiliary means -- albeit expensive -- by which to affect fluid temperature.

3.2 Boundary Layers

Although nuanced, the understanding of turbulence is critical to the successful design of unit operations, which often involve flow considerations at multiple length scales. While the Reynolds number provides a relatively blunt instrument by which the engineer may characterise turbulence, deeper insight can be gained by considering the role of turbulence in generating eddies through the bulk of the flowing volume. As flow reaches the wall, a distinct set of behaviours emerge that affect both momentum and heat transfer.

Figure 3.5 provides an illustration for the initial onset, and growth, of a *boundary layer*, which occurs when a uniform flow stream contacts the wall (upstream of point c). In reality, the boundary layer is simply a construct, which allows the engineer to separate unique behaviour near the wall from that of the bulk flow: the height of the boundary layer is determined by the location at which local velocity reaches 99% of the mean (bulk) fluid velocity, as dictated by line "OL" in Figure 3.5.

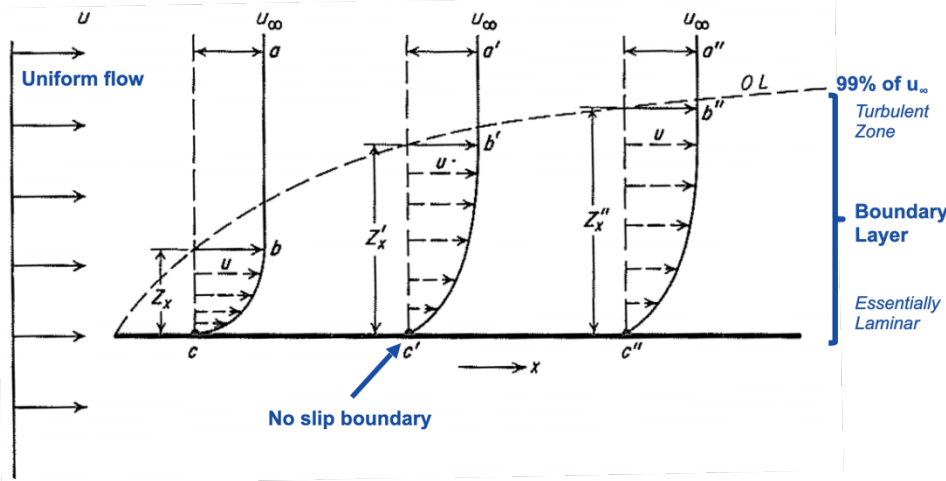


Figure 3.5. Illustration of a growing boundary layer (curve "OL") generated when a uniform flow pattern contacts the leading edge of a wall (left-hand side), modified from McCabe, Smith and Harriott (7th Edition).

The "growth" of the boundary layer shown in Figure 3.5 can be applied in two equivalent contexts: observing one physical location evolve in time, or observing one moving fluid packet evolve in space. Each of the examples shown illustrate the evolution of velocity *within* the boundary layer: importantly, the local velocity (u) is zero at the wall, matching the requisite "no-slip" boundary condition, and increases monotonically through the edge of the boundary layer (i.e. $u = 0.99 u_\infty$). The boundary layer itself may be considered to function analogously to the energy cascade shown in Figure 3.3: the portion of the boundary layer closest to the wall is functionally laminar, constituting the *viscous sublayer*; the middle portion constitutes a *buffer layer*; and the upper portion constitutes

the *turbulent zone*. An illustration of these three zones is shown in Figure 3.6, where the boundary layer grows in response to the bulk flow transitioning from laminar to turbulent (demarcated as the "onset of turbulence").

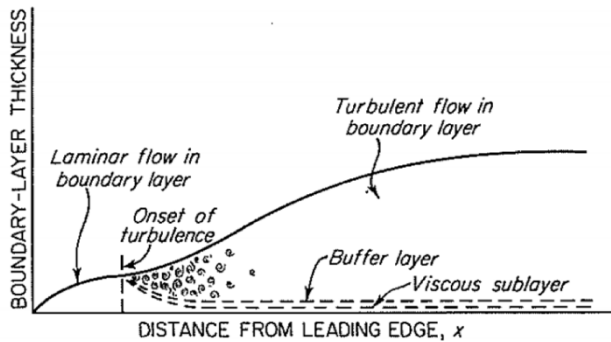


Figure 3.6. Evolution of boundary layer thickness as bulk flow transitions from laminar (left) to turbulent (right), illustrating the onset of three zones (viscous, buffer, and turbulent) with the establishment of fully turbulent flow. Reproduced from McCabe, Smith and Harriott (7th Edition).

The illustration in Figure 3.6 considers a system that is initially laminar, wherein the boundary layer thickness (δ) evolves with distance from the leading edge (x) according to Blasius:

$$(Equation 3.3) \quad \delta/x = 5/\sqrt{Re_x}$$

where the term Re_x represents the Reynolds number of the boundary layer, replacing v and D in Equation 2.3 with u_∞ and x , respectively. Thus, the thickness of the boundary layer in laminar flow evolves directly with the square root of distance from the leading edge (that is, from the onset of the boundary layer). In turbulent flow, the boundary layer thickness can similarly be predicted through Equation 3.4, where the numerator of the right-hand side and power of the boundary layer Reynolds number are semi-empirical, based on the statistical nature of turbulence:

$$(Equation 3.4) \quad \delta/x = 0.385/(Re_x^{0.2})$$

In turbulent flow, the boundary layer increases in thickness with distance from the leading edge (x) to the 0.8 power, or around 23% faster than in laminar flow. Figure 3.6 further illustrates the onset of the viscous sublayer and buffer layer in turbulent flow, which represent a minority of the overall boundary layer thickness once fully established.

If laminar flow is maintained in a ducted (e.g. cylindrical pipe) system, the growing boundary layers from both sides of the duct will grow monotonically until contact between them is established. The result is a parabolic flow profile, as shown in Figure 3.7. The distance (x_t) required to establish this steady-state laminar flow profile, where the flow is said to be "fully developed," is determined by Equation 3.5. For example, laminar flow in a cylindrical pipe with 2" (50 mm) inner diameter, operating at a Reynolds number of 1500, will require an entrance length of 12.3' (3.75 m). The solution for turbulent flow will be discussed in detail later, as it requires additional treatment of fluid mechanics.

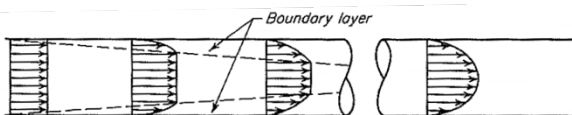


Figure 3.7. Illustration of boundary layer growth in ducted, laminar flow, resulting in a parabolic velocity profile at steady-state. Reproduced from McCabe, Smith and Harriott (7th Edition).

$$(Equation 3.5) x_t/D = 0.05 \cdot Re$$

In laminar flow, Equation 3.6 provides a basis to calculate the velocity at some distance (r) from the wall (at r_w), based on the shear stress at the wall (τ_w):

$$(Equation 3.6) u = \int_0^r du = -\frac{\tau_w}{r_w \mu} \int_{r_w}^r r dr = \frac{\tau_w}{2 r_w \mu} (r_w^2 - r^2)$$

From Equation 3.6, the maximum velocity occurring at the centreline ($r = 0$) of laminar flow is readily determined: $u_{max} = (\tau_w r_w)/(2\mu)$. While the Reynolds number (Equation 2.3) is calculated on the basis of *average* fluid velocity (\bar{u}) -- defined by the volumetric flow rate on the cross-sectional area -- the relationship between average and maximum fluid velocity in laminar flow can be derived from first principles, exploiting the parabolic flow profile shown in Figure 3.7:

$$(Equation 3.7) \bar{u} = \frac{\tau_w}{r_w^3 \mu} \int_0^{r_w} (r_w^2 - r^2) r dr = \frac{\tau_w r_w}{4 \mu}$$

Subsequently, the relationship between *average* and *maximum/centreline* fluid velocity in laminar flow is $\frac{\bar{u}}{u_{max}} = 0.5$. This constant laminar flow relationship provides a convenient basis for engineers who may be measuring a bulk quantity -- for example, volumetric or mass flow rate -- to determine the maximum velocity experienced by the fluids.

The consideration of boundary layers and fully-established flow is of paramount concern for unit operations and process engineers, with two primary considerations. First, if the engineer seeks to exploit flow for the purpose of heat or mass transfer, the requisite semi-empirical models (which are the subject of latter sections in this unit) *assume* flow is fully established: if this assumption is violated, the engineer can expect a deviation between the theory (model) and experiment (operation). Second, modern engineering is increasingly dependent on a network of sensors through processes and unit operations, whereby online management tools are used to maintain desired set-points. These tools may be adapted from engineering models, such as Aspen HYSYS that similarly *assume* flow has been fully-established, or they may be regressed empirically from historical operating data without necessarily invoking such assumptions. In either scenario, the placement of a measurement device at a point *before* flow is fully-established can result in significant deviations around the mean value, thereby jeopardizing the integrity of the measurement: put another way, the measurement deviations observed in Figure 2.6 become more substantial if the sensor is placed at a point of *establishing flow*.

While Equation 3.5 is useful for predicting the so-called *entrance length* required to obtain fully-established laminar flow, engineers will often rely on heuristics (that is, "rules of thumb") to guide the design and instrumentation of processes. In laminar flow, an entrance length of 100 pipe diameters is often used, while turbulent flow requires an entrance length of 50 pipe diameters that varies minimally with the Reynolds number. As pipe roughness increases, as may be a concern in systems with carbon steel that are prone to internal corrosion, the entrance length will increase beyond these heuristics. As will be discussed in greater detail with relevant unit operations, the impact of boundary layers on both heat and mass transfer processes must not be neglected: as both laminar and turbulent flow contain boundary layers with some degree of laminar region, the ability for turbulent eddies to access the wall is inhibited. Thus, if the unit operation is based on the contact

of the fluid and the wall, as might be the case in a simple jacketed pipe heat exchanger, the characteristics of the boundary layer contribute to the overall effectiveness of the process.

As discussed, most unit operations rely on turbulent flow to minimize the impact of boundary layers on heat and mass transfer. While the boundary layer in turbulent flow evolves according to Equation 2.7, the ultimate cross-sectional profile achieved is less parabolic than in laminar flow. Figure 3.1 compares fully-established profiles for laminar flow (dashed curve) and turbulent flow at $Re = 10,000$, as a fraction of the maximum local velocity at any point in the flow stream. As the degree of turbulence increases, a greater portion of the flow channel achieves the maximum velocity of flow: in Figure 3.1, the maximum velocity is experienced from relative distances of 10% on either side of the centreline. Extending this example, if the flow velocity were increased to achieve a Reynolds number of either 50,000 or 100,000, the relative distances of +/- 20% and +/- 40% of the centreline may be expected to be flowing at the maximum velocity. As such, higher Reynolds numbers generate a "bullhead" shape in the flow profile, as compared to the parabolic shape of laminar flow.

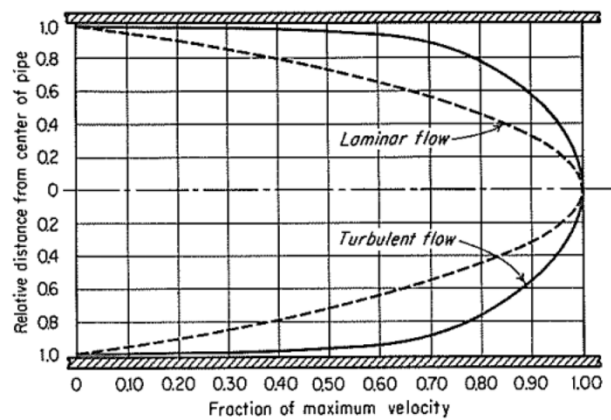


Figure 3.1. Normalized velocity profile for both laminar and turbulent ($Re = 10,000$) flow, reproduced from McCabe, Smith and Harriott (7th Edition).

Even at a mild turbulence of $Re = 10,000$ shown in Figure 3.1, the internal area between the dashed and solid curves represents a portion of material that will have a *higher residence time* for the laminar system. As such, a turbulent flow profile can be useful to the engineer, as it means a greater total mass of material is transmitted through the flow channel with time. There are two trade-offs for this improved flow efficiency: (i) *shear stress* on the wall increases with turbulence; and (ii) the size of the wall boundary layer, and its impacts on heat and mass transfer, similarly increase with turbulence.

Some unit operations, such as adsorption, are based not on the contact of a mobile fluid and a stationary wall, but rather the contact of mobile fluids with objects placed *within* the flow stream. The geometry of the object obstructing the flow stream becomes relevant in such a scenario. As shown in Figure 4.1, a parallel plate represents one bounding condition with minimal disruption to the flow stream, and a primary outcome of inverting the velocity profile: conceptually, this outcome may be considered to be the amalgam of laminar boundary layers from both the parallel plate and the enclosing wall. Conversely, the placement of a perpendicular plate represents a second bounding condition: instead of generating a new, local boundary layer, flow streamlines will be redirected around the plate, re-establishing the flow pattern after another (equivalent) entrance length. In this scenario, the local fluid immediately "behind" the plate will be relatively stagnant, with meaningful recirculation currents and the generation of eddies through a localised energy cascade as shown in Figure 3.3.

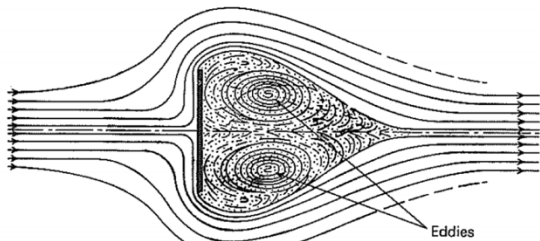
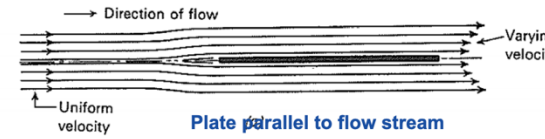


Figure 4.1. Illustration of two bounding conditions for the behaviour of fully-established flow around objects within the flow channel. Modified from McCabe, Smith and Harriott (7th Edition).

4.1 Drag

In considering the frictional loss of fluid colliding with the wall, the submerging an object in the flow stream will generate a similar loss in kind, called *drag*. Analogous to the friction factor, the *drag coefficient* (C_D) represents the magnitude of the loss term. One key distinction between friction losses and drag coefficients is in the relevant surface area: while most ducted flow systems have a well-defined cross-sectional area, drag coefficients require consideration of the *projected area* (A_p) of the immersed object, as shown in Figure 4.2.

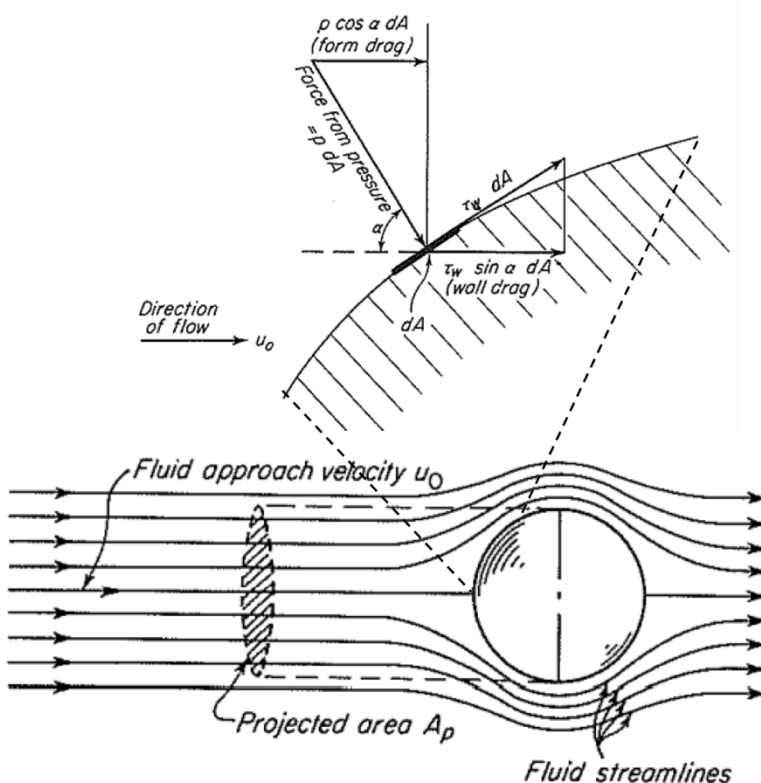


Figure 4.2. Example of fluid flow around an immersed sphere, with the projected area (A_p) of a circle: fluid can approach the immersed object at a number of angles. Modified from McCabe, Smith and Harriott (7th Edition)

Figure 4.2 illustrates a few key features of flow around immersed spheres. First, the fluid streamlines (that is, lines of constant velocity) bend around the object, and only return to fully established flow after the entrance length for the system is *repeated*. This is an important insight for the engineer who may consider installing objects that disrupt the flow pattern, as to where the downstream flow can be meaningfully measured again. Second, the *front half* of the sphere in Figure 4.2 will naturally experience a differential shear stress applied by the flowing fluid. The drag coefficient (C_D) is defined by Equation 4.1, which requires knowledge of the fluid velocity approaching the object (u_0):

$$(Equation 4.1) \quad C_D = (F_D / A_p) / ((\rho u_0^2 / 2) / 2) \approx \phi \cdot Re_p = \phi \cdot \frac{\rho u_0 D_p}{\mu}$$

Often, the estimation of drag force applied (F_D) integrated across the projected area of the object can be difficult to estimate, hence the approximation shown on the right-hand side of Equation 4.1. Within this approximation, ϕ is a proportionality function, and D_p is a *characteristic length* for the immersed object: the upstream/approach fluid velocity, viscosity (μ), and density (ρ) are otherwise used in the calculation of the local Reynolds number.

Semi-empirical relationships for the drag coefficient exist for most solids of interest, and may be estimated based on the area-to-circumference ratio of the projected solid in the limit that they have not been measured. For highly laminar systems where $Re < 1$, Stokes' Law provides an exact solution for drag force that further defines the drag coefficient:

$$(Equation 4.2) \quad C_D = 24 / (Re_p)$$

While the drag coefficient is difficult to predict during transition flow behaviour ($Re_p \approx 200$), it remains relatively constant at $0.4 < C_D < 0.45$ for local Reynolds number for $10^3 < Re_p < 10^5$, with minimal dependence on Reynolds number. As the local Reynolds number approaches 300,000, the drag coefficient decreases to approximately 0.1. Similar to the Fanning friction factor, a Moody-type diagram can be used to estimate the drag coefficient as a function of local Reynolds number for spheres, disks, and cylinders (Figure 4.3).

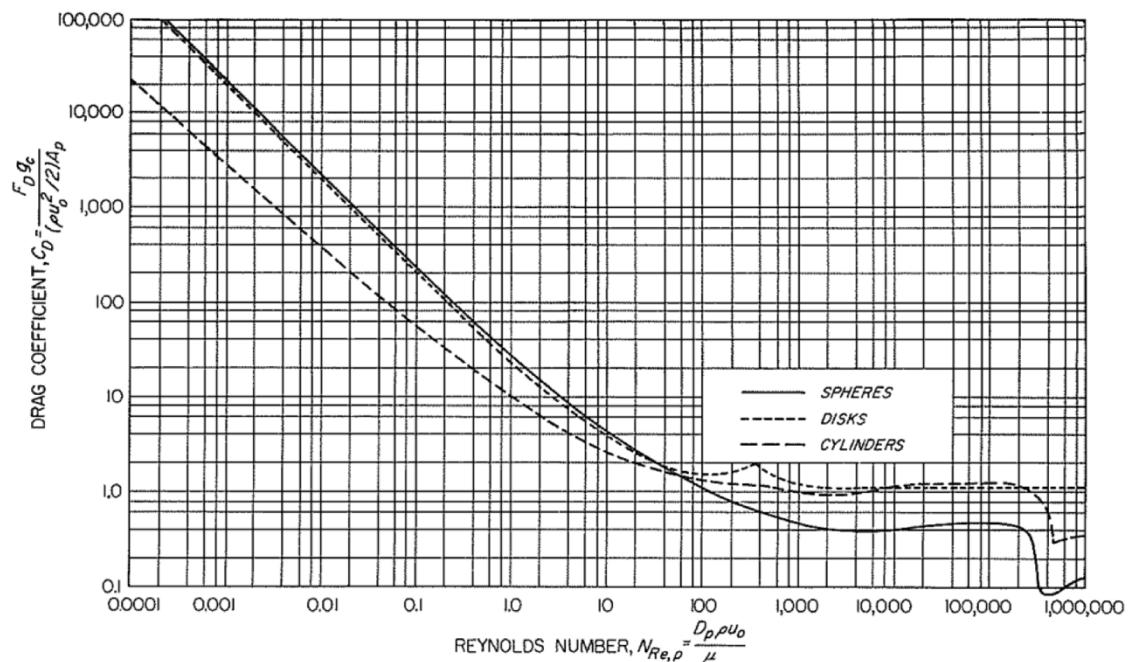


Figure 4.3. Relationship between drag coefficient (C_D) and local Reynolds number (Re_p or N_{Re_p}), reproduced from McCabe, Smith and Harriott (7th Edition).

With the exception of submerged disks in transition flow ($Re_p \approx 200$), drag coefficients decrease as the turbulence in a *laminar* flow regime increases, and tend to vary minimally with Reynolds number in a turbulent flow regime. Figure 4.4 demonstrates both experimental and theoretical examples of the interaction between fluids and submerged objects. At a transition Reynolds number (top panel), the cylinder contains a dye that is soluble within the external flowing fluid: the vortices induced by flow can be seen to remain stable after interaction with the cylinder, which is deemed a "vortex street" downstream of the object. As the fluid velocity is mild in this example, both large- and intermediate-sized eddies from the energy cascade (from Figure 3.3) can be observed. The immersed object's boundary layer follows the same behaviour as in Figure 3.6 for both laminar and turbulent flow. The centreline of flow directed at the face of the object (labelled as point "B" in the bottom panels of Figure 4.4) is called the "stagnation point," which corresponds to a local fluid velocity of zero and maximal flowing stress (that is, the entire "fluid head" is experienced at the face of the object). The contact area between the on-flowing fluid and the object increase as the fluid becomes more turbulent (demonstrated by the angle B-C from the centreline of the object). Consequently, the volume available for recirculation eddies becomes compressed, and the eddies contain greater turbulent energy, as the Reynolds number of the system increases.

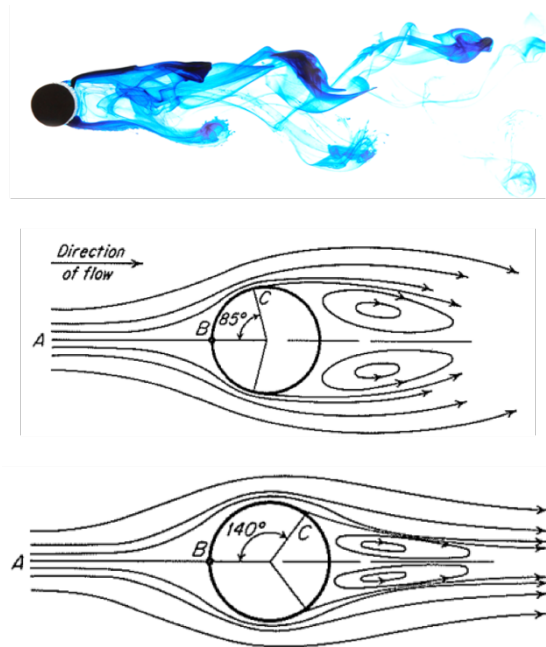


Figure 4.4. (top panel) Experimental example of wake shedding for a submerged cylinder at $Re_p = 200$, from Wikimedia Commons. (bottom panels) Illustration of streamlines for laminar (middle) and turbulent (bottom) flow around a submerged cylinder, reproduced from McCabe, Smith and Harriott (7th Edition).

The recirculation volume available "behind" the projected area of an immersed object correspond with energy loss, which can be minimised or eliminated by modifying the shape of the object: this process is referred to as "streamlining," where an example is shown in Figure 4.5. The correct choice of a streamlined object minimizes the detachment and magnitude of turbulent eddies at the tail of the object, and reduces the distance required for flow to again become fully established.

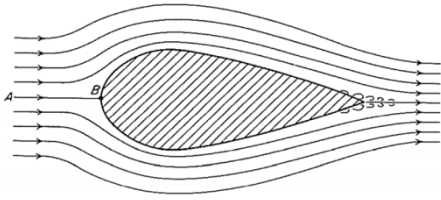


Figure 4.5. An example of streamlining, where the geometry of the immersed object minimises the extent of recirculation on the back face of the object's projected area. Reproduced from McCabe, Smith and Harriott (7th Edition).

4.2 Mobile Objects in Flow

In some engineering applications, the immersed object experiencing drag is *mobile*, as might be the case for a settling dense solid or rising vapour bubble in a liquid phase. The "particle" in such cases is subject to the drag force (F_D) described in Section 4.1, a bouancy force (F_B) that considers the density difference between the object and external fluid, and all gravitational or centrifugal external forces (F_E). Equation 4.3 balances and expands definitions for these forces, proscribing a definition for the velocity of the particle in time:

$$(Equation 4.3) \frac{du}{dt} = \frac{1}{m} \cdot (F_E - F_B - F_D) = \frac{1}{m} \cdot \left(m a_e - \frac{m \rho a_e}{\rho_p} - \frac{C_D u_0^2 \rho A_p}{2} \right) = a_e \frac{\rho_p - \rho}{\rho_p} - \frac{C_D u_0^2 \rho A_p}{2m}$$

where the density difference between the object (ρ_p) and external fluid (ρ) plays a controlling factor, alongside the particle mass (m), drag coefficient, projected area in flow (A_p), and velocity of the external fluid (u_0). Equation 4.3 is to describe both gravity acting on objects (where $a_e = g$, the constant for gravitational acceleration) and when the centrifugal force is controlling (where $a_e = r\omega^2$, involving the distance from origin r and angular velocity ω).

For objects that originally begin at rest, velocity will increase in line with Equation 4.3 until the force encouraging movement (that is, gravity or centrifugal) is fully balanced against the drag force. At this point, the object reaches its *terminal velocity*, where the time derivative of velocity ($\frac{du}{dt}$) goes to zero: the value of the terminal velocity can be determined by setting Equation 4.3 to zero, which is shown below for gravitational settling (Equation 4.4) and centrifugal separation (Equation 4.5):

$$(Equation 4.4) u_t = \sqrt{(2g(\rho_p - \rho)m / (A_p \rho_p C_D \rho))}$$

$$(Equation 4.5) u_t = \omega \sqrt{(2r(\rho_p - \rho)m / (A_p \rho_p C_D \rho))}$$



Example 3 -- Calculating terminal velocity of a sphere, using Equation 4.4 (video from [Microsoft Stream](#)).

It should be noted that gravitational "settling" involves both the downward motion of dense particles *and* the upward motion of buoyant particles (of any phase) in fluid. Example data for the scenario of a rising bubble are shown in Figure 4.6, which illustrate that intermediate-sized bubbles (between 1.3 and 3 mm) are reasonably predicted by the assumption of a rigid sphere, using the drag coefficient estimated from Figure 4.3. However, bubbles *larger* than 3 mm in diameter become ellipsoidal in nature: that is, the pressure experienced at and around the stagnation point (shown in Figure 4.5) can deform the bubble, the viscosity and density of which are substantially lower than the surrounding water.

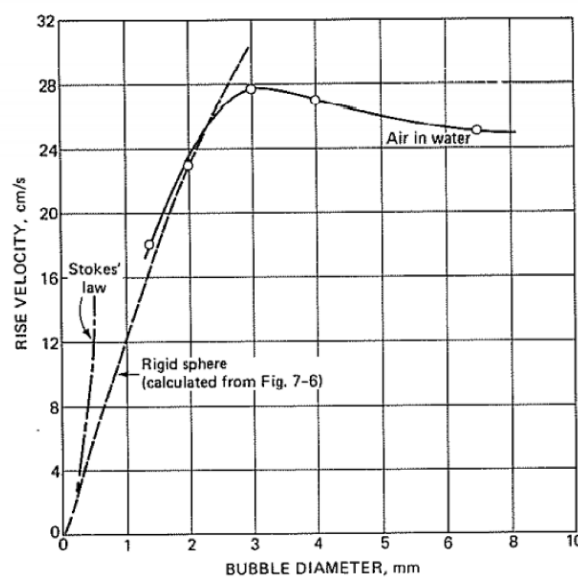


Figure 4.6. Measurement (points) and theory (dashed line) for the observed terminal rising velocity of air bubbles in water at 343 K, reproduced from McCabe, Smith and Harriott (7th Edition).

The behaviour shown in Figure 4.6 can be expected for all moderately-sized, immersed objects where the maximal stress applied at the stagnation point is greater than the yield stress of the object's phase (as per Figure 3.1), as the entire fluid velocity head ($\frac{v_0^2}{2}$) is converted to a pressure head acting on the object ($\frac{p_{stag.} - p_0}{\rho}$). It is worth noting that, for very small objects (e.g. air bubbles below 1 mm in diameter), the ability for the immersed phase to deform must further consider the interfacial tension, also called surface tension, between the object and the surrounding fluid. Generally, interfacial tension is the two-dimensional equivalent of pressure in three dimensions, with units of energy per unit area: as the absolute size of any object decreases, the interface contributes a greater fraction of "total" energy -- that is, the sum of interfacial tension and volumetric energy, such as Gibbs. At the limit of around 1 micron, interfacial energy/tension becomes the *dominant* contribution: this explains why micron-sized dust can appear to "float" with a particle density of above 2000 kg/m³. Thus, the deformation of very small particles requires sufficient stress to overcome *both* the yielding viscosity of the phase *and* the additional energy penalty of creating and maintaining surface area.

4.3 Flow in a Stationary Bed

The concept of "particle beds" feature heavily in Chemical Engineering applications, where a mobile fluid flows through a densely-packed collection of particles that are either stationary (discussed below) or mobile (called fluidization, discussed in Section 4.4). Depending on the desired heat or mass transfer outcome, such beds provide the engineer with a high surface area-to-volume environment. An example column is shown Figure 4.7, there the bottom half of the column is filled with small solids that form the "bed" through which a target fluid will flow: if the velocity of the flowing gas is sufficiently high, some or most of the particle bed can be suspended in air.

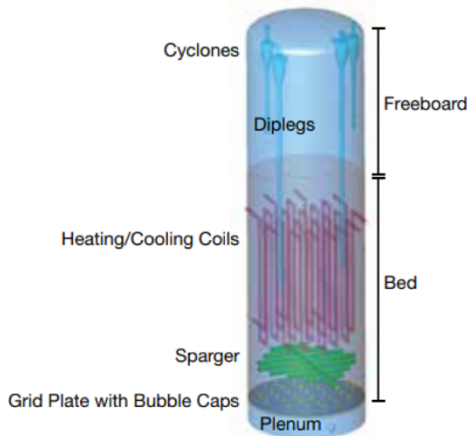


Figure 4.7. An example particle bed, where fluid (gas) is fed from the bottom of the column at a rate that controls column pressure (by using bubble caps): the use of a sparger ensures equal distribution of gas through the bed environment. Reproduced from Cocco et al., CEP (2014).

This section will consider lower flowing velocities, where the particle bed is considered to be "stationary." Each particle will experience some degree of flowing stress, giving rise to local boundary layers, in line with Figure 4.4: as such, the degree of turbulence imparted by the fluid will dictate both the contact area between fluid and solid -- which is of paramount importance to mass transfer operations -- and the extent of energy loss due to recirculation currents around the solids. As such, the characterisation of differential pressure across the bed requires the engineer to extrapolate the behaviour of flow around a single immersed object (as per Figure 4.4.) to flow

through a closely-packed network of hundreds or thousands of objects. This is accomplished by introducing an *equivalent channel diameter* (D_{eq}), which considers the individual particle diameter (D_p):

$$\Phi_s D_p \left(\frac{\epsilon}{1 - \epsilon} \right)$$

where ϵ represents the void fraction -- or the fraction of the total volume occupied by *fluid*, as opposed to the particle volume fraction that is, by definition, $(1 - \epsilon)$ -- and Φ_s represents the sphericity of the solid particles, defined as the surface area-to-volume ratio for a sphere divided by the surface area-to-volume ratio for the solid of interest. As a bounding condition, the sphericity of a sphere is unity. For a typical void fraction of 0.4, Equation 4.6 is $D_{eq} = 0.44\Phi_s D_p$, illustrating that the channel diameter is around *half* of the nominal particle diameter, depending on the sphericity of the particles employed. The sphericity of common materials is shown in Table 4.1, where Figure 4.8 provides an illustration of common packing materials.

Table 4.1. Common solids deployed in packed beds, reproduced from McCabe, Smith and Harriott (7th Edition).

Packing material	Sphericity
Spheres, cubes, short cylinders	1.0
Raschig rings where $D_i = 0.5D_o$	0.58
Raschig rings where $D_i = 0.75D_o$	0.33
Berl saddles	0.33
Ottawa sand	0.95
Rounded sand	0.83
Coal dust	0.73
Flint sand	0.65
Crushed glass	0.65
Mica flakes	0.28

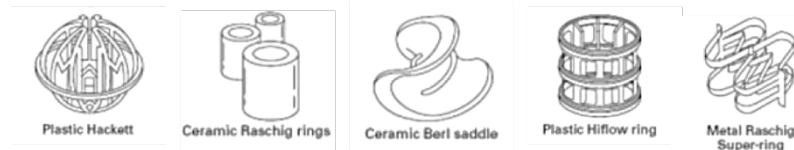


Figure 4.8. Common shapes of artificial (synthetic) solids deployed in packed beds, from Wikimedia Commons.

When considering how fluid may flow (as per Figure 4.4) around the exemplar packing materials shown in Figure 4.8, the variability in contact/surface area will naturally produce different outcomes. For example, flow between individual Raschig rings will follow a relatively uniform path, while Berl saddles will alter the direction of flow and result in, ultimately, a longer path. This property is called tortuosity, and requires consideration when attempting to predict the frictional pressure loss across packed bed materials. The Kozeny-Carman (Equation 4.7) and Burke-Plummer (Equation 4.8) relationships provide a basis for calculating this frictional pressure loss, which is traditionally reported with units of (differential) pressure loss per unit height of packed bed material and incorporates the contributions of effective diameter from Equation 4.6:

$$\frac{\Delta P}{L} = \frac{150 \bar{u}_0 \mu}{\Phi_s^2 D_p^2} \cdot \frac{(1-\epsilon)^2}{\epsilon^3} \quad \text{for } Re_p < 1$$

$$\frac{\Delta P}{L} = \frac{1.75 \rho \bar{u}_0^2}{\Phi_s^2 D_p^2} \cdot \frac{1-\epsilon}{\epsilon^3} \quad \text{for } 1000 < Re_p$$

where \bar{u}_0 represents the *superficial velocity* of fluid in the column, defined as the ratio of the volumetric flowrate of fluid on the cross-sectional area of the column. The use of superficial velocity provides a convenient basis for comparing multiple materials and bed configurations, each of which can affect the actual fluid velocity experienced by the particles.

The Kozeny-Carman relation (Equation 4.7) assumes that differential pressure is inversely proportional to the viscosity of the fluid, which is equivalently the basis for Darcy's Law that informs flow in porous media applications. As the Burke-Plummer relation scales with the square of fluid velocity, it returns a substantially larger differential pressure under turbulent flow than the Kozeny-Carman relation, where the converse is equally true under laminar flow conditions. Practically, the engineer can therefore use the single-form Ergun equation to predict the differential pressure across stationary beds, which accounts for viscous loss contributions in the first term (as per the Kozeny-Carman relation) and kinetic loss contributions in the second term (as per the Burke-Plummer relation):

$$\frac{\Delta P}{L} = \frac{150 \bar{u}_0 \mu}{\Phi_s^2 D_p^2} \cdot \frac{(1-\epsilon)^2}{\epsilon^3} + \frac{1.75 \rho \bar{u}_0^2}{\Phi_s^2 D_p^2} \cdot \frac{1-\epsilon}{\epsilon^3}$$

In the limit that mixtures of packing materials are employed in the bed, predicting frictional pressure loss requires the solid diameter D_p to be replaced with a mixture diameter that is normalised by the surface area of the N particles: $\bar{D}_{mix} = \sum_{i=1}^n N_i D_p^3 / \sum_{i=1}^n N_i D_p^2$. The Ergun equation informs the pressure required of the fluid injected in the packed bed and, subsequently, the cost and scale of gas compressor or liquid pump required for the unit operation.



Example 4 -- Calculating pressure drop in a packed bed, using Equation 4.9 (video from Microsoft Stream).

4.4. Fluidized Beds

In the scenario that the engineer introduces sufficient velocity to a packed bed such that the force applied to the stagnation point of each packing solid can overcome the gravitational or body force of that solid, some portion of the bed may become "fluidized." That is, a fraction of the solids will remain suspended in the flowing fluid phase, constituting a solid-in-fluid suspension. Fluidized beds play an important role through the energy and minerals industry. In the middle of the 20th century, fluidized catalytic cracking (or *cat. cracking* for short) enabled improved yield of high-value petroleum and kerosene (jet fuel), by degrading the long-chain hydrocarbons (typically associated with bitumen) at very high temperature. Similarly, fluidized beds have presented opportunities to improve the efficiency of chemical generation (as in the case of acrylonitrile), solid combustion, ore refinement, and gas adsorption.

The Kozeny-Carman (Equation 4.7) and Burke-Plummer (Equation 4.8) relations can respectively be used to solve for the minimum fluidization velocity ($\bar{u}_{0,\min}$) for the condition of $\Delta P = (\rho_p - \rho)gL$, where the same limiting particle Reynolds number conditions apply:

$$\Phi_s^2 D_p^2 \quad \text{for } Re_p < 1$$

$$\sqrt{\frac{\Phi_s D_p g (\rho_p - \rho) \epsilon_{\min}^3}{1.75 \rho}} \quad \text{for } 1000 < Re_p$$

where the bed porosity (ϵ) is replaced with the porosity at the minimum fluidization velocity (ϵ_{\min}). Figure 4.9 illustrates how the frictional pressure drop and the height of the bed -- which scales directly with porosity -- vary as a function of the superficial velocity of the incoming fluid (\bar{u}_0), where the vertical line demarcates the transition from a stationary (fixed) bed to a fluidized bed. As the minimum fluidization velocity is achieved, the pressure drop can be seen to vary minimally with further increases to fluid velocity as it meets the limiting criterion of total bed weight: above this point, the *height* of the fluidized bed will continue increasing linearly with the superficial velocity. Both pressure drop and height follow distinct curves *before* and *after* fluidization is achieved, denoted by the arrows in Figure 4.9. As solid are randomly packed in nature, fluidization followed by settling will typically produce a less efficient packing configuration, resulting in a larger stationary bed height and less sensitive relationship between pressure drop and superficial fluid velocity.

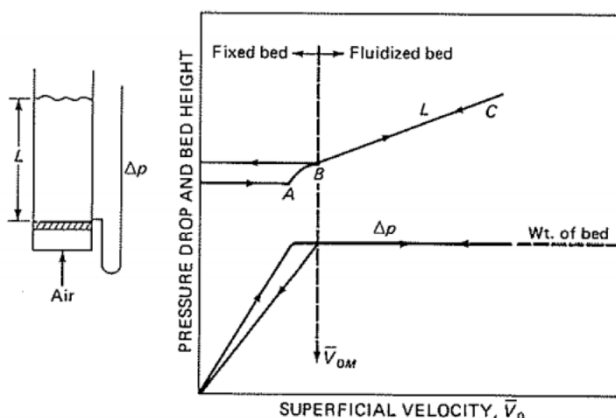


Figure 4.9. General relationship between differential pressure (drop) and total packed bed height, reproduced from McCabe, Smith and Harriott (7th Edition).

An illustration of fluidization states is shown in Figure 4.10, where superficial (gas) velocity increases from left to right. After achieving the minimum fluidization velocity, increasing fluid velocity will first produce a uniform expansion of the bed (as shown in Figure 4.9), with relatively uniform porosity throughout (deemed *smooth fluidization*). As fluid turbulence is inherently random in nature, the tortuous fluid pathway through the bed will naturally vary between boundaries of significant and minimal contact with the suspended solids. As superficial velocity increases beyond the point of smooth fluidization, the flow path will become biased toward regions with previously lower tortuosity (i.e. leftover from the previous volume of fluid): the result is the aggregation of solids throughout the column, with a portion of the fluid remaining relatively free of contact (referred to as both *aggregative fluidization* and *bubbling fluidization*). *Turbulent fluidization* and *fast fluidization* occur at yet higher superficial fluid velocities, when the pockets of concentrated fluid themselves become a turbulent phase of flow, which typically occurs between 1 and 2 ft/s for most solids. At velocities above this point, the bed may be referred to as either *conveying* or *circulating*, as solids are readily entrained in the fluid phase and can be returned to the bottom of the column by mechanical conveyor for re-entrainment: this condition can be useful if, for example, the temperature or material state of the solid must be re-generated.

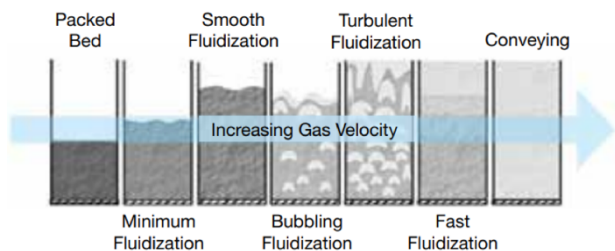


Figure 4.10. Condition of a packed bed across varying fluidization states, reproduced from Cocco et al., CEP (2014).

For superficial velocities above the minimum fluidization point, the Burke-Plummer relation can be re-arranged (Equation 4.12) to solve for the porosity of the bed and, through the definition of porosity, the height of the bed (L). Figure 4.11 provides an example of how this semi-empirical basis compares with experimental measurement.

$$\frac{150 \mu}{g (\rho_p - \rho) \Phi_s^2 D_p^2}$$

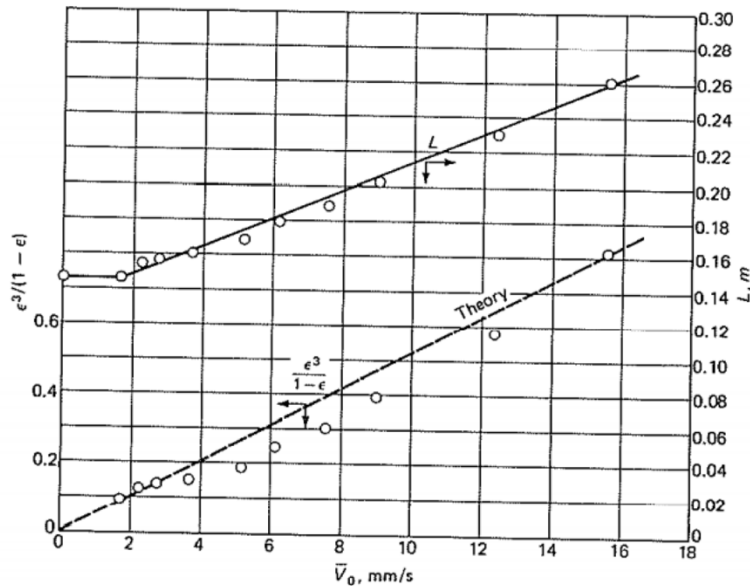


Figure 4.11. Example measurements (points) of bed porosity (left-hand ordinate) and height (right-hand ordinate) as a function of superficial gas velocity in a packed column, compared with theoretical predictions (lines) from Equation 4.12. Reproduced from McCabe, Smith and Harriott (7th Edition).

The condition of a *conveying* or *circulating* bed is informed by the limiting condition of the velocity predicted from the Kozeny-Carmen relation (the form of which matches Equation 4.10) is equal to the *terminal* velocity of the individual particles per Equation 4.4:

$$\frac{8.33(1-\epsilon_{min})}{\Phi_s^2 \epsilon_{min}^3}$$

which illustrates the role of both sphericity and fluidized porosity. Although the Burke-Plummer relation can be arranged in a similar form to Equation 4.13 (that is, by considering the terminal velocity of particles), the use of the Kozeny-Carmen relation provides a more conservative basis so as to ensure the size of gas compressor or liquid pump purchased is sufficient.

Temperature plays a critical role throughout unit operations, from its importance in defining the thermodynamic state of materials through to optimising the conditions for mass transfer. This section provides an abbreviated review of heat transfer concepts and relevant rate equations for use in unit operations. As will be shown, most "real" engineering problems typically a multitude of heat transfer modes and rates, which must be amalgamated to inform either the steady-state or transient temperature in a location of interest. The example in Figure 5.1 illustrates the role of three primary heat transfer modes to maintain temperature in a system: the warm house will lose heat through the walls and ceiling through conduction (discussed in Section 5.1), which is balanced at steady-state with the use of an electric or gas-fired heater to circulate warm air (convection, discussed in Section 5.2) and complemented by the minor impact of solar radiation.

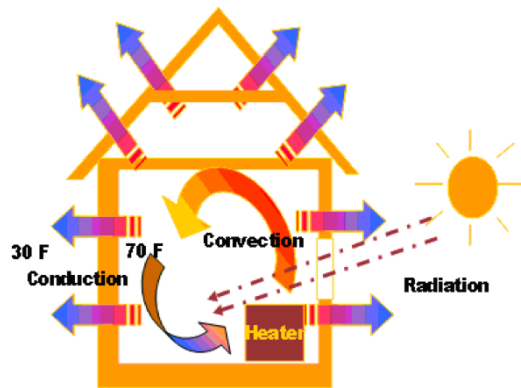


Figure 5.1. Heat transfer modes are often combined in practical systems to maintain a set-point temperature (reproduced from Wikimedia Commons).

5.1 Conduction

The rate of energy (that is, heat) transfer through materials varies with the phase of the material. The atoms or molecules in *solids* cannot store energy in translational or rotational modes, as only vibrational modes are available: as is discussed in the discipline of thermodynamics, this results in the general heuristic that the capacity (or ability) of solids to take on heat -- that is, the heat capacity -- *tends* to be an order of magnitude smaller than that of liquids or gasses. In the context of unit operations, the transfer of energy *through* a stationary phase -- including all solids and fluids at rest -- is called conduction, where Fourier's Law (Equation 5.1) determines the rate of heat flow (q) per unit area (A):

$$(Equation 5.1) \quad dq/dA = -k \frac{dT}{dx}$$

where the proportionality constant k corresponds to the *thermal conductivity* of the material -- that is, the ease with which vibrating molecules can transfer energy to nearby neighbours -- and the driving force (dT/dx) is defined by the temperature difference across the material. As practical unit operations tend to contain multiple, solid materials in contact (e.g. solid insulation placed around a cylindrical, metallic pipe), Equation 5.1 can be deployed to describe each material and the combined effect can be summed. Consider the example shown in Figure 5.2, where three solid materials (labelled A, B and C) are placed in series.

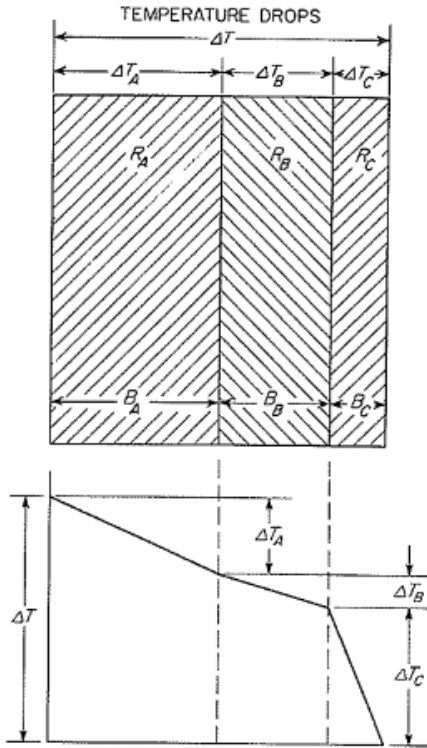


Figure 5.2. An example heat transfer system with three solid layers (A, B and C, where $T_A > T_B > T_C$), each with a difference resistance to conduction (where $R_A = k_A$) and thickness. Reproduced from McCabe, Smith and Harriott (7th Edition).

As the left-hand surface of phase A corresponds to the highest local temperature in the system, and the materials are immobile, heat will first be conducted across the thickness of phase A (corresponding to B_A) at a rate that is governed by the phase's resistance to heat transfer (generically, R_A as representative of the thermal conductivity). The lower panel of Figure 5.2 illustrates that the thermal conductivity of the phase dictates the slope of the temperature change: importantly, the construction of Fourier's Law (Equation 5.1) demonstrates that temperature within the material will change *linearly*. The total change in temperature across the material can be represented by Equation 5.2:

$$(Equation 5.2) \quad \Delta T = \sum_i \Delta T_i = \sum_i q_i B_i / (A_i \bar{k}_i) = \Delta T_A + \Delta T_B + \Delta T_C = \frac{q_A B_A}{A \bar{k}_A} + \frac{q_B B_B}{A \bar{k}_B} + \frac{q_C B_C}{A \bar{k}_C}$$

where the bar operator on thermal conductivity denotes a spatial mean (that is, considering the material may have differential thermal conductivity if, for example, a portion of it may have degraded during the lifetime of the unit operation). It is important to note that Equation 5.2 corresponds to a steady-state system. In most unit operations, the temperature boundary is established by continuous measurement, and the *initial* state of the material (that is, its *initial* thermal conductivity) is known through external characterisation. At steady-state, the rate of heat transfer between each of the three phases in Figure 5.2 will be equivalent (that is, $q_A = q_B = q_C = q$), as the phases share the same contact/interfacial area: as such, if the external temperature boundaries are known (ΔT), the overall rate of heat transfer per unit area can be determined:

$$(Equation 5.3) \quad \frac{q}{A} = \frac{\Delta T}{\frac{B_A}{\bar{k}_A} + \frac{B_B}{\bar{k}_B} + \frac{B_C}{\bar{k}_C}}$$

It is important to note that Fourier's Law, and it demonstrated uses in Equations 5.2 and 5.3, correspond to *steady state* heat transfer. If the temperature of the *boundaries* changes in time, Equation 5.1 cannot be used and a differential description of temperature in both space and time must be employed:

$$(Equation 5.4) \frac{\partial T}{\partial t} = \left(\frac{k}{\rho C_p} \right) \frac{\partial^2 T}{\partial x^2} = \alpha \frac{\partial^2 T}{\partial x^2}$$

where knowledge of the material's density (ρ) and heat capacity (C_p) are required. The bracketed terms in Equation 5.4 together represent the thermal diffusivity of the material (α), physically corresponding to the ability of the material to transmit heat relative to that which it retains (i.e. in vibrational modes for solids, or vibrational/rotational/translational modes for stationary fluids). Equation 5.4 can be solved explicitly where one initial condition and two boundary conditions are known in the system, or may be approximated through numerical methods for complex systems. The example in Figure 5.2 can be extended to a system with cylindrical coordinates, such as a metallic pipe with multiple insulation layers. At steady state, Fourier's Law can be integrated in cylindrical coordinates for a cylinder of thickness ($r_o - r_i$) and length (L):

$$(Equation 5.5) \int_{r_i}^{r_o} \frac{dr}{r} = \frac{2\pi L k}{q} \int_{T_i}^{T_o} dT$$

When solved for the temporal rate of heat transfer at steady-state (q), Equation 5.5 produces:

$$(Equation 5.6) q = \frac{k \bar{A}_L (T_i - T_o)}{r_o - r_i}$$

where the term \bar{A}_L corresponds to the *logarithmic mean area* as defined below:

$$(Equation 5.7) \bar{A}_L = 2\pi L \cdot \frac{(r_o - r_i)}{\ln(r_o/r_i)}$$

The logarithmic mean area, the right-hand fraction of which contains a definition of the *logarithmic mean radius* (\bar{r}_L) or "log-mean radius", is an important consideration of conductive heat transfer for *thick-walled systems*. Figure 5.3 compares the log-mean radius with the arithmetic mean radius as a function of wall thickness (where r_o and r_i respectively represent the outer and inner radii). In most unit operations, consideration of the log-mean radius and area is only required with very high operating pressures (which necessitate thick pipes with high burst pressures) or when insulation is of concern (typically, systems operating at extreme temperature limits, or with either mass transfer or chemical reactions taking place).

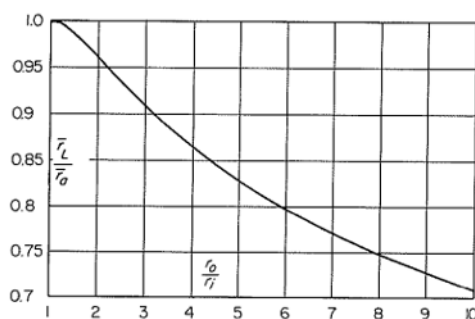


Figure 5.3. The log-mean radius (\bar{r}_L) deviates significantly from the arithmetic mean radius (\bar{r}_a) for cylindrical pipes with an outer radius (r_o) that is approximately 25% larger than the inner radius. Reproduced from McCabe, Smith and Harriott (7th Edition).

Where fluids are flowing through a system with heat conduction through the wall, as is often the case in unit operations, the effectiveness of heat transfer can readily be degraded through internal fouling. The formation and deposition of solids, such as mineral scales, is one primary cause of fouling, wherein the thickness and properties of the scale can act as a new "phase" of material (as per Figure 5.2) and thereby affect the overall rate of heat transfer. As such, the consideration of prospective fouling behaviour in flowing systems is a primary consideration for the chemical engineering, and a maintenance schedule must be employed to clean or replace fouled systems: if ignored, fouling can result in either the purchase of an unnecessarily large heat transfer operation or unacceptably poor performance in the heat transfer operation.

5.2 Convection

Fluids in motion are generally able to transfer energy more efficiently, as the distribution and magnitude of eddies shown in Figure 3.3 reduce the time required to reach thermal equilibrium in a volume. For systems in motion, Newton's Law of Cooling provides a basis to calculate the rate of heat transfer:

$$(Equation 5.8) \frac{dq}{dA} = h(T_{surface} - T_{bulk})$$

where U is the proportionality constant for convection, termed the *local heat transfer coefficient*, against the driving force of temperature difference between a surface ($T_{surface}$) and energy reservoir (T_{bulk}). The convective heat transfer coefficient varies with the heat transfer properties of the fluid and the degree of turbulence in the system. The correct nomination of coefficient is typically the most challenging part of solving a convective heat transfer problem, where empirical correlations are most often employed (as discussed below). Critically, the basis of considering heat transfer in a *flowing* system requires the engineer to assess both fluid mechanics and heat transfer characteristics simultaneously. Alongside the fluid mechanics that give rise to a (hydrodynamic) boundary layer, deviations in local fluid temperature (that is, between the fluid and wall) mean that temperature-dependent properties (for example, ρ , k , and C_p) will also vary locally in this region: the result is the generation of a "thermal" boundary layer, which follows similar behaviour in kind to the previously-discussed hydrodynamic boundary layer.

Figure 5.4 illustrates how hydrodynamic and thermal boundary layers evolve from the leading edge of a wall (that is, $x = 0$). When the wall is at a uniform temperature, both boundary layers will evolve toward fully-established flow through the laminar or turbulent behaviour discussed previously. If the wall has an unheated portion, as is shown in the bottom panel of Figure 5.4, the thermal boundary layer cannot begin to establish until fluids contact the heated portion of the wall: while both boundary layers will evolve to the same steady-state condition, such a "delay" in establishing the thermal boundary layer will increase the residence time required for fully-established flow.

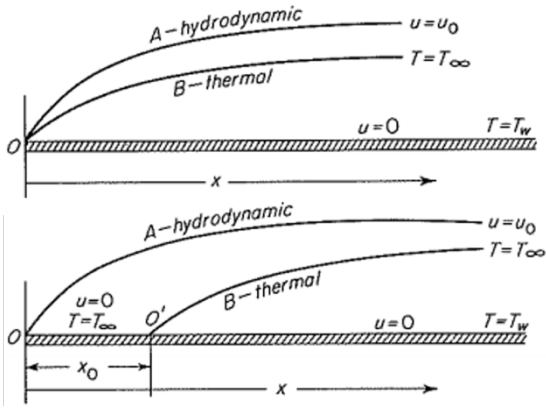


Figure 5.4. A comparison of hydrodynamic and thermal boundary layers for fluid in contact with a heated wall where $T = T_w$, for scenarios with a uniform wall temperature (top panel) and an unheated portion of the wall (x_0 , bottom panel). Reproduced from McCabe, Smith and Harriott (7th Edition).

To assess how the hydrodynamic and thermal boundary layers evolve relative to one another, one may consider how momentum diffuses through a fluid (represented by the kinematic viscosity, ν) relative to the diffusion of energy (again represented by α). This ratio is captured by the dimensionless Prandlt number:

$$(Equation 5.9) \quad \text{Pr} = \frac{\nu}{\alpha} = \frac{(\mu/\rho)}{k/(\rho C_p)} = \frac{C_p \mu}{k}$$

Where the Prandlt number has a value greater than unity, the *thermal boundary layer is thinner than the hydrodynamic boundary layer*: when the value is precisely unity, the thickness of the boundary layers is equivalent. As an example, water at 343 K and ambient pressure has a Prandlt number of approximately 2.5, indicating the hydrodynamic boundary layer will be larger than the thermal boundary layer.

5.3 Nusselt Correlations

Further to its use when considering local boundary layers, the Prandlt number, alongside the Reynolds number, is required to use the semi-empirical correlations that are able to inform convective heat transfer coefficients (h) across various scenarios. Such correlations require the use of the dimensionless Nusselt number (Equation 5.10), which represents the ratio of *convective to conductive heat transfer resistance*:

$$(Equation 5.10) \quad \text{Nu} = \frac{hD}{k}$$

As thermal conductivity (k) is a property of the material and not the flowing system (discussed in Section 5.1), semi-empirical correlations for the Nusselt number therefore allow the engineer to solve directly for h through the definition of the Nusselt number. One such correlation is shown in Equation 5.11, which is appropriate for **laminar flow** across a flat plate and is valid for $\text{Pr} > 1.0$ and $\text{Nu} > 10$:

$$(Equation 5.11) \quad \text{Nu} = 0.664 \sqrt[3]{\text{Pr}} \sqrt{\text{Re}} = 0.664 \sqrt[3]{\frac{C_p \mu}{k}} \sqrt{\frac{\rho u_o x_1}{\mu}}$$

where the right-hand expression expands definitions for the Prandlt and Reynolds numbers, respectively. For laminar flow in a pipe or duct, Equation 5.12 can be deployed:

$$(Equation 5.12) \quad Nu = 1.85 \left(Re \cdot Pr \cdot \frac{D}{L} \right)^{1/3} \phi_v \leq 3.66$$

where ϕ_v is a correction factor for the arithmetic mean viscosity of the fluid between the (μ) against the viscosity of water at the wall temperature (μ_w) and defined as $\phi_v = \left(\frac{\mu}{\mu_w} \right)^{0.14}$ with values greater than unity for heating and less than unity for cooling. As Equation 5.12 is limited to laminar flow, it is often taken at its limiting value of approximately 3.66.

Nusselt correlations are not well-established for transition flow, given the intermittent nature of the regime. In turbulent flow, where $Re > 6000$, two Nusselt correlations can be used:

$$(Equation 5.13) \quad Nu = 0.023 \cdot Re^{0.8} \cdot Pr^n$$

$$(Equation 5.14) \quad Nu = 0.023 \cdot Re^{0.8} \cdot Pr^{1/3} \cdot \phi_v$$

where Equation 5.13 is the Dittus-Boelter correlation, valid when the fluid is being heated with Prandlt exponents of $n = 0.4$ and $n = 0.3$ when the fluid is being heated or cooled, respectively, and Equation 5.14 is the Sieder-Tate correlation (alternatively referred to as the Colburn equation). In using these correlations, the engineer must first determine the correct Reynolds and Prandlt number for the system, calculate the Nusselt number from an appropriate correlation, and -- through the definition of the Nusselt number shown in Equation 5.10 -- then calculate the appropriate convective heat transfer coefficient. Characterising the region of transition flow, in which $2100 < Re < 6000$, the intermittent nature of turbulent eddies necessarily require a more empirical solution, which is proposed in Equation 5.15.

$$(Equation 5.15) \quad \frac{h_i}{c_p \rho V} = 1.86 \frac{\left(\frac{D}{L} \right)^{1/3}}{Re^{2/3} \cdot Pr^{2/3}} \phi_v$$

Equation 5.15 is a semi-empirical correlation applied to the Colburn analogy, which follows a similar form to the above correlations, but does *not* use the Nusselt number. Figure 5.5 provides an illustration of the so-called "Colburn-j" analogy for transition flow patterns, where $j_H = Nu / (\Phi_v \cdot Re \cdot Pr^{1/3})$, which is valid for prandlt numbers between 0.6 and 100: the negative slope corresponding to Reynolds numbers between 1000 and 2000 corresponds to laminar flow, above which the Colburn-j correlation is presented.

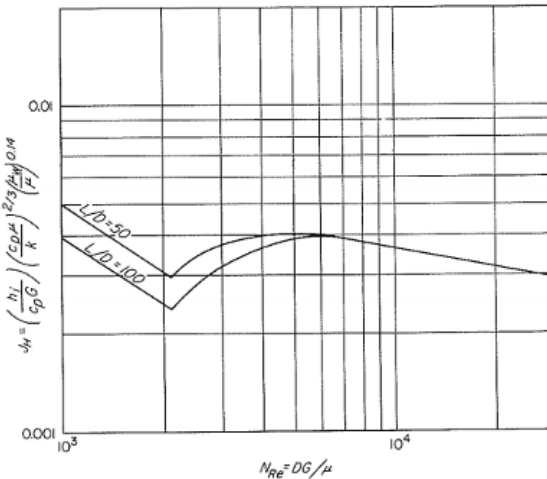


Figure 5.5. The "Colburn-j" factor as a function of the Reynolds number, for two different length scales of interest. Reproduced from McCabe, Smith and Harriott (7th Edition).

The above correlations consider flow *inside* an enclosed system, such as water flowing through a pipe. A second suite of Nusselt-type correlations can be deployed for flow *outside* temperature-controlled surfaces, which are discussed below. This may be the case for outdoor heat exchange systems, where air or water either naturally or forcibly flows across a heat exchange surface. For the scenario of forced flow across (that is, normal to) one or more *cylinders* to exchange heat, Equation 5.16 can be used:

$$(Equation 5.16) \quad Nu_o = \frac{h_o D_o}{k_f} = (0.35 + 0.56 \cdot Re_f^{0.52}) \cdot Pr_f^{0.3}$$

where the Nusselt number is defined for the outer diameter and convective heat transfer coefficients of the cylinders, and the Reynolds and Prandlt numbers are defined for the *external* fluid flowing across the diameter of cylinders. Engineers tend to prefer forced convection in natural settings -- for example, through the use of fans to direct air or water -- to maintain fluid flow that is normal to the heat exchange surface. Figure 5.6 illustrates how the Nusselt number varies with the direction of external flow, where a coordinate of 90 degrees ($\theta = 90^\circ$) corresponds to flow normal to the surface associated with optimal Nusselt numbers. If the engineer is not able to maintain normal flow, the unit operation design must consider the effect of changing wind or water direction that, as per Figure 5.6, can affect the convective heat transfer coefficient (being directly proportional to the Nusselt number) by a factor of 2-3: this consideration may require, for example, that the heat exchange surface (i.e. number and/or length of pipes) be doubled or tripled, thereby affecting capital and operating expenditure for the unit operation(s).

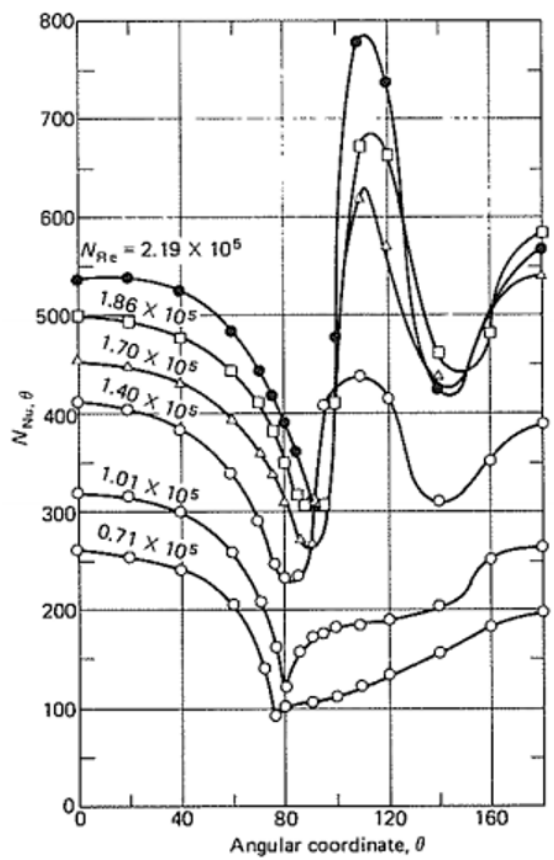


Figure 5.6. Dependence of the Nusselt number in forced external convection on the direction of flow, for curves of constant Reynolds number in the external fluid. Reproduced from McCabe, Smith and Harriott (7th Edition).

Where natural convection is selected, and the above-described cost impacts are acceptable, heat transfer considerations must also incorporate the effect of local fluid buoyancy. That is, an external fluid transferring heat through natural convection, such as a stationary cooling pond, will experience changes in local thermophysical properties (including density) as the fluid heats or cools upon contact with the heat exchange surface. This behaviour is captured by the dimensionless Grashof number, which captures the balance of buoyancy to viscous forces in a flowing fluid:

$$(Equation 5.17) \quad Gr = \frac{D_0^3 \rho_f^2 \beta g \Delta T_o}{\mu_f^2}$$

where ΔT_o represents the absolute difference between the wall and bulk fluid (that is, $|T_{wall} - T_\infty|$) and the coefficient of thermal expansion (β) is a thermophysical property of the fluid, defined as

$\beta = \frac{(\partial V)}{\nu} \cdot P$ and representing the isobaric slope of molar volume with temperature (as may be determined from thermodynamic equations of state) on the coefficient of volumetric expansion (ν). As is discussed in chemical thermodynamics, the ideal gas equation of state produces a precise solution of $\beta = 1/T$. For systems with natural convection, a similar Nusselt-based solution strategy can be employed, using Equation 5.18 with empirical values for b and n available in Table 5.1.

$$(Equation 5.18) \quad Nu = b(\Pr \cdot Gr)_f^n$$

Table 5.1. Empirical parameters for Equation 5.18 based on the condition of natural convection, reproduced from McCabe, Smith and Harriott (7th Edition).

Convection Condition	Valid for $Pr \cdot Gr =$	b	n
Vertical plates and vertical cylinders	$10^4 - 10^9$	0.59	0.25
	$10^9 - 10^{12}$	0.13	0.333
Horizontal plates	$10^5 - 2 \cdot 10^7$	0.54	0.25
	$2 \cdot 10^7 - 3 \cdot 10^{10}$	0.14	0.333
Horizontal cylinders	$3 \cdot 10^5 - 3 \cdot 10^{10}$	0.27	0.25
	$\log(Pr \cdot Gr) > 4$	0.53	0.25

5.4 Complex Heat Transfer Rates

As practical unit operations typically require the consideration of multiple conductive and convective components, the overall heat transfer resistance and rate are of critical concern. An example of this behaviour is shown in Figure 5.7, where solid wall separates a warm fluid from a cold fluid (as is the case in heat exchange operations). The fluid temperature changes geometrically approaching either boundary layer (curves $T_g - T_e$ and $T_b - T_a$), where a convective heat transfer coefficient (h) is required for each of the fluid sides: interestingly, the fluid temperature within the boundary layer changes more radically, given the lower degrees of turbulence in this region (note that the convective heat transfer coefficient accounts for these contributions, captured by the curves $T_e - T_{wc}$ and $T_{wh} - T_b$). Finally, heat is conducted across the wall material, resulting in a linear relationship between T_{wc} and T_{wh} .

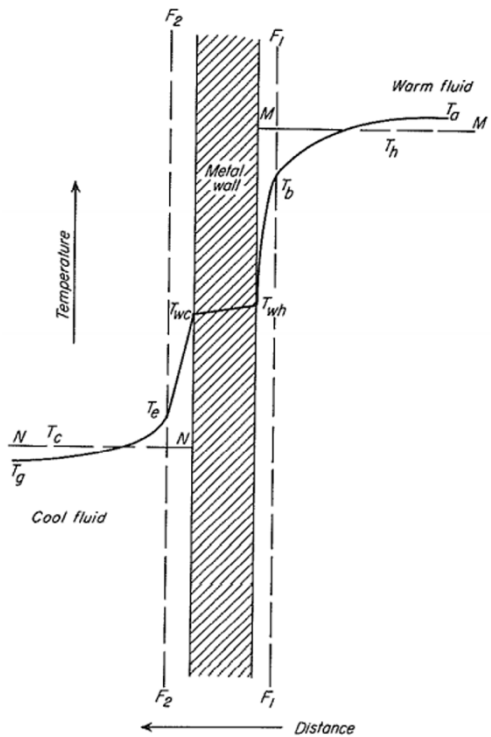


Figure 5.7. Example complex heat transfer relationship, where convection transfers energy from a warm fluid to the wall, conduction transfer energy across the solid wall, and convection again transfer energy from the wall to a cool fluid. Reproduced from McCabe, Smith and Harriott (7th Edition).

While the example in Figure 5.7 contains three discrete heat transfer relationships of interest, the solution strategy can, in fact, expand to account for *any* number of relevant contributions. Equation 5.19 demonstrates this approach, where *each of the individual heat transfer resistances are summed to determine the ultimate change in fluid temperature*:

$$\text{Equation (5.19)} \quad \Delta T = dq \cdot \left(\sum_m \frac{1}{h_m dA_m} + \sum_n \frac{x_n}{k_n dA_n} \right) = dq \left(\frac{1}{h_i dA_i} + \frac{x_w}{k_w dA_w} + \frac{1}{h_o dA_o} \right)$$

where the generalised solution involves summation of m and n convective (Equation 5.1) and conductive (Equation 5.8) heat transfer modes, respectively. The right-hand term illustrates the application to Figure 5.7, where h_i and h_o are solved individually using Nusselt-type correlations appropriate to the conditions of the warm and cool fluids. In this generalised approach of Equation 5.19, one length scale can be extracted from the bracketed term (that is, distance *in to the page* in Figure 5.7) to reveal the definition of an *overall heat transfer coefficient (U)*, which is similarly generalised to account for m and n convective and conductive modes, respectively:

$$\text{(Equation 5.20)} \quad U = \sum_m \sum_n \frac{1}{\frac{1}{h_m} + \frac{x_n}{k_n A_w}}$$

This definition of the overall heat transfer coefficient is often used in industrial flow simulation software, wherein the engineering will be required to determine the appropriate coefficient manually as an input to the simulation. Alternatively, where software may be able to estimate the coefficient from an internal library of thermophysical properties and correlations, Equation 5.20 provides the engineer with a useful means by which the integrity of the solution can be double-checked. Equation 5.20 deploys the definition of log-mean diameter for conduction through the wall (as shown in Equation 5.7), although it is noted that this treatment is only required for so-called

"thick walled" problems. When used manually, the overall heat transfer coefficient can be deployed in Equation 5.21, alongside the total surface area for heat transfer (A_T) and the averaged driving force for heat exchange (shown generically as ΔT , which will be discussed further in Section 6):

$$(Equation 5.21) \quad q_T = UA_T\Delta T$$



Example 5 -- Calculating the overall heat transfer coefficient, using Equation 5.20 (video from Microsoft Stream).

To provide context, typical values of thermal conductivity (k) in unit operations are on the order of 1 W/m/K for high-calibre insulation and 50 W/m/K for common metal alloys used in construction, as shown in Table 5.2: it should be noted that these are indicative values only, where formal references (e.g. peer-reviewed research papers or repositories thereof) should be employed. Convective heat transfer coefficients vary both with the fluid (i.e. thermodynamic) and turbulence in the system, with typical ranges shown in Table 5.3.

Table 5.2. Typical thermal conductivities of common materials.

Material	k (W/m/K)
Copper	300
Aluminium	200
Steel	50
Cement	1.05
Fiberglass	0.1 to 0.4
PVC	0.19
Polystyrene	0.16
Rubber	0.075-0.1
Glass fibre	0.04

Polyurethane foam 0.024-0.035

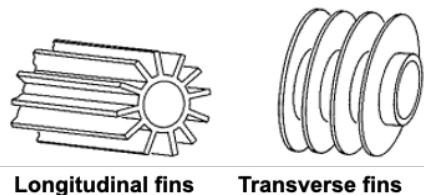
Table 5.3. Common ranges for convective heat transfer coefficients.

Scenario	Range h (W/m/m/K)
Natural convection of gas	1-2
Forced convection of gas	10-50
Natural convection of liquid	25-500
Forced convection of liquid	900-2500
Forced convection of liquid + condensation of a vapour phase	1000-4000

A comparison of Equation 5.20 with Tables 5.2 and 5.3 reveals an important heuristic: *conduction tends to be the rate-limiting step in heat exchange*. In most circumstances (with copper as a notable exception), the degree of "resistance" ascribed to conduction will be more than 95% of the overall resistance, where it is not uncommon to see this value exceed 99%. As such, copper is a common material used to improve overall heat transfer rates in complex systems (e.g. in professional cookware).

5.5 Extended Heat Transfer Surfaces

As demonstrated by the generalised heat transfer rate (Equation 5.21), the engineer is effectively provided with three control levers: the heat transfer coefficient, which varies primarily with the conditions of fluid mechanics; the surface area of heat exchange; and the driving force in the operation, either as a direct or corrected temperature difference (as will be discussed in later sections). As such, the modification of heat transfer area presents one opportunity through which the engineer can improve the efficiency of the operation while minimising additional cost. Examples of such extended surfaces (commonly called "fins") are shown in Figure 5.8.



Longitudinal fins Transverse fins

Figure 5.8. Example of "fins" that can be used to extend the heat transfer surface, both of which are orientated with flow from left-to-right across the page. Reproduced from McCabe, Smith and Harriott (7th Edition).

The orientation of fins relative to flow -- with bounding conditions of longitudinal and transverse -- provide an opportunity for the engineer to utilise the thermal conductivity of the material to more readily exchange heat with fluid on the exterior of the fin surface. The characterisation of a basic fin depends on both the height of the fin (and, thereby, its surface area) and the local temperature within this region, as shown in Figure 5.9.

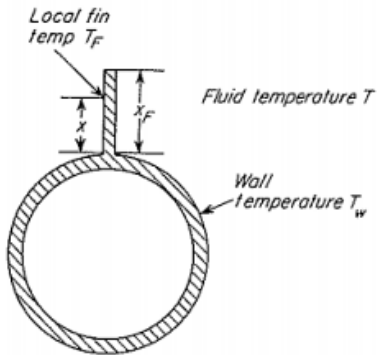


Figure 5.9. Relevant characteristics of a basic fin, the temperature of which (T_F) will vary along its distance from the wall. Reproduced from McCabe, Smith and Harriott (7th Edition).

At steady-state, the fin temperature will vary between the bounding conditions of T_w and T , as illustrated in Figure 5.9. The ratio of these temperature differences is captured by the fin efficiency (η_f), which utilises the spatially averaged temperature within the fin ($T_{F,avg}$):

$$(Equation 5.22) \quad \eta_f = \frac{T - T_{F,avg}}{T - T_w}$$

The spatial dimension of the fins are captured through a single dimensionality term (a_F), which varies with the fin perimeter (L_p), cross-sectional area (S), alongside the fin material's thermal conductivity (k_m) and convective heat transfer coefficient at the exterior of the fin (h_o):

$$(Equation 5.22) \quad a_F = \sqrt{\frac{h_o L_p}{S k_m}}$$

Both the fin dimensionality and efficiency can be combined with the base heat transfer area (A_b) *without* the fin present, and deployed in an overall heat transfer relationship:

$$(Equation 5.23) \quad U = \frac{1}{\frac{1}{h_i} + \frac{1}{h_o(\eta_f a_F + A_b)}}$$

which, for example purposes, only considers internal and external convection. Thus, the engineer is presented with an opportunity to increase the efficiency of heat transfer, by appropriately selecting the fin material and the height-to-surface area ratio. Fins can be found in a variety of unit operations, and are particularly useful when ambient fluids exist on one side of the heat transfer relationship. For example, they can commonly be found in the outdoor unit of household reverse-cycle air conditioning systems, or atop microchips in laptop/desktop computers with moderate processing power.

Heat exchangers are one of the core unit operations deployed in Chemical Engineering, as both stand-alone operations (e.g. within refrigeration cycles) and as complements to operations with chemical reactions or mass transfer. This section provides an overview of four common heat exchanger types: (i) shell and tube; (ii) double-pipe; (iii) condensers; (iv) boilers or evaporators. As highlighted in the final entry of Table 5.3, heat exchangers where a phase change takes place -- such as the condensation of steam -- provide an additional performance gain when compared with typical liquid convection, wherein condensers and boilers require are treated in detail below.

6.1 Shell and Tube Heat Exchangers

A basic shell-and-tube (S-T) heat exchanger is shown in Figure 6.1, where the first (typically cooler) fluid enters the vessel at the bottom left of the illustration and flows through pipes that span the length of the unit operation (the "tube side") before exiting on the top-left of the illustration.

Volumes on either side of the tubes ("channels" labelled in Figure 6.1) enable the tube-side fluid to reach a homogeneous temperature at the entry to each tube, and prior to exiting the unit operation (where it may be used in a further operation that could be sensitive to temperature fluctuations): when viewed from the cross-section, these tubes are typically arranged in either a triangle or square configuration (referred to as the "pitch") to enable the efficient flow of fluids around them. A second fluid (typically warmer) enters from the central position atop the unit operation flows *across* (normal to) the tubes in the body of the exchanger (the "shell side"). This design enables the engineer to control the flowing conditions, and thus the relevant convective heat transfer coefficients, that will ultimately govern the effectiveness of heat transfer.

Shell-and-tube heat exchangers are sufficiently common in the process engineering field, such that their design and safety standards are prescribed through the Tubular Exchanger Manufacturers Association (TEMA) and ASME-API Unfired Pressure Vessel Code, respectively. The naming of shell-and-tube exchangers follows a two-number convention (such as the "1-1 Exchanger" shown in Figure 6.1), where the first and second numbers respectively indicate the number of "passes" on the shell and tube sides, respectively.

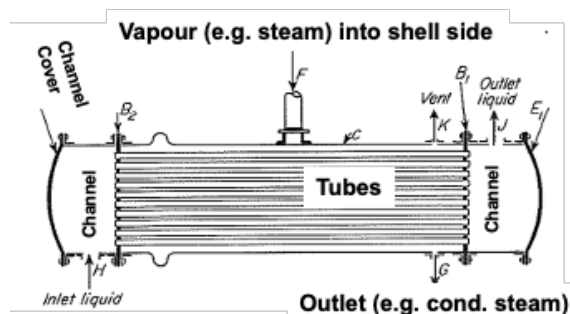


Figure 6.1. Example of shell-and-tube heat exchanger, where liquid is warmed through contact with steam. Adapted from McCabe, Smith and Harriott (7th Edition).

While the absolute temperature of heat transfer fluids remains important to their thermophysical properties (e.g. heat capacity changing with temperature), the unit operations themselves are typically characterised by the *approach* temperatures at steady-state. As shown by example in Figure 6.2 (corresponding to the 1-1 Exchanger in Figure 6.1), the temperature of the condensing vapour will retain a constant value of T_h as it is undergoing a phase change. The inlet liquid is initially at a temperature of T_{ca} , which will warm to a final temperature of T_{cb} through continued exposure with the condensing steam. Thus, the *initial* approach temperature (ΔT_1) represents the maximal difference between either of the two fluid temperatures, while the *final* approach temperature (ΔT_2) represents the minimal difference at the end of the unit operation. As the warming fluid follows a logarithmic behaviour (shown in Figure 6.2), characterisation of an *average* approach temperature ($\overline{\Delta T}_L$) thus requires a similar log-mean treatment as described in Section 5 for conduction through thick-walled pipes. The definition of this log-mean approach temperature is shown in Equation 6.1, and is defined exclusively by the two approach temperatures (ΔT_1 and ΔT_2).

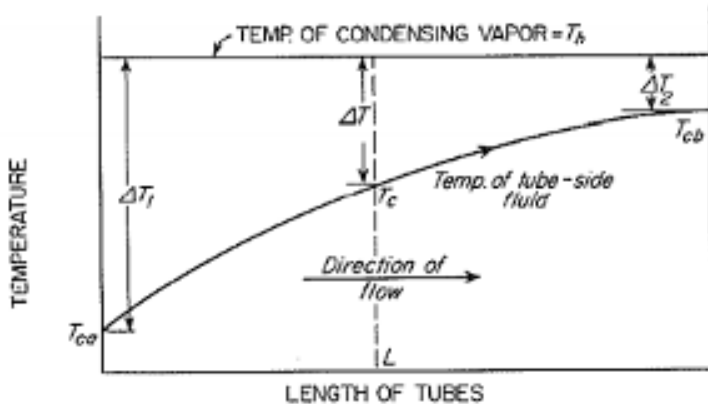


Figure 6.2. Illustration of the changing approach temperature for a 1-1 shell-and-tube exchanger with condensing steam on the shell side. Reproduced from McCabe, Smith and Harriott (7th Edition).

$$\overline{\Delta T_L} = \frac{\Delta T_2 - \Delta T_1}{\ln \frac{\Delta T_2}{\Delta T_1}}$$

Equation 6.1 is often referred to as the Log-Mean Temperature Difference (LMTD) method, and can be derived from first principles by considering the differential expression in Equation 5.5 with a variable driving force (ΔT). Importantly, the result of the LMTD method provides an appropriately averaged driving force for heat exchange: it is therefore deployed in the overall heat transfer rate equation shown in Equation 5.21, with knowledge of the average heat transfer coefficient for the unit operation (U) and the surface area of heat transfer (A_T). It should be noted that the LMTD approach should not be used when U changes significantly over the unit operation.

While the use of a log-mean temperature difference is not strictly required for 1-1 exchangers, as are common in refrigeration systems where T_h is the ambient (e.g. household) temperature, it is required (with an appropriate correction) to characterise both *multi-pass* exchangers and, depending on the circumstance, where fluid(s) are undergoing a chemical reaction. While chemical reactions are not strictly treated in this curriculum, the consideration of multi-pass exchangers is an important domain of shell-and-tube design, as they can provide more efficient heat exchange. An example of multi-pass exchangers is shown in Figure 6.3, where the top and bottom panels illustrate the flow of warm (red) and cool (blue) fluids through a 1-2 exchanger and 2-4 exchanger, respectively.

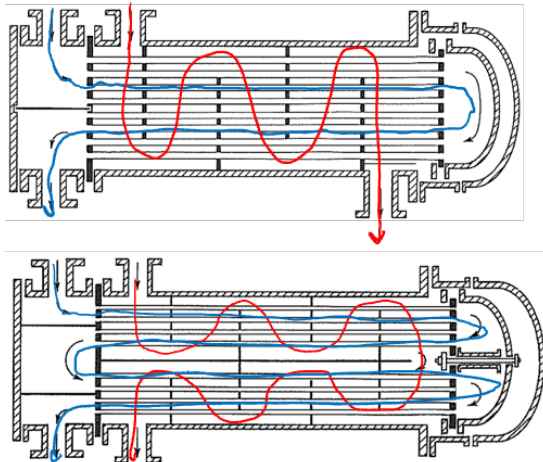


Figure 6.3. Illustration of warm (red) and cool (blue) fluids flowing through 1-2 (top) and 2-4 (bottom) multipass heat exchangers, adapted from McCabe, Smith and Harriott (7th Edition).

For the 1-2 exchanger pictured, vertical baffles are employed (indicated in Figure 6.3 by vertical black lines) to direct the warmer, tube-side fluid across the tubes in multiple passes. The use of these baffles improves overall heat transfer, by prevent stagnation and increasing the turbulence of shell-side fluids. The 1-2 designation indicates that the shell-side fluid retains a singular pass through the vessel, while there are two tube-side passes: this can be observed by tracing the blue curve (Figure 6.3) from the inlet at the top left-hand port, where fluids first flow through one tube before transiting through a *second* set of tubes on the bottom. Importantly, the introduction of multiple passes in the tube side typically results in a nearly three-fold increase in the heat transfer coefficient, thereby significantly increasing the effectiveness of the unit operation without significantly increasing the materials required. Similarly, the 2-4 exchanger pictured retains the same general baffle structure, but the tube side has been split in to *four passes* (as pictured from the entry point on the top, left-hand port). The four sets of tubes therefore require the addition of a longitudinal baffle that forces the warm fluid in to two "halves" of the operation, as pictured by the red flow-path in Figure 6.3: this configuration can provide an even *higher* overall heat transfer coefficient than for a 1-2 exchanger, the magnitude of which depends on the solid materials employed, number of tubes, and configuration of baffles.

As the number of tube passes increases, so too does the number of approach temperatures that must be considered. An generic set of approach temperatures is shown in Figure 6.4, where the shell is assumed to contain the warmer fluid. Importantly, the introduction of the intermediate fluid temperature (T_{ci}) represents the extent to which the first tube pass is able to warm fluids, which then experience the second pass. This treatment can be extended for a system with multiple *shell* passes (dashed curves, right-hand panel of Figure 6.4), where four tube passes result in two intermediate temperatures.

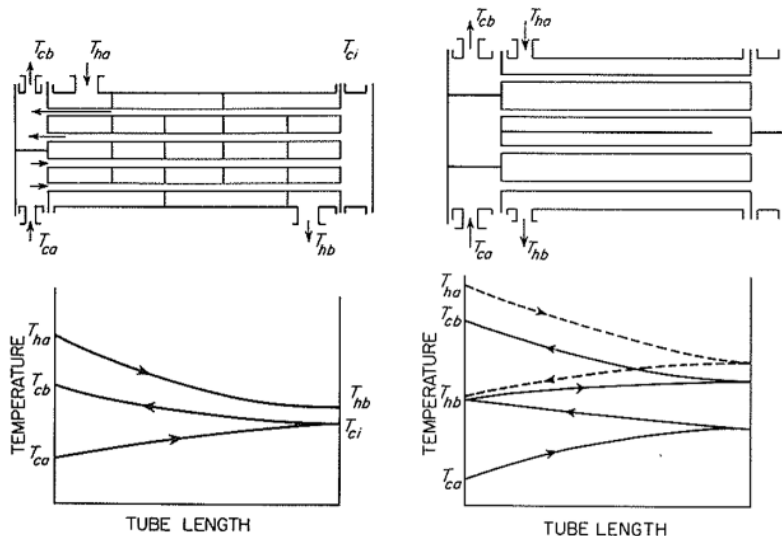


Figure 6.4. Illustration of temperature profiles in multi-pass exchangers with warm fluid on the shell side: (left panel) a 1-2 exchanger, and (right panel) a 2-4 exchanger. Reproduced from McCabe, Smith and Harriott (7th Edition).

When using a multi-pass exchanger, the LMTD driving force ($\overline{\Delta T}_L$) must be multiplied by a correction factor F_G :

$$(Equation 6.2) F_G = \frac{(Z^2+1)^{1/2} \cdot \ln\left(\frac{1-\eta_H}{1-Z\eta_H}\right)}{(Z-1) \ln\left(\frac{2-\eta_H[Z+1-(Z^2+1)^{1/2}]}{2-\eta_H[Z+1+(Z^2+1)^{1/2}]}\right)}$$

where the factor Z represents the ratio of the true temperature decrease on the true temperature gain, and the factor η_H is the *effectiveness* of the heating process: that is, $Z = \frac{T_{ha}-T_{hb}}{T_{cb}-T_{ca}}$ and $\eta_H = \frac{T_{cb}-T_{ca}}{T_{ha}-T_{ca}}$. Although Equation 6.2 was derived for a system with two tube passes (note the temperature definitions of Z and η_H compare with Figure 6.4), it can reasonably be applied to other multi-pass exchangers with a limiting condition of $F_G > 0.8$. Practically, the factor Z can equivalently be defined by the ratio of the product of mass flow rate and heat capacity, for the cool fluid on the warm fluid.

Calculating the overall heat transfer coefficient in shell-and-tube systems follows the same approach as in Equation 5.21, requiring knowledge of the overall heat transfer coefficient, total heat exchange surface area, and LMTD driving force. While flow through the tube side is reasonably-straight forward (as the tubes themselves are either laminar or turbulent *ducts*, with well-defined Nusselt correlations), and conduction through the tube wall varies with material selection and wall thickness, the Donohue equation is often used to approximate the convective heat transfer coefficient for the flow in the shell side:

$$(Equation 6.3) \frac{h_o D_o}{k} = 0.2 \left(\frac{D_o G_e}{\mu} \right)^{0.6} \left(\frac{c_p \mu}{k} \right)^{0.33} \left(\frac{\mu}{\mu_w} \right)^{0.14}$$

which contains four empirically-regressed factors applied to the thermophysical properties of the shell-side fluid, some of which are compared to reference values (e.g. the viscosity of water, or μ_w), and the term $G_e = \sqrt{G_b G_c}$ represents the weighted average mass velocity (with units of units of mass per area per time) of fluid parallel with the tubes and is defined by the mass velocity of fluid

parallel with the tubes (Equation 6.4) and mass velocity of fluid in cross-flow with the tubes (Equation 6.5).

$$(Equation\ 6.4)\ G_b = \frac{\dot{m}}{f_b \frac{\pi D_s^2}{4} - N_b \frac{\pi D_o^2}{4}}$$

$$(Equation\ 6.5)\ G_c = \frac{\dot{m}}{P D_s \left(1 - \frac{D_o}{p}\right)}$$

In these expressions, f_b represents the fraction of cross-sectional area in the shell that is occupied by the baffle window (e.g. 25 per cent baffles result in $f_b = 0.1955$), D_s and D_o respectively represent the internal shell and external tube diameters, N_b represents the number of tubes within the baffle window, P represents the baffle pitch (with units of length), and p is the centre-to-centre distance between tubes within the baffle window. In most cases, manufacturers will provide the geometry parameters required to solve Equations 6.3 through 6.5, which allows the engineer to consider the impact of varying mass flow rate (\dot{m}) on the heat transfer coefficient of the shell side, noting that the Donohue equation tends to provide conservative (i.e. low) estimates.

For a 1-1 exchanger where *ambient (outside)* air flows across a single-pass tube bundle, Equation 6.6 provides a basis to estimate the external convective heat transfer coefficient, which similarly follows a Nusselt-type correlation and includes the use of an arrangement factor (F_a) as shown in Table 6.1. Such external (i.e. outdoor) heat exchangers provide the opportunity to use natural convection across a tube bundle containing the target fluid. Table 6.1 illustrates the impact laminar/transition (i.e. < 1) and turbulent (i.e. > 1) flow of the external fluid flow on the arrangement factor.

$$(Equation\ 6.6)\ \frac{h_o D_o}{k} = 0.287 \left(\frac{D_o G}{\mu}\right)^{0.61} \left(\frac{c_p \mu}{k}\right)^{0.33} F_a$$

Table 6.1. Arrangement factors (F_a) for crossflow heat exchangers with a square pitch.
Reproduced from McCabe, Smith and Harriott (7th Edition).

p/D_o	$Re = 2,000$	$Re = 8,000$	$Re = 20,000$	$Re = 40,000$
1.25	0.85	0.92	1.03	1.02
1.5	0.94	0.90	1.06	1.04
2.0	0.95	0.85	1.05	1.02

As engineers are increasingly concerned with the impact of unit operations on the natural environment -- which itself can be considered as the amalgam of ecology, geology (soil), marine science, and climate -- the elimination of unnecessary process equipment or synthetic fluids is an important consideration. One such advance can be obtained from heat exchange operations that can make use of ambient air (deploying Equation 6.6 and Table 6.1), or naturally-occurring water sources. Such air-cooling systems are typically designed with horizontal bundles of tubes carrying warm process fluids, the surface areas of which can be extended through the use of fins (Section 6.4). In common applications, tubes of 1" (25 mm) diameter are employed with lengths between 8 and 30 ft. (2.4 to 9 m), where the use of fins can extend heat transfer areas up to 500 m² in order to cool process fluids up to 673 K.

6.3 Double-Pipe Heat Exchangers

Particularly when temperature maintenance or modification is used to complement a second unit operation (i.e. focussed on mass transfer or reacting systems), double-pipe heat exchangers provide the engineer with a convenient basis. An example is shown in Figure 6.5, with one fluid flowing on the annular side of a jacket that transfers heat to or from a second fluid flowing inside of an internal cylindrical pipe. While the example in Figure 6.5 includes curvature in the pipe network, double-pipe (or jacketed) heat exchangers can be deployed horizontally.

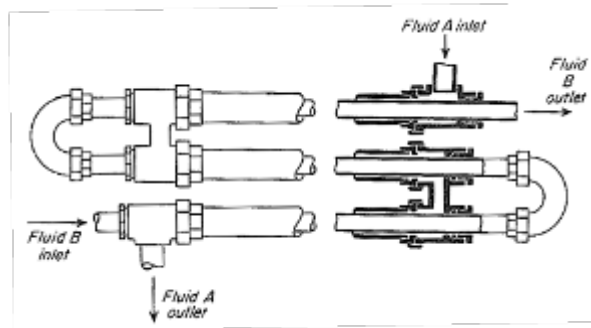


Figure 6.5. Illustration of double-pipe or jacketed heat exchanger, enabling heat transfer between two fluids (A and B). Reproduced from McCabe, Smith and Harriott (7th Edition).

As the flow configuration in a double-pipe heat exchanger is based around fluid flowing along a cylindrical pipe with additional flow inside the pipe, the basic Nusselt correlations shown in Section 5 can be used to estimate the convective heat transfer coefficients on both sides of the system: with knowledge of the inner material (e.g. stainless steel or copper), the overall heat transfer coefficient for the system can be readily calculated as a function of flow rate. Critically, double-pipe exchangers can be configured with one fluid flowing in the same direction as another ("parallel flow") or one fluid flowing in an opposite direction to the other ("counter-current flow"). Although there are some notable exceptions, counter-current flow is typically used, because it provides better constancy in the approach temperatures at the beginning and end of the exchange network. An example of this behaviour is shown in Figure 6.6, where a comparison with the LMTD definition (Equation 6.1) illustrates the value of counter-current exchange.

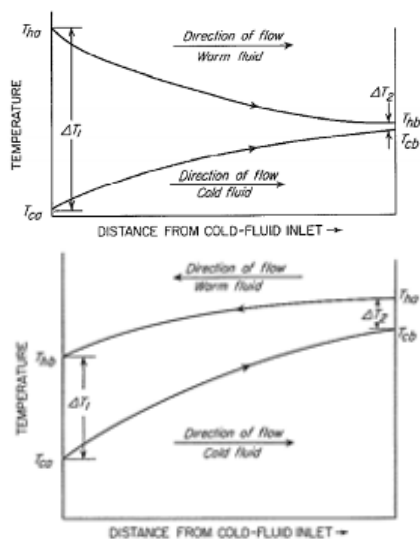
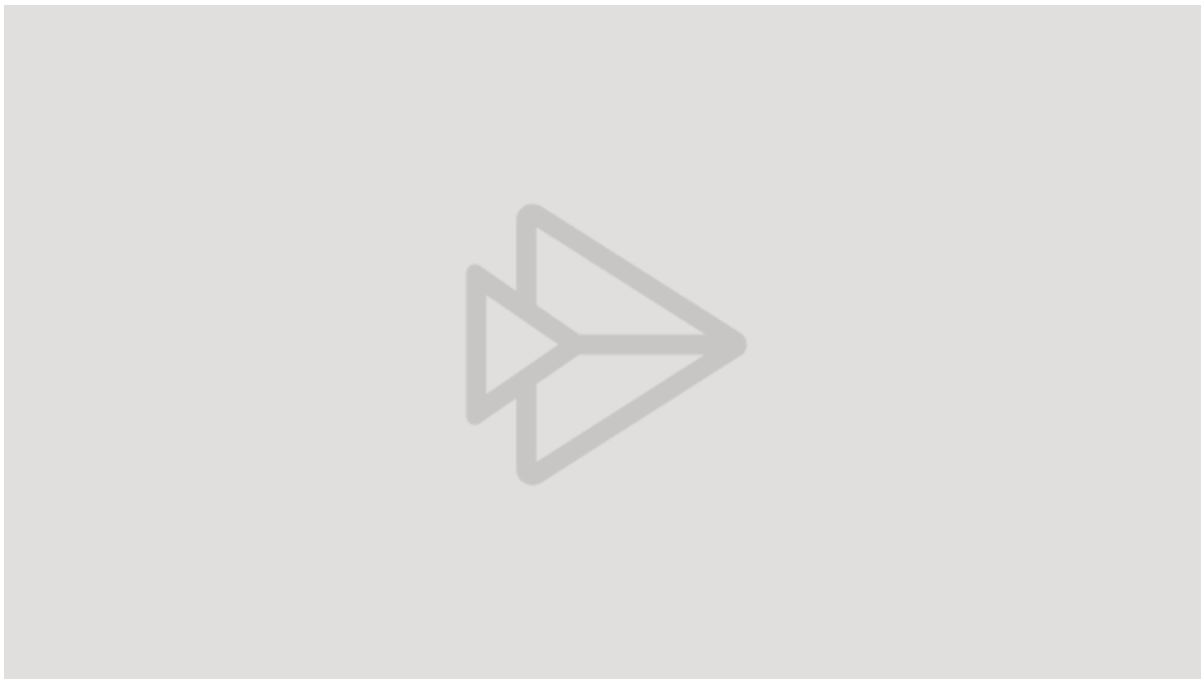


Figure 6.6. Illustration of approach temperatures in a parallel (or co-current) double-pipe heat exchanger (top), and a counter-current configuration (bottom). Reproduced from McCabe, Smith and Harriott (7th Edition).



[Example 6 -- Performance of a jacketed single-pass heat exchanger \(video from Microsoft Stream\).](#)

6.3 Plate-Type Heat Exchangers

While plate type exchangers receive significant treatment in other curricula (such as Heat and Mass Transfer), they will only be considered here from the role of the relevant Nusselt-type correlation, which is provided in Equation 6.7. The typically high surface areas in plate-type heat exchangers utilise the lessons of extended surfaces ("fins") in improving the surface area for heat transfer: this allows the heat exchanger to achieve an appreciably similar convective heat transfer coefficient to shell-and-tube (Section 6.1) or double-pipe (Section 6.2) exchangers, which can operate at much higher velocities. Typically, liquid-liquid plate-type heat exchangers should operate with low fluid velocities (e.g. 0.2 to 1.0 m/s), resulting in Reynolds numbers of less than 2,100 when the small space between plates is considered. The extended surfaces within these exchangers continue to produce eddies even at Reynolds numbers in the low hundreds:

$$(Equation 6.7) \frac{hD_e}{k} = 0.37 \cdot Re^{0.67} Pr^{0.33}$$

where the equivalent diameter (D_e) is taken to be four times the hydraulic radius, or typically twice the spacing between the plates. Plate-type exchangers provide a performance limit approaching true counter-flow (as described above), wherein LMTD correction factors are near unity. As such, they are commonly deployed in industries where strict control of internal fluid temperatures are required, including food processing and dairy.

6.4 Heat Transfer Units

Although not deployed heavily in this treatment of heat transfer, there exists a symmetry between heat and mass transfer operations that will become relevant in Sections 8 through 11. The number of so-called "heat transfer units" (N_H) in an operation is given by Equation 6.8:

$$(Equation 6.8) \quad N_H = \frac{T_{cb} - T_{ca}}{F_G \cdot \overline{\Delta T_L}} = \frac{UA}{\dot{m}_c c_{p,c}}$$

where the numerator represents the temperature gained by the cool fluid (or equivalently lost by the warm fluid), relative to the LMTD driving force (noting the multi-pass correction factor F_G is not always required): manipulation of the LMTD definition can provide a second, equivalent definition of N_H shown on the right-hand side of the expression. The number of transfer units provides the engineer with a basis for *scaling* a heat exchange design for different applications, without re-considering every detail. For example, a water cooler that uses ambient air for household applications may contain 4 transfer units: if the application were to be doubled in scale, such as for a small office building, then the engineer could simply consider how many *additional* transfer units would be required. Similarly, Equation 6.9 provides the engineer with an efficient means of determining the *impact* of changing process conditions (e.g. a sudden change in T_{ca}) on the number of transfer units present.

Critically -- as will emerge again in the more complex discussion of mass transfer operations -- the *number* of (heat) transfer units is contextualised by the *effectiveness* of the transfer units (ϵ). In heat transfer, this effectiveness is defined by the capacity ratio of the two fluids:

$$(Equation 6.9) \quad \epsilon = \frac{T_{cb} - T_{ca}}{T_{ha} - T_{ca}} = \frac{N_H}{1 + N_H}$$

which functionally represents the actual change in temperature (of the cold fluid) on the *potential* change in temperature between the fluids, and can equivalently be related to the number of heat transfer units. For the above example with 4 heat transfer units in a household application, the effectiveness is 80%, meaning the cold fluid is brought to about 4/5 of the temperature of the warm fluid. Importantly, as is shown in the second equality of Equation 6.8, the number of heat transfer units, and subsequently the *effectiveness* of the units, can be related to the *thermal capacity* of the fluids: that is, the ratio of the lower-capacity fluid on that of the higher capacity fluid, where fluid capacity is determined by the product of mass flowrate and heat capacity (which is assumed not to vary).

Functionally, this metaphor provides a convenient analogue for complex mass transfer operations, wherein each "mass transfer unit" is paired against its effectiveness, in order to determine the total *scale* of the option that is required. Put another way, an operation seeking to transfer some finite amount of mass (that is, number of molecules) between two phases is functionally constrained by the number of contact points (as may be exemplified by the single-stage "flash vessel" discussed in Section 1) and the efficiency of that contact point (e.g. with a limited residence time, turbulent flow will transfer mass more efficiently than laminar flow).

While Section 6 considered heat exchange between fluids without a phase change present -- that is, where only *sensible* heat is transferred between the phases -- advanced heat transfer operations can make use of *latent* heat, where one or more fluids is changing in phase. As the condensing (vapour-to-liquid transition) or evaporating (liquid-to-vapour transition) phase may contain any number of components, the *nature* of the phase change process being deployed is important to consider. Basic systems may deploy a single component, such as steam (i.e. water), ethylene glycol, glycerine, nitrobenzene, or isoheptane, amongst others: such systems are often easier for the engineer to design, as comprehensive reference tables or calculations are readily accessible for thermophysical properties (e.g. the steam tables).

Condensing systems are generally considered to be either *dropwise* or *film-type*. In dropwise condensation, the heterogeneous nucleation of droplets occurs continuously, at the point of contact between the (cooling) vapour and a (cold) heat transfer surface: consider the effect of placing a cold glass of iced tea outside on a humid summer day, where individual droplets of water will condense from the warm air. Conversely, film-type condensation occurs with more effective heat transfer and where there is a larger extent of condensable content in the vapour phase: one might consider what would happen if droplets were forming so rapidly as to generate a flowing film on the heat transfer surface. Consequently, the treatment of film-type condensation requires the engineer to understand so-called "flowing film" behaviour, where a thin liquid film separates the heat transfer surface (typically a cooled solid) from the warmer vapour phase. The momentum of this fluid film is controlled by gravity, wherein its "thin" nature typically invokes the assumption that it is at a constant temperature defined by the interface of (i) the wall and (ii) vapour within the flowing boundary layer. As gravity action tends to produce slowly flowing films, heat is transferred through a combination of conduction and convection, where the *effective* heat transfer coefficient (h_x) is determined by the ratio of the thermal conductivity (k_f) on the film thickness (δ):

$$(Equation 7.1) \quad h_x = \frac{k_f}{\delta}$$

Proportionally, the film thickness is between 100 and 1000 times smaller than the diameter of the vessel (e.g. the tube) in which the fluid is condensing. When film-type condensation occurs, the heat transfer surface is further said to be "wetted," where the entire surface is assumed to be in contact with the film: conversely, dropwise condensation occurs on "non-wetted" surfaces, where the surface free energy of the solid (contextualised by *both* the vapour and liquid phases) controls the shape and ultimate size of droplets that can form. While Equation 7.1 can be readily estimated with knowledge of the liquid's thermal conductivity and an assumption of condensing tube diameter (e.g. 10 mm), the effective heat transfer coefficient for dropwise condensation tends to have an upper limit of around 115 W/m²/K.

Figure 7.1 provides an illustration of the local convective heat transfer coefficient, alongside film thickness, for a falling liquid film as a function of the distance from the top of the tube on which the liquid is condensing. The example illustrates that the local heat transfer coefficient varies inversely with the film thickness (as would be expected). This relationship can be generalised in Equation 7.2 as a function of film viscosity and density (μ_f and ρ_f , respectively), alongside the liquid loading in the system (Γ , or the mass flow rate of liquid per unit length of the periphery).

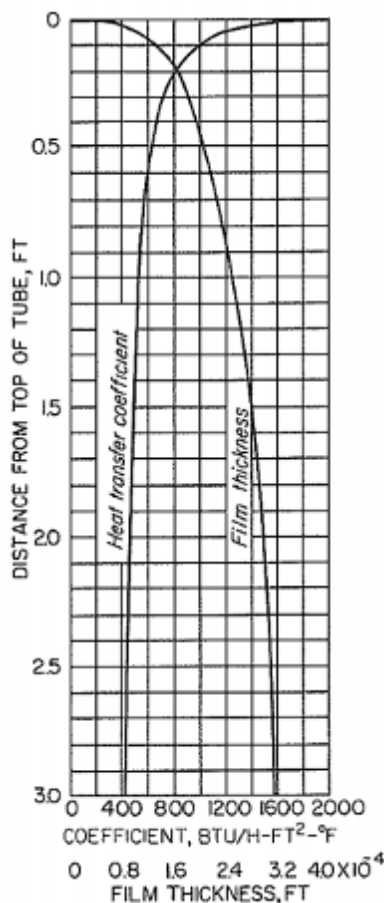


Figure 7.1. Example of film thickness and heat transfer coefficient variation for a condensing film, drawn downward by gravity. Reproduced from McCabe, Smith and Harriott (7th Edition).

$$(Equation 7.2) \quad \delta = \left(\frac{3\Gamma\mu_f}{\rho_f^2 g} \right)^{\frac{1}{3}}$$

In calculating the steady-state film thickness, the engineer can use a thermodynamic relationship (e.g. pressure-enthalpy curves) to determine the equilibrium balance between vapour and liquid for local conditions. Equation 7.2 therefore provides a similar curvature to the example shown in Figure 7.1, whilst considering local fluid properties. When the film thickness has been established, the resultant convective heat transfer coefficient can be estimated through the generalised correlation in Equation 7.3:

$$(Equation 7.3) \quad h = \frac{4}{3} k_f \left(\frac{\rho_f^2 g}{3\Gamma\mu_f} \right)^{\frac{1}{3}}$$

where, notably, the thermal conductivity of the fluid (k_f) becomes relevant. When the condensing fluid is of a pure species, as may be the case in steam, the condensate loading term (Γ) can further be expanded and simplified based on its thermodynamic origin for condensation along *vertical tubes or cylinders*:

$$(Equation 7.4) h = 0.943 \left(\frac{k_f^3 \rho_f^2 g \lambda}{\Delta T_o L \mu_f} \right)^{1/3}$$

where λ represents the latent heat of vaporization (e.g. as may be deduced from the Clapeyron equation) and ΔT_o considers the temperature difference between the condensing vapour and the heat exchange surface for the total length of tube L . Equations 7.3 and 7.4 provide a similar relational form to the example shown in Figure 7.1, enabling the engineer to determine the steady-state heat transfer coefficient for the condensing liquid film, which may be combined with conduction and (internal) convection resistances to determine the overall heat transfer coefficient (U) for deployment in Equation 5.21.

Equation 7.5 follows a similar form to Equation 7.4, but is suited for flow across a horizontal bundle of N tubes with a condensing species where the latent heat of phase change (λ) can be readily determined:

$$(Equation 7.5) h = 0.729 \left(\frac{k_f^3 \rho_f^2 g \lambda}{N \Delta T_o D_o \mu_f} \right)^{1/4}$$

In more complex condensing vapour systems, a Nusselt-type correlation (Equation 7.6) can also be employed to predict the local heat transfer coefficient, based on the exit Reynolds and Prandtl numbers for the system. Notably, this correlation does not follow the precise use of the Nusselt number, as again the thermal conductivity of fluid in the falling film contributes to the overall solution. In designing systems with condensing vapours, a trial-and-error approach is often used by the engineer: that is, the rate of condensation (which dictates the ultimate thickness of the condensing film) is affected by, and further affects, the Reynolds and Prandtl numbers of the out-flowing vapour.

$$(Equation 7.5) \frac{h}{k_f} \left(\frac{\mu_f^2}{\rho_f^2 g} \right)^{\frac{1}{3}} = \sqrt{Re^{-0.44} + (5.82 \cdot 10^{-6}) Re^{0.8} Pr^{1.3}}$$

In the limit that the condensation of a superheated vapour is required -- that is, the pressure and temperature conditions of the vapour are outside the two-phase VLE region -- the condensation operation must be considered as a two-step process: first, the vapour is cooled in a *de-superheater* (i.e. a basic heat exchanger) before then entering a *condenser*.

7.1 Basic Condensers

The basic shell-and-tube heat exchange design discussed in Section 6.2 is commonly employed for condensation, with single-pass and two-pass example configurations shown in Figure 7.2. In both designs, the heat exchange fluids (that is, the condensing vapour and the *coolant*, which removes the latent heat of condensation) are not in physical contact, but instead the heat exchange is conducted through the tube bundle material: such operations are differentiated from *contact condensers* discussed below, wherein both fluids are in physical contact. In the single-pass example shown in Figure 7.2 (left panel), the coolant fluid (typically water) flows through all tubes (labelled

"A") between the inlet and exit reservoirs (D_2 and D_1 , respectively), and the condensing fluid enters from position "F" on the shell to be removed as a liquid ("condensate") at position "G." Basic (1-1 Exchange) condensers are practically limited in scale, where excessive heat exchange demands can require such a large number of tubes and/or such a low velocity within the tubes so as to render the unit sub-economic. This can be remedied by employing a multi-pass design, an example of which is shown in the right-hand panel of Figure 7.2: importantly, the correction factor (F_G) for the LMTD driving force is *not required for condensers*, as the shell side will remain at constant temperature during phase change. In this example, the specification of a "floating head" indicates that one side of the tube bundle is not structurally connected to the wall, allowing it to move or "float" as changing temperatures (e.g. during start-up or shut-down) can result in differential thermal expansion between the solid materials. Without such a specification, the severe expansion or contraction potential of the tube material (relative to the shell material) can result in the tubes buckling and/or pulling loose from tube sheets, thereby damaging the unit operation.

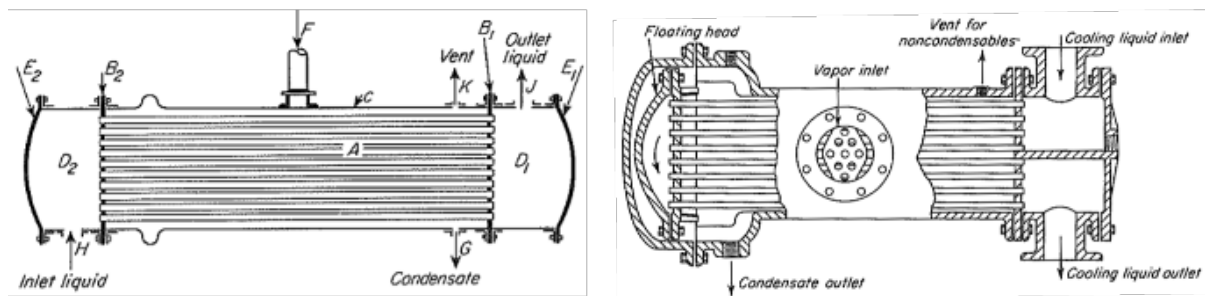


Figure 7.2. Example design for shell-and-tube heat exchanger, deployed as (left) a single-pass condenser and (right) a two-pass floating-head condenser. Reproduced from McCabe, Smith and Harriott (7th Edition).



[Example 7 -- Shell and tube heat exchanger \(video from Microsoft Stream\).](#)

Similar to the shell-and-tube design shown in Figure 7.2, *dehumidifiers* are deployed in a vertical orientation for the purpose of removing dilute water from air ("relative humidity"). An example dehumidifier is shown in Figure 7.3, where liquid water or coolant flows through the shell side, to remove humidity (water) from vapour drawn in at the top of the unit operation: similar to horizontal

shell-and-tube systems, a floating head is employed at the bottom of the unit operation to prevent damage to the system, where a final liquid knock-out stage is pictured at the bottom of the process. As relative humidity (that is, the equilibrium water content *soluble* in air, typically taken to be 79 mol% nitrogen and 21 mol% oxygen) decreases directly with temperature, the vapour drawn in the top of the operation is cooled to a point where a majority of the water (constituting the initial relative humidity) can no longer remain dissolved in the vapour phase, resulting in condensation along the interior of the tubes.

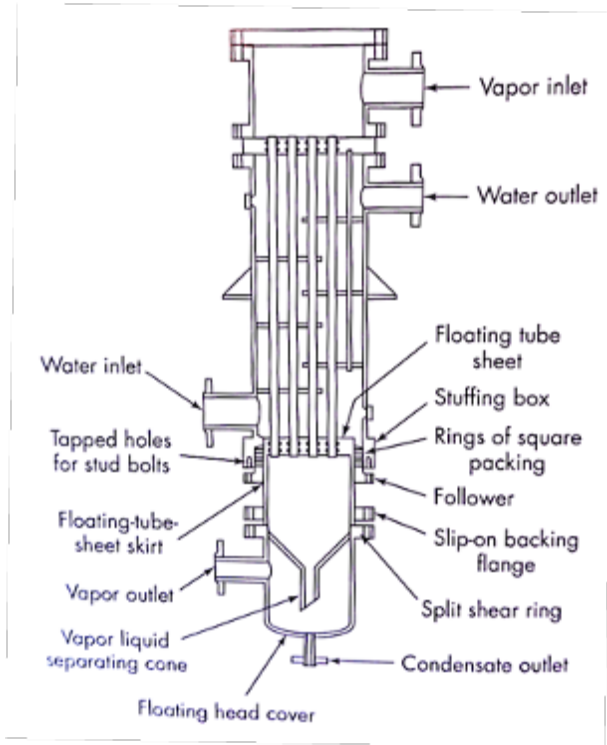


Figure 7.3. Example dehumidifier design used to remove dilute quantities of water from air, where heat is exchanged with liquid water (pictured) or a coolant flowing through the shell side. Reproduced from McCabe, Smith and Harriott (7th Edition).

In household applications, water removed from the "condensate outlet" can be recycled and used on the shell side of the dehumidifier: prior to entering the shell side, it is typically cooled to well below ambient (i.e. room) temperature through a thermoelectric (Peltier) element. As such, the degree of cooling, and thus the ultimate amount of relative humidity that can be removed from the vapour, is directly proportional to the electricity drawn from the elements. The vertical orientation of this design encourages the sweep of fluids through the shell and tube sides, thereby preventing stagnation pockets of the vapour.



Example 8 -- Log-mean temperature difference example (video from [Microsoft Stream](#)).

Apart from shell-and-tube/dehumidifier applications, *contact condensers* are typically smaller, and less expensive (per volume condensed), operations that function by direct physical contact between a coolant and the condensing vapour. An example design is shown in Figure 7.4, where a coolant (typically water) is sprayed into a central contact chamber: spraying a liquid through a nozzle will naturally generate a distribution in the resultant droplet sizes of coolant, where higher upstream pressures and smaller nozzles can be used to *atomize* droplets (meaning the average resultant droplet is between 1 and 20 microns in diameter). While the inlet water can be pre-cooled similar to dehumidification, further cooling in the droplets can be achieved by Joule-Thomson expansion across the nozzle: as discussed in thermodynamics, the extent of J-T cooling scales with the difference in pressure across the valve. The chilled water/coolant droplets critically provide a *very* high surface area with the condensing vapour, enabling rapid heat transfer and resultant condensation. Additional coolant flows in to the centre of the vessel, ensuring the liquid/condensate discharge remains liquid-filled, while non-condensed vapour exits through the side of the vessel. For industrial applications, contact condensers may stand up to 10 m (34 ft) tall, with either limited or no need for gas compression or liquid pumping systems.

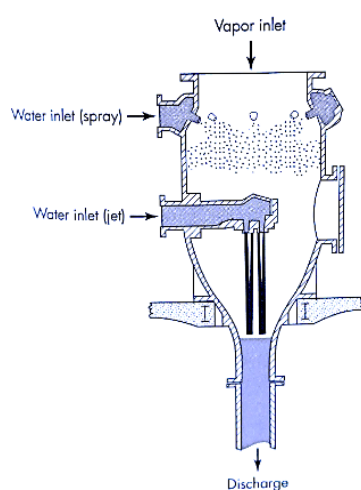


Figure 7.3. Example of a contact condenser, where the a coolant is sprayed to rapidly cool the condensing vapour phase. Reproduced from McCabe, Smith and Harriott (7th Edition).

For the engineer, the specification of a contact condenser chiefly depends on the degree of atomization achievable from the nozzles, which dictates the surface area for heat exchange. While nozzle vendors can provide a reasonable estimate of the droplet size distribution for each differential pressure condition, such droplet sizes can also be estimated from first principles. As the atomization process is naturally turbulent, the viscosity of most coolant fluids plays a negligible role: instead, the droplet size is governed by turbulent forces (that is, drag forces acting to "break up" large droplets, similar to the eddy distribution shown in Figures 3.3 and 4.2) that are balanced against interfacial tension between the droplet and external vapour phase (which acts as a "restorative force" attempting to reunite or coalesce small droplets). For different applications, ranging from contact condensers to up-welling bubble flow, the Weber number (Equation 7.6) balances such drag (destructive) and interfacial (restorative) forces:

$$(Equation 7.6) \quad We = \frac{\rho_p v_p^2 D_p}{\gamma}$$

where the momentum energy of the dispersing phase (that is, ρ_p and v_p) are considered, alongside the equilibrium liquid-vapour interfacial tension (γ , a thermophysical property defined by *both* phases) and the diameter of the particle (D_p , as in Figure 4.2). Typically, experimental and pilot-scale studies are used to regress semi-empirical relationships relating the Weber number and equilibrium droplet size, which are readily available in the engineering literature. Critically, the form of the Weber number affirms that the engineer can decrease droplet size by increasing the velocity of the atomizing liquid spray (itself being directly related to differential pressure) and/or *decreasing* the liquid-vapour interfacial tension (as may be the case when dilute surface active agents, or surfactants, are injected in the liquid phase).

7.2 Reboilers

While there are limited methods available to control the condensation of liquid, the engineering community has long utilised the control of liquid boiling: the generation of steam was an enabling factor in the first industrial revolution. As the process of condensation seeks to transition a vapour phase to liquid *without* enabling the formation of solid (that is, freezing), there is limited value in attempting to accelerate the driving force for condensation. Conversely, boiling seeks to deploy a unit operation for the generation of vapour, wherein substantial increases in the driving force are not able to transition the result (vapour) to a second phase. In other words, the engineer is not inherently limited in how hard they can "push" a boiling system, outside of concerns around equipment integrity and process safety.

Figure 7.4 illustrates four *types* of boiling that can be accessed as a function of the driving force applied (ΔT , or the temperature difference between the heating surface and the liquid with which it is in contact. The region between points "A" and "B" represent the lowest intensity condition, where a minimal temperature driving force produces a low heat transfer coefficient (h , shown on the right-hand plot) and mild heat flux (q , shown on the left-hand plot). In this region, heat transfer in the liquid is dominated by natural convection with the limited nucleation of bubbles on the heating surface (each of which may persist for some time, before rising to the surface of the liquid pool). Between points "B" and C", the rate of bubble nucleation (on the heating surface) increases substantially, increasing in order-of-magnitude increases in the convective heat transfer coefficient and rate of heat exchange. Critically, each bubble that nucleates, detaches, and rises to the liquid pool surface generates local turbulence (explaining the increase in heat transfer coefficient): as such,

the effectiveness of the boiling process depends on the frequency of bubble nucleation, and the region between points "B" and "C" is referred to as *nucleate boiling*.

Under the condition that bubbles provide optimal (i.e. turbulent) mixing -- that is, the bubbles are small enough that they rise slowly, thereby maximising their local mixing potential -- point "C" represents the "maximum flux" for such nucleate boiling. At this position, the engineer has maintained a driving force (that is, surface temperature less the temperature of phase change) such that the process of boiling itself promotes the best-case convective heat transfer coefficient for future bubble nucleation, thereby aiding the boiling process. If the surface temperature is increased beyond this point (that is, from points "C" to "D"), bubbles are nucleated so frequently that they coalesce, resulting in a higher buoyancy force for the (larger) bubble that causes it to rapidly rise to the surface (thereby decreasing the cumulative turbulence imparted on the liquid phase). This condition is known as *jet* or *transition boiling*, and is marked by a decrease in the heat transfer coefficient and overall heat flux (that is, a less efficient condition is achieved for a *greater* driving force applied). For driving forces above point "D" (referred to as the Leidenfrost point), bubbles are nucleated so frequently, and so readily coalesce, that a *persistent film of gas is stabilised*, which introduces a new heat transfer film (not dissimilar to the condensing film resistance discussed above) that decreases the heat transfer coefficient. This region is, logically, referred to as *film boiling*. The substantial driving force applied at this condition is typically sufficient to overwhelm the poor heat transfer coefficient, resulting in a higher net heat flux than the maximum flux achieved in nucleate boiling (point "C").

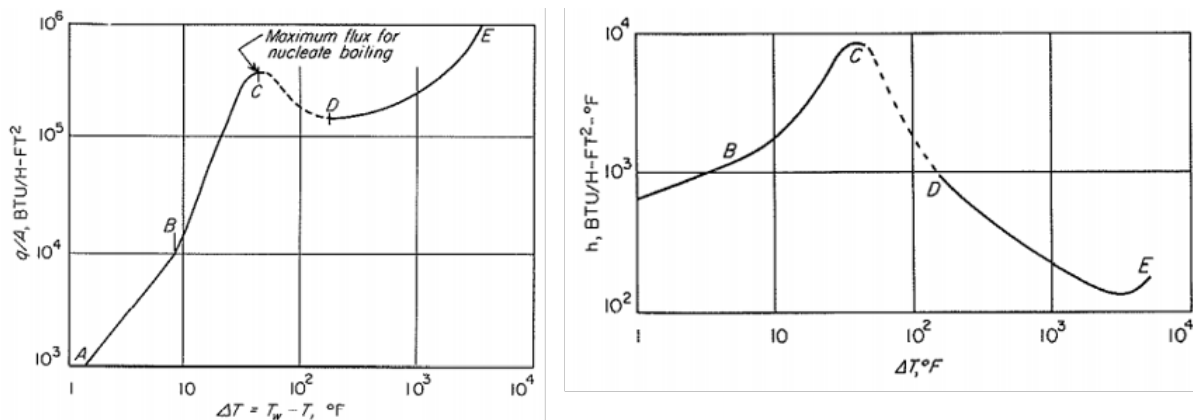


Figure 7.4. For the example of water at 373 K, the heat flux (left panel) and liquid heat transfer coefficient (right panel) as a function of thermal driving force, or the difference between the liquid (373 K) and heating surface. Reproduced from McCabe, Smith and Harriott (7th Edition).

As an aside, each of the regions in Figure 7.4 (nucleate boiling, transition boiling, and film boiling) can be observed visually as a pot of water is heated on the stove, whereby the frequency of bubble nucleation is connected to the turbulence in the liquid (and the time required to achieve the "next" stage of boiling). Similarly, the three regions can be *heard* by listening to an electric tea kettle being heated from room temperature, where the noise level will increase proportional to the frequency of bubble nucleation.

Kettle-type reboilers are one of the most basic applications, which, having been deployed in the first industrial revolution, are still used today. An example design is shown in Figure 7.5, where a similar "floating head" shell-and-tube design is used to transfer heat from warm fluid (typically steam) flowing through tubes to cool liquid entering the shell side. When compared with a standard shell-

and-tube heat exchanger, two modifications can be detected: a large volume is maintained above the tubes (referred to as the "boiling pool") to produce a near-constant rate of vapour generation, the height of which is maintained by an overflow weir that directs hot (i.e. boiling) liquid out of the bottom of the vessel. Figure 7.6 compares the experimentally-determined heat flux measured for a Kettle-type tube bundle boiling water with what theory (i.e. Figure 7.4) might predict for a *single* tube. The result demonstrates that vapour generated in the lower portion of the tube bundle progressively aids heat transfer in the upper portion of the bundle, resulting in a more efficient heat transfer process. Although both tube bundles and (theoretical) single tubes are subjected to the constraints of jet and film boiling, the presence of the bundle shifts the curve toward lower driving forces and generates a more efficient boiling process.

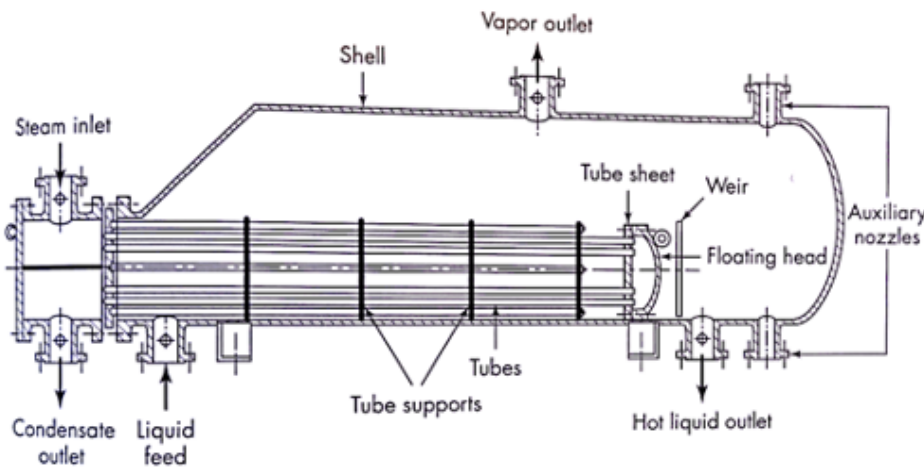


Figure 7.5. A kettle-type reboiler, where cool liquid enters in the shell side and is heated by fluid flowing through two tube passes (typically steam). Reproduced from McCabe, Smith and Harriott (7th Edition).

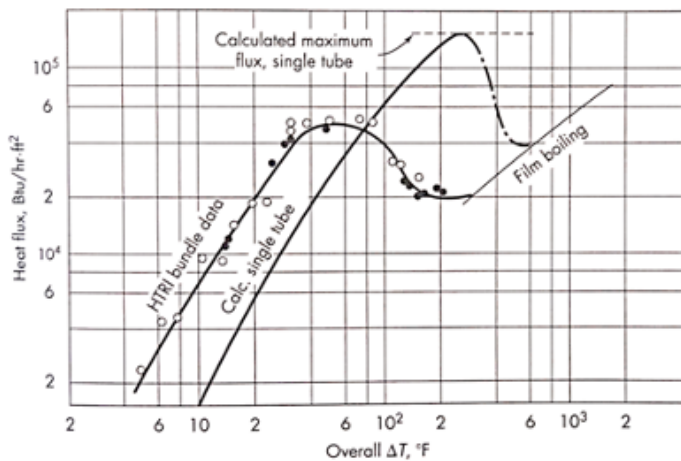


Figure 7.6. Comparison of heat flux in a kettle-type tube bundle (experimental points) with the theoretical performance of a single tube (solid curve). Reproduced from McCabe, Smith and Harriott (7th Edition).

7.3 Evaporators

The diversity of reboiler designs scales with that of shell-and-tube heat exchangers, enabling the engineer to select the heat flux conditions most suitable for the liquid phase of interest. In many applications, the objective is to vaporise an aqueous solution, where water is typically carrying either contaminants or impurities (e.g. salt) or a dilute product following chemical reaction (e.g. pharmaceutical synthesis): this domain is the namesake of evaporators, which are designed to *partially* vaporise a solution while simultaneously concentrating the impurity/product in the remaining liquid phase.

Evaporators function by heating the (typically aqueous) solvent liquor through a vertical shell-and-tube type heat exchanger. As shown in Figure 7.7, the heat exchanger is connected to a single-stage flash vessel, where boiled vapour is taken from the top product and the remaining liquid is recirculated on a loop through the bottom of the tube bundle. In this particular example, liquid is vaporised as it "climbs" through the bundled tubes, thereby functioning as a "climbing film" evaporator: both condensate (that is, condensed steam) and vapor exit the shell-side of the heat exchanger, where the ratio of condensate-to-vapor vented is dictated by the superheat of the steam upon entry. Conversely, a "falling film" evaporator draw the target liquor from the top to the bottom of the heat exchange tubes: such a design can be useful when species in the liquor are highly sensitive to heat exposure (e.g. milk) and require a minimal residence time in the heat exchange network. Finally, evaporators can be configured with forced circulation, whereby the vertical shell-and-tube design in Figure 7.7 is replaced with a simple, kettle-type reboiler pictured in Figure 7.5: an example is pictured in Figure 7.8.

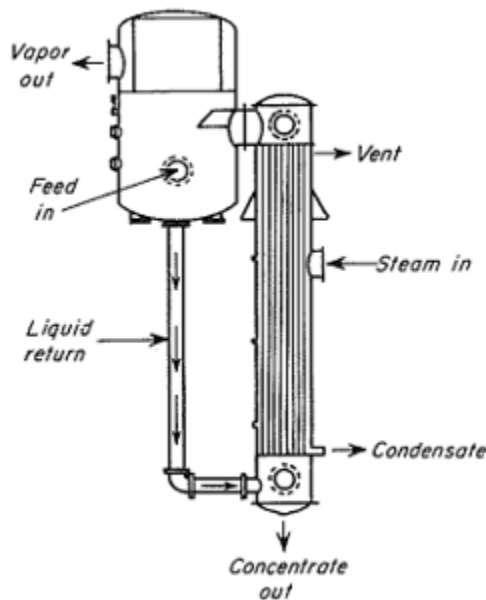


Figure 7.7. Diagram of a basic evaporator, where steam occupies the shell side of a vertical shell-and-tube type exchanger to heat a target liquor ("condensate") to its boiling point. Reproduced from McCabe, Smith and Harriott (7th Edition).

If the steam is sufficiently superheated, no condensate will be produced: if the heating vapour is used once and discarded, the evaporator is said to be single-effect, where a multiple-effect evaporator will deploy multiple units in series, with the exiting steam of one unit deployed as an inlet to the second stage (and so on). Single-effect evaporators tend to demonstrate poor efficiency, with the example of 1.3 kg of steam required to evaporate (or vaporise) 1 kg of water in a typical design. An example of triple-effect evaporator is shown in Figure 7.8, in a so-called "forward feed"

design where the initial liquid feed is introduced in the first (that is, highest pressure) column, and pressure decreases with each subsequent (numbered) column: the warm vapour from each "effect" serves as a heating medium for the next effect. At the end of the third stage, the thick, product liquor is pumped out of the "third effect" in this example, where the final vapour phase is purified through the use of a simple, contact condenser (as discussed above). Although forward-feed multi-effect evaporators are the most common, backward-feed can be employed to handle mildly viscous liquors (at the cost of additional liquid pumps).

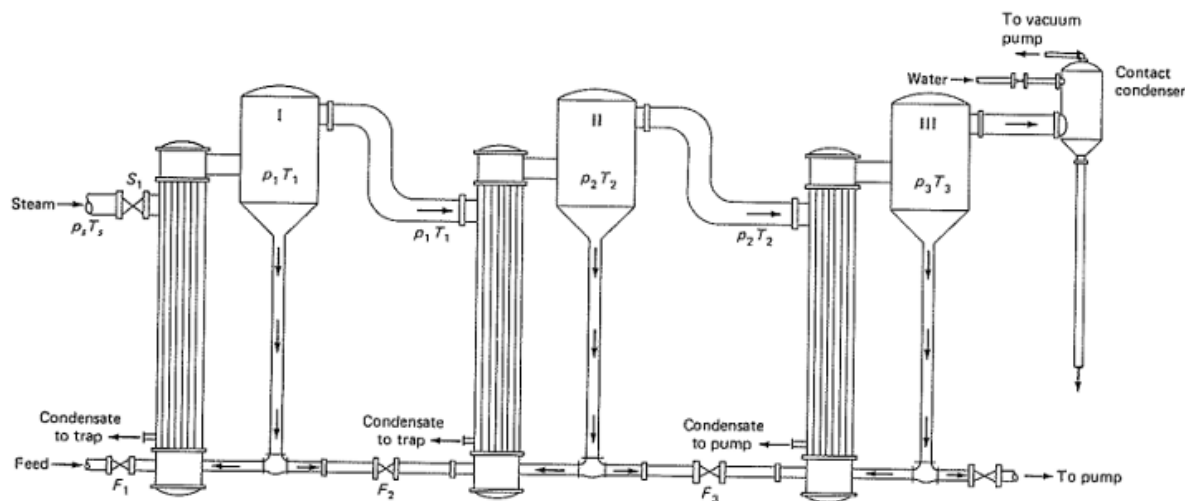


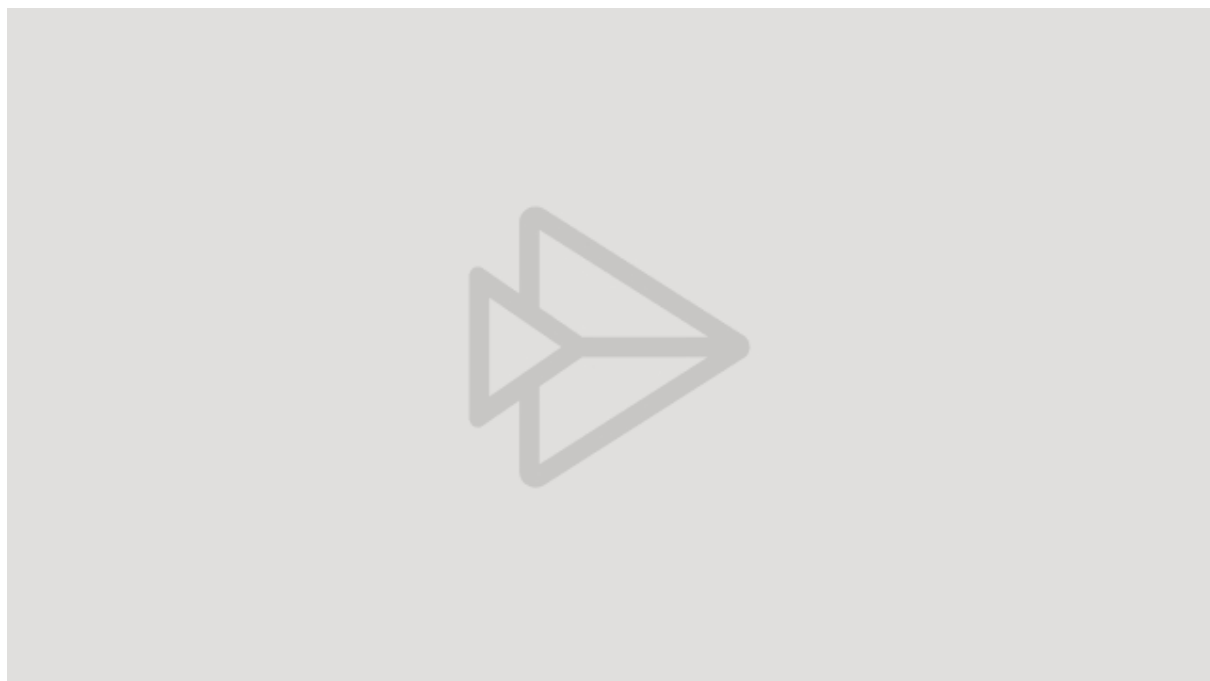
Figure 7.8. Diagram of a triple-effect evaporator configured for "forward feed," where multiple units are used in sequence to improve the overall efficiency of the process operation. Reproduced from McCabe, Smith and Harriott (7th Edition).

As evaporators are typically deployed in aqueous solutions, there are three key considerations in their engineering design. First, the concentration of impurities or products in the aqueous solution will change as evaporation takes place. In many applications, this "concentrating" outcome can change the thermophysical properties of the remaining liquor: as one example, the boiling point of water increases directly with the dissolved salt content (exemplifying a "colligative property," up to the solubility *limit* of around 26 wt% NaCl in water), meaning the evaporation of water will increase the boiling point of the subsequent liquor in a positive feedback cycle. If the liquor contains a highly sensitive product (e.g. an expensive pharmaceutical agent, following chemical reaction), the relation of solute concentration on boiling point must be understood to avoid damaging the product (solute).

Second, the solute may act as a surface active agent (or surfactant, referenced above): as the potency of surfactants typically increases with their concentration, the "concentrated liquor" generated at the end of the heat exchanger may be able to readily stabilise small vapour bubbles in the liquid phase with minimal turbulence (as Equation 7.6 demonstrates, interfacial tension is directly balanced against equilibrium particle/bubble diameter). In the scenario that the solute is a *strong* surfactant, it can result in a *large* amount of gas being entrained as bubbles in the liquid phase, leading to the formation of a *foam*. As with most phase dispersions, foams are metastable: they will degrade over time, resulting in pure liquid and vapour phases in equilibrium. Critically, strong surfactants can readily produce foams that require between hours and weeks of time to resolve, if the system is not heated or chemically treated ("breaking the foam"): if not considered in the design, this process can prevent the unit operation from ever reaching steady-state.

Finally, the presence of dissolved species in the aqueous phase can naturally lead to *scale* formation, as can readily occur in saline water. Although a mineral scale can take years to fully develop due to minute differences in equilibrium solubility of dissolved ions, their presence in the heat exchanger

introduces a second, conductive heat transfer resistance that reduces overall efficiency. Often times, their removal can require extreme maintenance operations, such as the use of concentrated acid and/or mechanical scraping.



Example 9 -- Evaporator for industrial milk production (video from [Microsoft Stream](#)).

If the liquor of interest is highly viscous, a forced circulation evaporator (Figure 7.8) can be employed, where a centrifugal pump is used to drive liquor through the tube side of a kettle-type reboiler (typically with steam heating on the shell side). The forced convection flows liquor through the tubes at a rate of between 2 and 5 m/s, or an order of magnitude larger than the natural convection expected for either falling-film or climbing-film evaporators. The pressure head generated from the pump is resolved in the flash vessel (separating the produced vapour from the concentrated liquor), but critically is used to prevent boiling *within* the tubes. As such, the feed can be superheated prior to partial vaporisation at the end of the tube bundle (through the accumulated pressure drop and temperature increase inside the tubes): a simple deflector plate can be placed in the flash vessel to direct liquid (droplets or pockets/slugs) downward, simultaneously preventing erosion from continuous spray contacting the wall of the flash vessel.

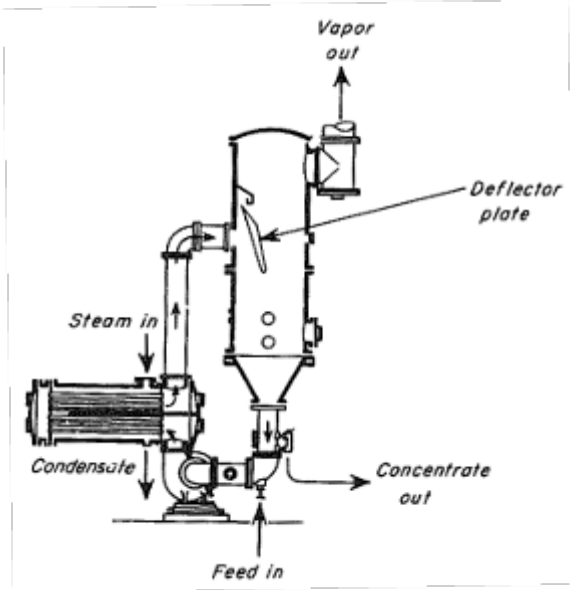


Figure 7.8. Diagram of a forced circulation evaporator, functionally representing the combination of a kettle reboiler (with two tube passes) and basic evaporator. Reproduced from McCabe, Smith and Harriott (7th Edition).

For liquors of *extremely* high viscosity, as may be the case for gelatin, rubber latex, antibiotics, or concentrated fruit juices, an agitated-film evaporator may be employed (Figure 7.9). As the liquor typically enters near the top of the vessel, vertical blades (connected to a central, rotating shaft) induce centrifugal motion, thereby forcing liquid droplets toward the internal vessel wall. As the cylinder is encased in a double-pipe or jacketed heat exchanger (typically containing steam), heating of the liquid droplets/film induces partial vaporisation as the liquid flows downward. Apart from nominating the steam condition (e.g. the degree of superheat), the engineer can subsequently nominate the agitator speed and number of blades, in order to control the *residence time* of liquid in the evaporator: that is, with greater centrifugal force, droplets are less affected by the gravity field and will take longer to migrate downward to the exit ("concentrate" in Figure 7.9).

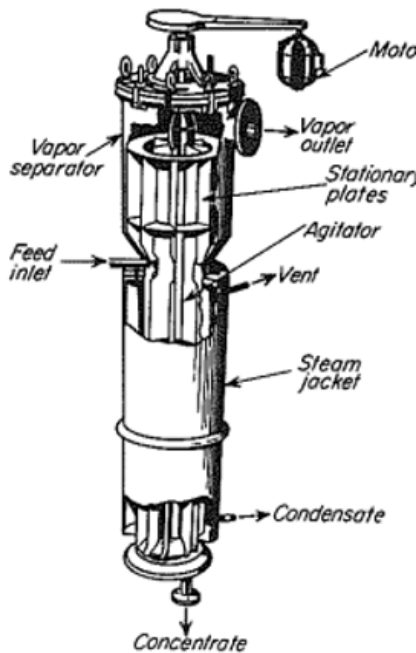


Figure 7.9. Diagram of an agitated-film evaporator, where centrifugal motion concentrates liquid droplets at the exterior wall for heating by a surrounding jacketed exchanger. Reproduced from McCabe, Smith and Harriott (7th Edition).

The internal heat transfer coefficient in agitated film evaporators can be approximated through Equation 7.7, where n represents the agitator speed (in rotations per hour) for a number of blades (B):

$$(Equation 7.7) \quad h_i = 2 \sqrt{\frac{k\rho C_p n B}{\pi}}$$

Agitated-film evaporators, although uniquely suited for viscous liquors (up to 10,000 times that of water), can engender high capital costs due to their internal complexity (when compared with falling-film evaporators), higher maintenance costs (due to rotating internal mechanics), and the relatively small capacity of individual units (as the centrifugal force scales with distance from the axis of rotation, thereby introducing a physical limitation to absolute diameter). However, they are able to generate high heat transfer coefficients under viscous conditions, where natural film or forced circulation evaporators fail. Indicative ranges of overall heat transfer coefficients for all three evaporator types are provided in Table 7.1, where the (natural) film-based evaporators may be characterised by long-tube vertical bundles and forced circulation evaporators can be characterised by either horizontal or vertical long-tube bundles (as per Sections 5 and 6). Where the viscosity of water is often used as a reference standard at 1 centipoise ("1 cP"), Table 7.1 illustrates that agitated-film evaporators can achieve a similar overall heat transfer coefficient for a liquor that is 10,000 times the viscosity of water (or approximately the viscosity of honey).

Table 7.1. Indicative overall heat transfer coefficients for evaporators. Reproduced from McCabe, Smith and Harriott (7th Edition).

Type	$U \text{ (W/m}^2/\text{K)}$
Long-tube vertical evaporators	

<i>Natural convection (falling or climbing film)</i>	1000-2500
<i>Forced convection</i>	2000-5000
<i>Agitated-film evaporators (assuming Newtonian fluids)</i>	
1 cP viscosity	2000
100 cP viscosity	1500
10,000 cP viscosity	600

While multiple engineering subdisciplines are equipped to address basic unit operations of heat exchange, it is solely the chemical engineer who is responsible for determining how to control the flow of mass through a system. From Section 1, thermodynamics provides a context by which engineers may understand the distribution of N components through M phases in an equilibrium system: critically, when a change in process conditions (that is, pressure or temperature) is introduced, the chemical engineer is charged with determining how the N components will redistribute with precision, and exploiting this knowledge to achieve the growing needs of the society. Raoult's Law provides a formalism through which the distribution of components between phases may be achieved at *equilibrium* -- inclusive of treatment for non-ideality in the vapour and liquid phases, respectively through activity and fugacity coefficients -- yet this framework is not sufficient to predict how molecules might migrate within a phase, or between phases, when the system is *not* at equilibrium. Such questions are the domain of mass transfer, functionally representing the third of three driving forces in Equation 1.2 (accounting for changes in the number of molecules, $d n_i$, each with a molecular free energy of μ_i).

Considering Equation 1.2 momentarily, one might recognise that volume (the domain in which pressure is transmitted) is more intuitive to understand than entropy (the domain in which temperature is transmitted): given the conceptual and computational complexity of chemical potential (μ_i), it reasonably represents the most complex domain (that in which mass is transmitted). As such, mass transfer is often taught by drawing parallels with heat transfer (the middle domain), wherein the rate equations of both follow the general formalism of Equation 1.3: the rate of transfer is given by the product of the *relevant* driving force, the area across which that driving force acts, and the resistance of the system to the relevant driving force. The remainder of this curriculum considers four primary mass transfer operations, and the practical implementations thereof: absorption (Section 9), distillation (Section 10), adsorption (Section 11), and membrane separation (Section 12).

8.1 Diffusion

The first such analogue is drawn between the diffusion of heat and the diffusion of mass, where Fick's First Law of Diffusion considers a one-dimensional problem at *steady-state*:

$$(Equation\ 8.1)\ J_a = -D_V \frac{dC_a}{dx}$$

where J_a is the diffusive flux of the component ("a") in mols per transfer area per time (mol/m²/s), D_V is the resistance term called volumetric diffusivity (with SI units of m²/s, representing the ease with which a molecule can migrate through a given volumetric phase), and the driving force is represented by the *linear gradient* or slope of concentration per distance in the one-dimensional problem (dC_a/dx). Equation 8.1 may be considered as the mass transfer "analogue" to Fourier's Law, where a thermal gradient is replaced with a concentration (mass) gradient and the thermal conductivity of the material (representing the ease with which heat can diffuse through materials) is

replaced with diffusivity. Strictly speaking, Fick's Law of Diffusion can be applied to a plane *parallel* to the source of diffusing molecules (e.g. a sugar cube placed carefully in a tea cup, so as not to introduce turbulence), and considers the flow of molecules *perpendicular* to that plane: a simplified example is shown in Figure 8.1, where a vertical line demarcates the plane to which Fick's Law of Diffusion is applied. While diffusivity (D_V) is a thermophysical property of the diffusing species (*relevant* to the species and phase in which it is being dissolved), moving the vertical line left or right will quickly reveal that the slope of concentration changes with position (that is, the magnitude of the slope is much larger on the left of the image than on the right). This reveals an important insight in mass transfer: the *diffusive flux is not constant throughout the system*. The negative sign in Equation 8.1 is ultimately cancelled out by the slope of the concentration: if the black arrows in Figure 8.1 indicate the "positive x" direction, the slope can be seen to *always be negative* (put another way, mass will diffuse from high concentration to low concentration, in the same way heat transfers from warmer to colder positions). As will be discussed later, further manipulation of the Gibbs free energy, such as an increase in pressure or temperature, *can* be used to reverse this naturally-occurring gradient, but is not common in unit operations.

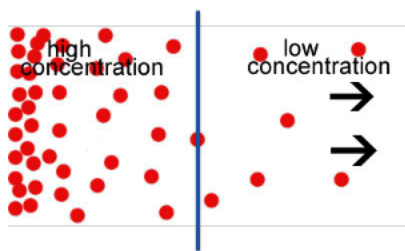


Figure 8.1. Simplified representation of the diffusion of species "a" (red circles) in a medium of species "b" (white space), where Fick's Law of Diffusion (Equation 8.1) would be applied to the vertical blue line. Reproduced from Wikimedia Commons.

In considering the migration of an *individual* molecule in Figure 8.1 (that is, focussing in on a single, red circle of species "a"), one can ascribe the *average* velocity u_a : the term average is used to denote that the molecule itself will diffuse along a tortuous path (as originally identified by Brownian motion), similar to turbulent eddies occasionally moving perpendicular to, or against, the general velocity of the flow stream. When this average velocity (u_a) is multiplied by the concentration of the component at a given point (C_a), the molar flux is revealed (N_a). When the plane is in motion (i.e. consider the diffusion potential if Figure 8.1 *itself* were to move from the left- to right-hand side of the screen with a velocity u_0), the diffusive flux (J_a) in Equation 8.1 can be defined as the difference in molar flux at the molecule's velocity less the background velocity:

$$(Equation 8.2) J_A = C_A u_A - C_A u_0 = C_A (u_A - u_0)$$

This allows Fick's First Law of Diffusion to extend to systems in motion, so long as they are at *steady state* (i.e. no property is changing in time). This is a critical assumption, as engineers are often charged with measuring or monitoring unit operations to determine whether the product species is being generated to an appropriate quality (e.g. in the case of a life-saving pharmaceutical). If the engineer's measurement is *not* at steady state for *most* unit operations (adsorption being a notable exception), any subsequent modelling or analysis -- either by hand or through simulation -- is categorically invalid. This framework can be extended to solve directly for the molar flux of a component ("A"), where liquid systems (Equation 8.3) follow the convention of using concentration (mol per volume, where $C_A = \rho_M y_A$) and gas systems (Equation 8.4) follow the convention of mole fractions.

$$(Equation 8.3) \quad N_A = C_A u_0 - (D_v + \varepsilon_N) \frac{dc_A}{dx}$$

$$(Equation 8.4) \quad N_A = y_A N - (D_v + \varepsilon_N) \rho_M \frac{dy_A}{dx}$$

where the first term represents the background concentration of the species, and the second term represents the change in the amount of species due to diffusion (following the basis of Equation 8.1). If the flowing system is static or laminar, meaning the turbulent eddies described in Figure 3.3 are absent, the term ε_N is set to zero: this term represents the "eddy diffusivity," or the amount of *additional* diffusion that takes place as eddies in the energy cascade carry molecules throughout the system. While eddy diffusivity is proportional to the turbulence in the system (that is, the magnitude of energy distributed *through* the energy cascade), the correct prediction of eddy diffusivity requires both complex derivation and semi-empirical regression against experimental data. As with molecular diffusivity, experimental measurements or previous peer-reviewed studies provide the engineer with the most reliable basis for such estimates.

In the example of an ideal gas containing two components ("A" and "B") at equilibrium, any change in the *local* concentration of first component must be counteracted by an inverse change in the concentration of the second to meet the requirement of constant density: that is, $dC_A + dC_B = d\rho_{mix} = 0$. As Equation 8.2 relates these concentrations to the local molar flux of each component, Equation 8.1 can be written for both components to yield the condition that the molar fluxes (which *can* change locally at equilibrium) must be equal and opposite: $J_A + J_B = 0$. Together, these two conditions reveal a powerful insight: in this ideal gas system, the diffusivity of component "A" within component "B" is *equal* to the diffusivity of component "B" within component "A" (written as $D_{AB} = D_{BA}$). A similar treatment can be applied to a binary liquid mixture with constant density (as may be the case if the two components have negligible activity). This theoretical framework provides the engineer with intuition on the *limiting* condition of diffusivity between two species.

Equimolar counter-diffusion provides another benchmark example for the engineer, similar to the binary ideal gas discussed above, where the net volumetric and molar fluxes for a two-component system are both zero. Considering a concentration gradient of component "A" across a local region of thickness δ with no convection (that is, $u_0 = 0$), Equation 8.5 is the result of integrating both the diffusive and molar fluxes of the component between some initial ($C_{Ai} = \rho_M y_{Ai}$) and final ($C_A = \rho_M y_A$) concentration:

$$(Equation 8.5) \quad N_A = J_A = \frac{D_v}{\delta} \rho_M (y_{Ai} - y_A) = \frac{D_v}{\delta} (C_{Ai} - C_A)$$

where ρ_M is the molar density (i.e. moles per volume). Critically, Equation 8.5 illustrates the first of two key insights in equimolar counter-diffusion: the concentration *gradient* of the component is constant across the distance (δ). A simple mass balance reveals that component "B" follows an equal and opposite concentration profile in space, with a concentration gradient of equal magnitude and opposite sign to that of component "A". This is illustrated in Figure 8.2 for both components, where the abscissa ("distance from interface") scales from 0 to δ . The exemplar case of equimolar counter-diffusion is useful when considering, for example, how two miscible gas species will mix if they are initially in separate vessels and the barrier/partition between them is removed (revealing the "interface") in Figure 8.2.

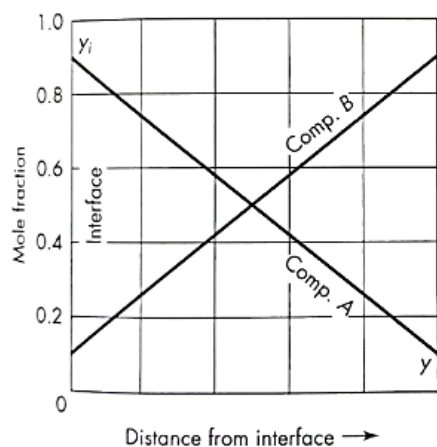


Figure 8.2. Illustration of equimolar counter-diffusion in a binary gas, where the interface is rich in component "A" and the bulk is rich in component "B". Reproduced from McCabe, Smith and Harriott (7th Edition).

One-way diffusion provides a third and final exemplar case for a binary system, where only component "A" is able to diffuse and component "B" is otherwise immobile or stagnant (meaning it cannot diffuse). To assess this scenario for a laminar system, Equation 8.4 (with eddy diffusivity, ε_N , set to zero) can be integrated for distances 0 to δ between respective mole fractions of y_{Ai} and y_A to reveal a relationship for molar flux:

$$(Equation 8.6) \quad N_A = \frac{D_v \rho_M}{\delta} \ln \left[\frac{1-y_A}{1-y_{Ai}} \right] = \frac{D_v \rho_M}{\delta} \frac{(y_{Ai}-y_A)}{\ln \left[\frac{1-y_A}{1-y_{Ai}} \right]}$$

where the right-most definition employs a more robust log-mean mole fraction, which provides robustness of the solution for a greater diversity of applications (similar to the case of log-mean radius or LMTD in heat transfer calculations). Critically, the log-mean term is *always* less than unity, meaning the molar flux of component "A" in one-way diffusion will *always* be less than that of equimolar counter-diffusion: in other words, if molecules of component "B" aren't *making room* for the incoming diffusion of component "A", the overall diffusion process will proceed with less efficiency. Concentration profiles arising from Equation 8.6, in concert with a mass balance, are captured in Figure 8.3.

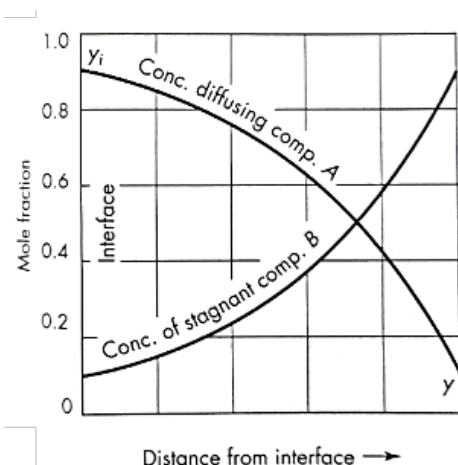


Figure 8.3. Illustration of one-way diffusion in a binary gas, where the interface is rich in component "A" and the bulk is rich in component "B". Reproduced from McCabe, Smith and Harriott (7th Edition).



Example 10 -- Calculating diffusivity (video from [Microsoft Stream](#)).

8.2 Molecular Diffusivity

The resistance term employed in Equation 8.1 (volumetric or molecular diffusivity, D_v) functionally represents the "ease" with which one molecule of species "A" can dissolve in a phase of species "B". As this definition suggests, diffusivity therefore depends on both the *species and phase(s)* present. While this property is inherently thermophysical (wherein predictions should be available through an understanding of thermodynamics), the difficulty in thermodynamic predictions of multi-component interactions presents a constraint: as one example, consider the challenge in calculating activity and fugacity coefficients for a system of 50 components across both aqueous and organic phases, which must be determined before the consideration of a *rate equation* (which requires diffusivity) can be predicted. For this reason, diffusivity is most often determined through semi-empirical relationships (for simple systems), or preferably through laboratory experimentation (as a best practice and requirement for complex systems).

From the basic theory of diffusion in *gasses*, volumetric diffusivity is functionally related to the average molecular velocity (\bar{u}) along the tortuous *mean free path* (λ) taken by the molecule, as exemplified by Brownian motion: that is $D_v \cong \frac{1}{3} \bar{u} \lambda$. This relationship is rarely employed, as predictions of the mean free path and associated velocity are difficult to capture: however, the mean free path is known to vary with temperature to the first power and molecular velocity varies with the square root of temperature, resulting in a (theoretical) dependence of molecular diffusivity on temperature to the power of 1.5. This dependence is captured in the Chapman-Enskog relation, where the Lennard-Jones 6-12 potential is applied to a binary gas containing two components:

$$(Equation 8.7) D_{AB} = \frac{0.001858 T^{1.5} \left[\frac{M_{W,A} + M_{W,B}}{M_{W,A} M_{W,B}} \right]^{0.5}}{P \sigma_{AB}^2 \Omega_D}$$

where the collision diameter (σ_{AB}) is averaged based on the individual collision diameters of the components that can be found from lookup tables (such as Appendix 19 of McCabe, Smith and Harriott (7th Edition): in its simplest arithmetic form, $\sigma_{AB} = 0.5(\sigma_A + \sigma_B)$, although more complex

and concentration-dependent models can be employed to refine the accuracy of the solution. In Equation 8.6, the collision integral (Ω_D) functionally represents the frequency with which the two molecules *will* collide (thereby affecting the mean free path): while these values can also be accessed through lookup tables, they similarly depend on the force constants for the molecular potential model employed (e.g. the above-referenced textbook Appendix is informed by the Lennard-Jones 6-12 potential, where research in the discipline of *ab initio* physical chemistry searches for more accurate and elaborate replacements with parallel application in molecular dynamics simulation). The Chapman-Enskog relation, with the nuanced and complex assumptions required to inform its collision parameters, exemplify the difficulty in predicting volumetric or molecular diffusivity in real-world applications. For this reason, diffusivity in the *gas* phase is currently reliant on precise laboratory measurements.

For gas diffusion in porous media, as is the case in adsorption (Section 11), the ability for gas molecules to diffuse is restricted by the size of the pores, as demonstrated in Figure 8.4: the pore diameter must be *large* enough for the molecule(s) to fit, above which the size of the pore controls the amount of material that can flow through it. When the pore radius is comparable in scale to the mean free path of the diffusing molecule (that is, $R_{pore} \approx \lambda$), the semi-empirical relation for Kundsen diffusion can be employed (Equation 8.8).

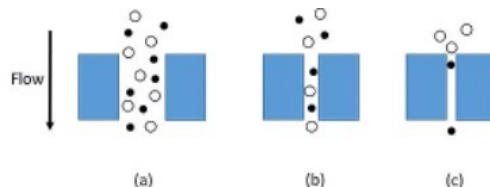


Figure 8.4. Illustration of two components diffusing through a model pore, where pore diameter (a) > (b) > (c). Reproduced from Wikimedia Commons.

$$(Equation 8.8) D_K = 9700 \cdot R_{pore} \cdot \sqrt{\frac{T}{M_w}}$$

If the size of pores is of moderate size, when compared to the molecules, the porous diffusivity (D_{pore}) can be calculated with contributions of both Kundsen and volumetric (bulk) diffusivity:

$$(Equation 8.9) \frac{1}{D_{pore}} = \frac{1}{D_K} + \frac{1}{D_{AB}}$$

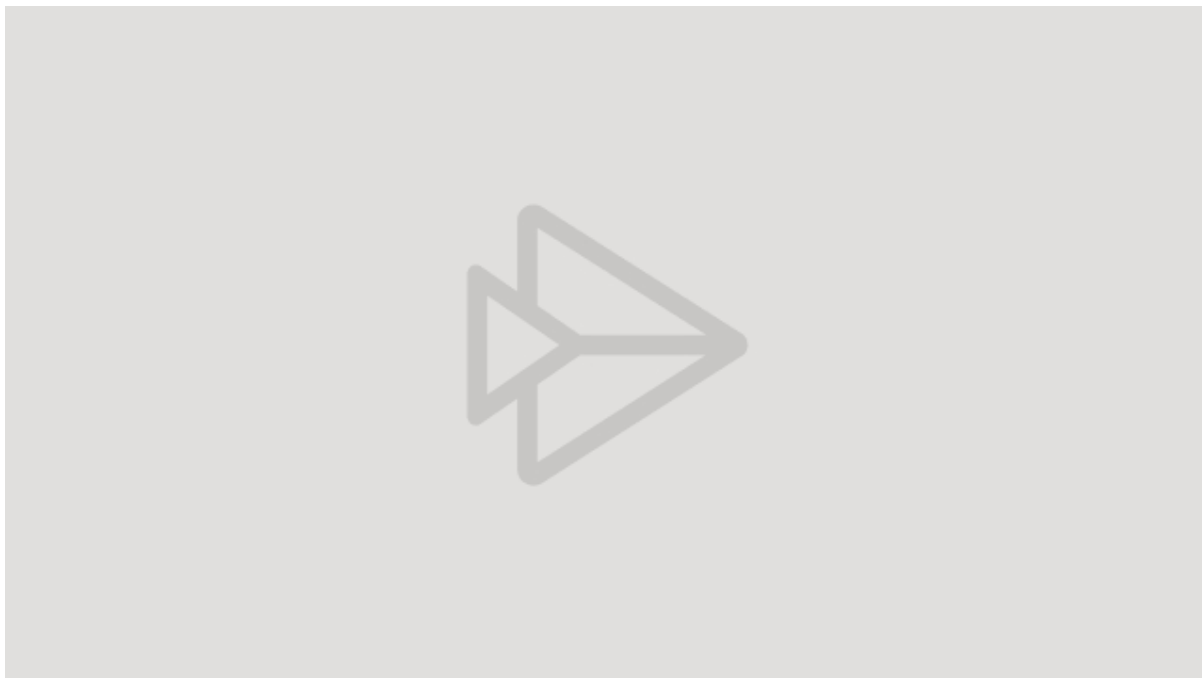
In liquid systems, the diffusivity of components is generally between four and five orders of magnitude below that of the gas phase: as the intuitive result of liquid molecules having significantly less energy, with a much higher probability of (local) collision, when compared to their counterparts in the gas phase. Although theory from physical chemistry is less well-developed, two basic frameworks have been proposed. The Stokes-Einstein relation considers molecules as spheres that experience drag (similar to Figure 4.2), where the diffusivity therefore depends on the radius of the spherical "molecule" (r_m) and the Boltzmann constant ($k = 1.380 \cdot 10^{-23} \text{ J/K}$):

$$(Equation 8.10) D_v = \frac{kT}{6\pi r_m \mu}$$

For the treatment of non-spherical molecules with molecular weights below 400, the Wilke-Chang relation provides a semi-empirical basis to predict diffusivity:

$$(Equation 8.11) D_v = (7.4 \cdot 10^{-8}) \frac{(\psi_B M_w)^{0.5} T}{\mu V_A^{0.6}}$$

where viscosity must be used with units of centipoise (1 cP = 1 mPa*s), V_A is the molar volume of the solute (in cm³/g/mol) at its *normal boiling point*, and ψ_B is the *association parameter* for the solvent (typically requiring empirical regression against experimental data) that scales, for example, with the extent of electrolyte activity in the system. For the exemplar case of an aqueous system with *no* electrolytes, the equation can be approximated: $D_v = \frac{13.26 \times 10^{-5}}{\mu_B^{1.14} V_A^{0.589}}$, with diffusivity with units of cm³/gmol and the viscosity of the system represented purely by the viscosity of water (μ_B).



Example 11 -- Calculating the diffusivity of benzene (video from [Microsoft Stream](#)).

8.3 Mass Transfer Rates

While considerations of molecular diffusivity provide a theoretical, or semi-empirical, basis for determining the willingness of different molecules to migrate through each other, the usefulness of such predictions is largely focussed on static or laminar flow. Conversely, the chemical engineer will often exploit the ability of turbulent eddies to more efficiently reach a (new) equilibrium condition, as was demonstrated in the treatment of heat exchange operations and remains true in mass transfer. In this context, *mass transfer coefficients* (denoted by k_i , where the subscript indicates the phase of matter to which the coefficient is relevant) can be considered as analogous to convective heat transfer coefficients (h_i). Mass transfer coefficients, or MTCs, can be readily deployed in multi-component systems with turbulence.

In the example case of equimolar counter-diffusion in a stagnant (boundary) layer, the MTC for component "A" can be defined:

$$(Equation 8.12) k_c = \frac{J_A}{C_{Ai} - C_A} = \frac{D_v(C_{Ai} - C_A)}{\partial} \frac{1}{(C_{Ai} - C_A)} = \frac{D_v}{\partial}$$

where the right-hand simplification reveals a fundamental definition (diffusivity on the thickness of the stagnant or non-turbulent layer). In turbulent flow, the MTC is defined generally, as a function of the liquid or vapour mole fraction of the component:

$$(Equation 8.13) \quad k_y = \frac{J_A}{y_{Ai} - y_A} = k_c \rho_M$$

where, in liquid, x_A would replace y_A . This general definition provides a relation to thermodynamics, where the molar density of the mixture can be defined through an appropriate equation of state (e.g. $\rho_M = P/RT$ in an ideal gas mixture). By deploying Equation 8.5 to define diffusive flux (J_A), the molar flux of component "A" can be defined in terms of its MTC for *one-way diffusion* across unsteady, turbulent flow:

$$(Equation 8.14) \quad N_A = \frac{k_y(y_{Ai} - y_A)}{(1-y_A)_L}$$

where a similar log-mean mole fraction driving force is used as with Equation 8.6. In both Equations 8.13 and 8.14, the concentration (or mole fraction) of the bulk system (that is, C_A or y_A) is not represented by the *centreline* of the flow (e.g. in a cylindrical pipe), but instead represents the volume average concentration or mole fraction of component in the system. An illustration of this definition is shown in Figure 8.5, where the concentration of the species "A" naturally mimics the velocity and thermal profiles of the laminar or turbulent flow pattern, inclusive of a boundary layer with thickness δ . Unlike velocity, the *volume averaged* concentration is *less* than the global maximum concentration in the centre of the flow stream, and the driving force for mass transfer is defined relative to the concentration at the wall (C_{Ai}).

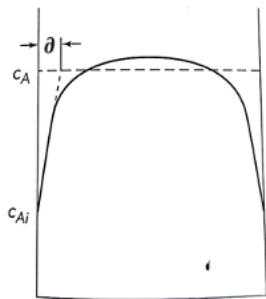


Figure 8.5. Illustration of the concentration of a species (on the ordinate) as a function of distance across the flow channel (on the abscissa), which mimics the velocity profile of turbulent flow and includes a boundary layer of thickness δ . Reproduced from McCabe, Smith and Harriott (7th Edition).

In deploying MTCs for use in practical unit operations, which seek to transfer some species between two phases across an interface, the engineer must necessarily assume equilibrium is established at the interface between the phases. Thus, the transfer of species across the interface encounters resistance from *both* phases, which can be amalgamated similarly to the treatment of internal and external convective coefficients in heat transfer. Critically, the "volume averaged" concentration discussed around Equation 8.14 can therefore be replaced with the *equilibrium concentration* of the species in the phase of interest (that is, y_A). A chemical engineer is therefore *required* to design and manipulate mass transfer operations, as *these equilibrium concentrations emerge from Raoult's Law in the subdiscipline of thermodynamics*: the chemical engineer must invoke any assumptions around the extent of non-ideality in the vapour and/or liquid phase(s), apply respective treatments with

fugacity and activity coefficients, and determine the equilibrium concentration (or mole fraction) of the component that the system will seek to achieve.

In such systems, the *overall* mass transfer coefficient is designated through a capital K (analogous to the overall heat transfer coefficient U), which is defined on a mole fraction basis for the example of vapour-liquid system:

$$(Equation 8.15) \frac{1}{K_y} = \frac{y_A^* - y_{Ai}}{k_x(x_A - x_{Ai})} + \frac{y_{Ai} - y_A}{k_y(y_{Ai} - y_A)}$$

where the first and second terms respectively represent the *resistance* to mass transfer in the liquid and vapour phases. Importantly, the liquid phase term considers the concentration difference in the liquid (as shown, on a mole fraction basis) relative to the amount of the species that *would be in equilibrium for its vapour*. The "equilibrium line" shown in Figure 8.6 is, by definition, the result of solving Raoult's Law for the quantity y/x . When the liquid and vapour phases, with respective "bulk" mole fractions of x_A and y_A (Figure 8.6), the quantity y_A^* illustrates the amount of component "A" that the liquid phase *expects* to see in the vapour: the discrepancy between y_A and y_A^* in Figure 8.6 therefore represents the *driving force for mass transfer*. Figure 8.6 merits a few moments of concentrated study, as the concept of this driving force (that is, the relation between y_A , x_A , and y_A^*) is critical to designing and analysing absorption (Section 9), distillation (Section 10), and adsorption (Section 11) systems.

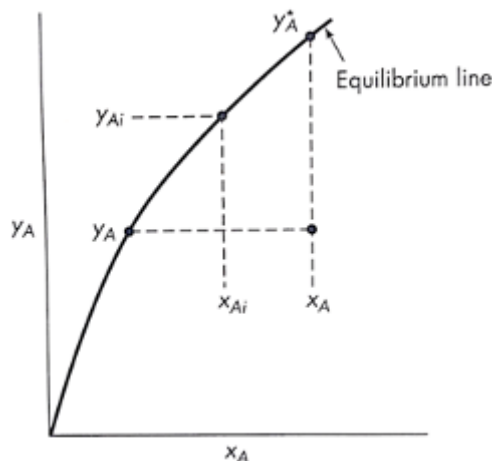


Figure 8.6. Illustration of the driving forces for mass transfer between the liquid and vapour phases in "xy" space at constant temperature and pressure. In this context, the "equilibrium line" represents a solution to Raoult's Law for Chemical Engineers, solved for y/x , Reproduced from McCabe, Smith and Harriott (7th Edition).

Figure 8.6 further illustrates the interfacial mole fraction of component "A" on the shared interface between the vapour (y_{Ai}) and liquid (x_{Ai}) phases. Although this condition is represented by a single *point*, it does not mean the values of y_{Ai} and x_{Ai} are equal: this is a second unique feature of mass transfer when compared to mass transfer, as there is naturally a *large* discrepancy in the mole fraction of component on each side of the interface. This is represented by Figure 8.7 as a function of distance on either side (gas vs. liquid) of the interface, for an exemplar distillation (left panel) and absorption (right panel) processes -- that is, where distillation *typically* seeks to migrate a component from the liquid to the gas phase, while absorption typically functions inversely.

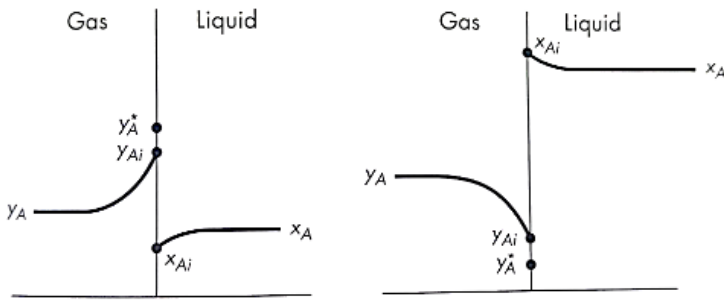


Figure 8.7. Illustration of the concentration of component A across the gas-liquid interface, in the example of a distillation (left) and absorption (right) process. Reproduced from McCabe, Smith and Harriott (7th Edition).

As with the equilibrium plot (or "xy diagram") in Figure 8.6, the definition of the interface mole fractions in Figure 8.7 warrants detailed inspection for its conceptual value. In the example of distillation (left-hand panel), the liquid-side interface is *deplete* in the component relative to its bulk, *because Raoult's Law dictates that a larger fraction of component A should exist in the gas phase (y_A^*) than exists at either the gas-side interface or in the gas bulk*. The opposite expression is true for the example of absorption (right-hand panel), where the liquid-side interface expects to see *less* of component A in its nearby vapour than it sees in practice (that is, $y_A^* < y_{Ai}$), enabling mass transfer from the gas to the liquid phase.

The driving force for mass transfer is shown on a per-phase basis in Equation 8.15 (e.g. the amount of "excess" or "deficit" each phase recognises upon contact with the other). However, with an appreciation of Raoult's Law as applied to Figures 8.6 and 8.7, this driving force can be represented by a singular term (**m**) in Equation 8.16 that balances the MTCs for the liquid and vapour phases to yield the overall mass transfer coefficient (K_y).

$$(Equation 8.16) \frac{1}{K_y} = \frac{\mathbf{m}}{k_x} + \frac{1}{k_y}$$

where **m** is the slope between the two bounding points of Figure 8.6 (y_A and y_A^* , which is given by x_A). Of course, the equilibrium line shown in Figure 8.6 is not linear, but displays a reasonable curvature. However, if the "difference" between the phases' concentrations were smaller (i.e. the vapour phase was *less* in deficit of component A, and/or the liquid phase was *richer* in component A), the distance between these two points would naturally decrease. It is for this reason that complex mass transfer operations (where multiple equilibrium stages are connected in sequence, similar to Figure 1.3) must be designed with an appropriate *number* of equilibrium stages, such that the driving force for mass transfer in *each* stage is reasonably limited. In other words, a sufficient number of points should be placed on the equilibrium curve in Figure 8.6, so the linear slope between each deviates minimally from the equilibrium curve given by Raoult's Law.

In practice, the engineer will deploy semi-empirical correlations in order to determine the MTCs of each phase (that is, k_x and k_y in Equation 8.16), and will use Raoult's Law (either manually or through a calculation tool) to identify the driving force for mass transfer (**m** in Equation 8.16). In combination, this allows the engineer to calculate the molar flux of components between the phases through Equation 8.13, and to determine the *overall* mass transfer coefficient through Equation 8.16.

8.4 Mass Transfer Coefficients

Completing the analogue between heat and mass transfer, the determination of MTCs in convective systems (noting Equation 8.12 is used for stagnant flow, similar to conductive heat transfer) is accomplished through the deployment of two dimensionless numbers. The Schmidt number (Sc) represents momentum diffusivity (i.e. the extent of diffusion engendered by fluid motion) relative to molecular diffusivity (i.e. from a stagnant system):

$$(Equation 8.17) \quad Sc = \frac{\nu}{D_v} = \frac{\mu}{\rho D_v}$$

where kinematic viscosity (ν), or equivalently dynamic viscosity on density, are balanced against molecular diffusivity from Section 8.2. For gasses, the Schmidt number is typically on the order of 0.5 to 2, while for liquids has a typical range between 10^2 and 10^5 . Functionally, the Schmidt number is deployed for mass transfer similar to the use of the Prandtl number in heat transfer. As might be expected, the second dimensionless quantity (the Sherwood number, Sh) is therefore deployed on a correlative basis to determine the balance between convective and diffusive mass transfer:

$$(Equation 8.18) \quad Sh = \frac{k_c D}{D_v}$$

where the MTC is represented generically (k_c , without specifying a phase), D represents the characteristic length of the system, and D_v is the molecular diffusivity. Nearly identical to the correlations for the Nusselt number discussed in Sections 5 and 6, the engineer must select the appropriate Sherwood correlation for the mass transfer system of interest and, through the definition in Equation 8.18, can then determine the appropriate MTC for the phase. For example, Equation 8.19 is a basic Sherwood correlation for flow through a laminar boundary layer on a flat length of characteristic length b :

$$(Equation 8.19) \quad Sh = \frac{k_c D}{D_v} = 0.664(Sc)^{1/3}(Re)^{1/2}$$

Similarly, Equation 8.20 provides the Sherwood correlation for laminar flow inside a pipe. It should be noted that this correlation -- identical to the Nusselt correlation in Equation 5.12 -- obeys an upper limit of 3.66. Equation 8.20 is also commonly deployed for flow in hollow-fibre membranes, which are the subject of Section 12.

$$(Equation 8.20) \quad Sh = 1.76 \left(\frac{\pi D}{4L} \cdot Sc \cdot Re \right)^{1/3} \leq 3.66$$

For ducted pipes with turbulent flow, the Sieder-Tate correlation has been adapted, where the exponents have been mildly refined based on experimental studies:

$$(Equation 8.21) \quad Sh = 0.023 \cdot Re^{0.81} \cdot Sc^{0.44} \cdot \phi_v^{0.14}$$



Example 12 -- Film thickness in mass transfer resistance (video from [Microsoft Stream](#)).

At ducted pipes with turbulent flow *and* high Schmidt numbers (from approximately 430 through 100,000), Equation 8.22 can be deployed:

$$(Equation 8.22) \quad Sh = 0.0096 \cdot Re^{0.913} \cdot Sc^{0.346}$$

External flow that is normal to a single cylinder (for $10 < Re < 10^4$) is addressed by Equation 8.23, while external flow normal to a tube bundle is approximated by Equation 8.24.

$$(Equation 8.23) \quad Sh = 0.61 \cdot Re^{1/2} \cdot Sc^{1/3}$$

$$(Equation 8.24) \quad Sh \cong 1.28 \cdot Re^{0.4} \cdot Sc^{0.33}$$

Although Equations 8.20 through 8.22 are useful in mass transfer operations within pipes -- such as in determining how an internal "flow coating" used to reduce wall friction in pipe flow may dissolve over time -- most mass transfer operations would consider transfer to or from one immersed object in another phase, as exemplified by dropping a sugar cube into a cup of tea. For flow past a single, isolated sphere (similar to Figure 4.2), Equation 8.25 can be used to estimate the Sherwood number for external Reynolds numbers below 1000 (again, based on the characteristic length of the object's projected area), where Equation 8.26 can be used if the flow stream is turbulent.

$$(Equation 8.25) \quad Sh = 2.0 + 0.6 \cdot Re^{1/2} \cdot Sc^{1/3}$$

$$(Equation 8.26) \quad Sh = (4.0 + 1.21 \cdot [Re \cdot Sc]^{2/3})^{1/2}$$

If there are *many* objects in the flow path, such as would be the case for a packed bed, Equation 8.27 can be deployed for beds that contain either spherical or cylindrical objects (the mean diameter of which is the characteristic length), for bed void fractions between 40 and 45%:

$$(Equation 8.27) \quad Sh = 1.17 \cdot Re^{0.585} \cdot Sc^{1/3}$$

Alternative correlations to Equation 8.27 exist for beds with different packing materials, such as hollow particles or rings. Finally, the consideration of mass transfer from a suspended *deformable* phase to another -- inclusive of rising or falling bubbles/droplets in another fluid phase -- is given by Equation 8.28:

$$(Equation 8.28) \text{ Sh} = 1.13 \cdot \text{Re}^{1/2} \cdot \text{Sc}^{1/2}$$

Where appropriate Sherwood correlations are not available in the peer-reviewed literature, or from official reference texts (e.g. Perry's Chemical Engineering Handbook), the engineer may be required to consider an experimental campaign. Such approaches require systems with well-defined and controllable surface area, where form drag (if appropriate) and turbulence (including boundary layer separation) can be avoided: one such approach is the use of a so-called "wetted wall tower," where a thin film of liquid is drawn down the inside of the column by gravity.

Absorption columns are a useful, and often inexpensive tool, with which chemical engineers can remove one or more target components of interest in a solute (where different grades of water are commonly employed). An example unit is shown in Figure 9.1, wherein the inlet liquid (called the "weak liquor") is typically either a pure solvent or dilute solution, and is distributed evenly through the top of the packing material. Gravity draws the weak liquor down through the packing material in the column, where it exists at the bottom as a "strong liquor" that contains an *equilibrium* amount of some target component(s) of interest. Conversely, "rich gas" enters through the bottom of the column, where the designation of "rich" indicates the phase contains a large amount of the target component(s) of interest, and flows upward across the packing material where it contacts the liquor: the gas then exits through the top of the column as a "lean gas," having been depleted in the target component(s).

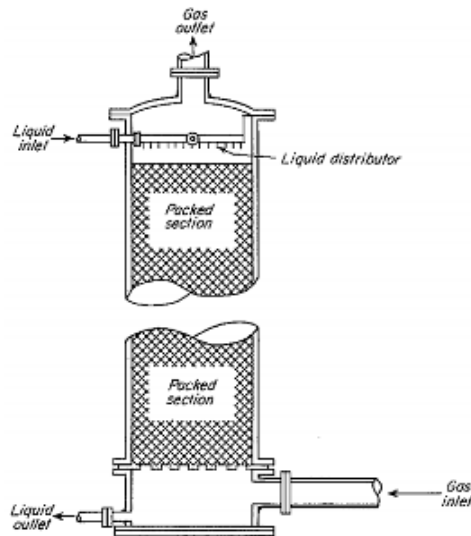


Figure 9.1. Diagram a simple absorption column, where a nominated packing material provides a high surface area of contact to facilitate mass transfer between a liquid (solvent) and a gas containing some target component(s) of interest. Reproduced from McCabe, Smith and Harriott (7th Edition).

Such absorption column designs are commonly employed to remove CO₂ or H₂S, as the polarity of both components makes water (of nearly any grade) a useful solvent. After an absorption operation, the strong liquor can be regenerated for reuse, either by changing pressure-temperature conditions (as used in single- or multi-stage distillation, discussed in Section 10) or by employing a

complementary "stripping" or desorption column. Functionally, stripping columns operate identically to absorption columns, except the fluids are selected to enable transfer of some target component(s) *from* the liquid phase *to* a gas phase that is initially deplete in the component(s).

9.1 Packing Materials

As absorption or stripping columns typically operate without meaningful pressure or temperature control, the engineer must have a precise knowledge of the equilibrium condition that will be achieved for the existing gas and liquid streams: while mild pressure or temperature control can be applied to modify the equilibrium condition, doing so can result in significant increases in costs and introduce additional safety concerns. While the inlet gas, by definition, must have a mild pressure condition to enable flow, the engineer may be required to deploy the Kozeny-Carman relation (Equation 4.9) to ensure the frictional pressure loss in the gas phase will still enable sufficient flow at the end of the column. The engineer's primary decision lies in the appropriate selection of appropriate packing material, which controls the ultimate surface area between the gas and liquid phases.

As absorption columns are typically chosen for their minimal cost, ideal packing materials are similarly inexpensive, must be inert (to avoid reaction with the gas- or liquid-phase components), and have sufficient shape irregularity so as to generate void fractions between 60 and 90%.

Alongside Section 4, examples of traditional packing materials for absorption columns are shown in Figure 9.2, where an example set of characteristics are shown in Table 9.1: as would also be provided by packing material vendors, this table captures the contact surface area (per volume of material in the column), resultant porosity of the bed, and the packing factors that are required to solve the Kozeny-Carman relation (Equation 4.9).

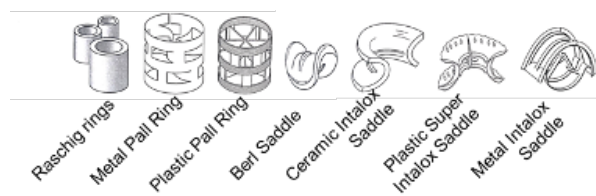


Figure 9.2. Example packing materials used in absorption/ stripping columns. Reproduced from McCabe, Smith and Harriott (7th Edition).

Early absorption columns also deployed crushed stone and simple, ceramic spheres, as low-cost materials. While Berl saddles and Raschig rings were developed to improve surface area, they are typically only deployed today for basic absorption operations. More advanced approaches have been developed, as shown in Table 9.1, to maximise the surface area while *minimising* the packing factor (subsequently decreasing the frictional pressure loss through the system).

Table 9.1. Characteristics of example packing materials in absorption columns, where bulk density and total surface/contact area are given per volume of material in the column. Adapted from McCabe, Smith and Harriott (7th Edition).

Type	Material	Nominal size (in.)	Density (lb/ft ³)	Surface area (ft ² /ft ³)	Porosity (ϵ)	Packing factor (F_p)
Raschig rings	Ceramic	0.5	55	112	0.64	580
		1.0	42	58	0.74	155

		1.5	43	37	0.73	95
		2.0	41	28	0.74	65
Pall rings	Metal	1.0	30	63	0.94	56
		1.5	24	39	0.95	40
		2.0	22	31	0.96	27
	Plastic	1.0	5.5	63	0.90	55
		1.5	4.8	39	0.91	40
Berl saddles	Ceramic	0.5	54	142	0.62	240
		1.0	45	76	0.68	110
		1.5	40	46	0.71	200
Intalox saddles	Ceramic	0.5	46	190	0.71	200
		1.0	42	78	0.73	92
		1.5	39	59	0.76	52
		2.0	38	36	0.76	40
		3.0	36	28	0.79	22

For the example of 1" ceramic Intalox saddles pictured in Figure 9.2, the properties of which are in Table 9.1, the frictional pressure loss (ΔP) as a function of gas mass velocity is shown in Figure 9.3. The figure represents a typical characterisation of absorption columns, where "dry line" has a slope of 1.8, indicating the frictional pressure loss of pure air flowing through the column: as the liquid flowrate in the column increases (G_x from 3,000 to 36,000 lb/ft²/hr), frictional pressure loss increases relative to the dry condition. As can be observed, lower air velocities produce frictional pressures with parallel slope to the dry line *independent* of the liquid velocity: the point at which the slopes are no longer equal (for each liquid velocity) is commonly referred to as the "loading point," and is taken to be a lower functional operating limit for the column.

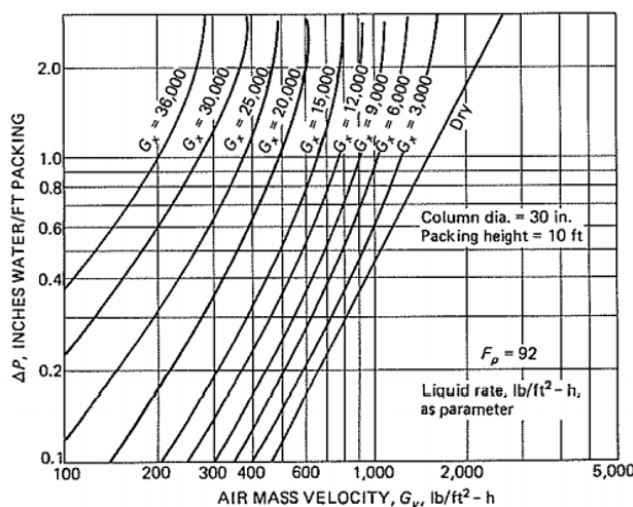


Figure 9.2. Frictional pressure loss as a function of air mass velocity for absorption using 1" Intalox saddles. Reproduced from McCabe, Smith and Harriott (7th Edition).

If the liquid mass velocity is *much* higher than the gas mass velocity, both phases may longer be evenly distributed across the surface area of the packing material. When there is a mild discrepancy, liquid may collect in localised pockets, inhibiting effective mass transfer local basis. This condition is referred to as a "localised flood," wherein the local region of packing materials are assumed to be

immersed in the liquid. As the discrepancy increases, multiple regions throughout the column are subjected to localised flooding conditions: the *gas* is said to have achieved its "flooding velocity" at this condition, which varies with both the liquid mass velocity and the type/size of packing material. The relationship between (gas) flooding velocity and liquid mass velocity -- for the same absorption column characterised by Figure 9.2 -- is shown in Figure 9.3. Importantly, the *optimal* operating condition for absorption columns is immediately prior to the flooding velocity, at which point the highest gas-liquid contact area is achieved.

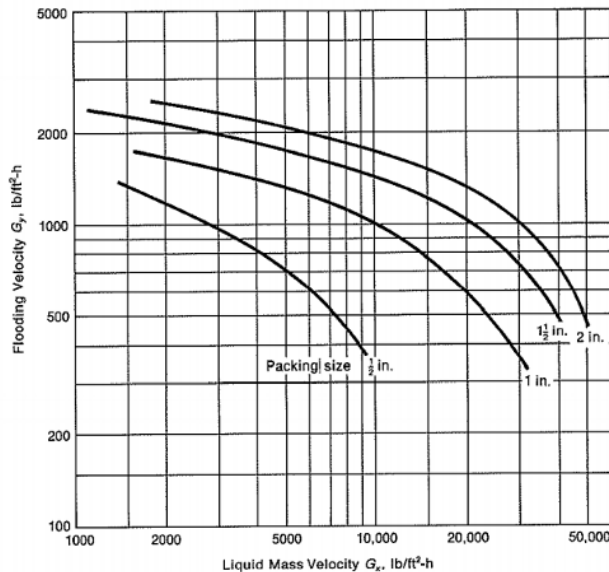


Figure 9.3. Gas flooding velocity as a function of liquid mass velocity, for four nominal diameters of Intalox saddles in a 30" diameter column with 10 ft. of packing material. Reproduced from McCabe, Smith and Harriott (7th Edition).

While there is no well-refined correlation to estimate the flooding velocity for each packing material and gas/liquid combination, the pressure drop at the flooding point can be estimated through Equation 9.1, which is valid for packing factors (F_p) between 10 and 60: Equation 9.1 returns pressure drop per unit length of packing material, in "inches of water per foot" (where 1 in. H₂O/ft = 817 Pa/m). For appropriate packing factors, Equation 9.1 can be combined with the Kozeny-Carman relation (Equation 4.9), allowing the engineer to consider the impact of varying the packing material selection (representing ϵ , D_p , and Φ_s) at constant flooding velocity (\bar{u}_0 , when $\Delta P \rightarrow \Delta P_{flood}$).

$$(Equation 9.1) \quad \Delta P_{flood} = 0.115 \cdot F_p^{0.7}$$

Alongside the use of Kozeny-Carman, Eckert proposed a general correlation (Figure 9.4) to determine pressure drop for dumped (i.e. random) packing materials in a column, where gas and liquid mass flux (G_y and G_x) are in units of lb/ft²/s; liquid viscosity (μ_x) is in cP; gas and liquid densities (ρ_y and ρ_x) are in lb/ft³; and g_c represents gravitational acceleration for imperial units (32.174 lb-ft/lb_f/s²). Figure 9.5 presents the empirical correlations from Strigle, which functions identically to the correlations by Eckert, with the exception that the packing factor (F_p) is taken to the power of 0.5 and the kinematic viscosity (ν) replaces the dynamic viscosity (ρ). The correlations by Strigle also make use of a "capacity factor" in the ordinate, which is defined as $C_s = u_0 \sqrt{\rho_y / (\rho_x - \rho_y)}$. As illustrated in both figures, the condition of 2" H₂O/ft (1630 Pa/m) represents a heuristic limit of the pressure drop at the flooding point in the column.

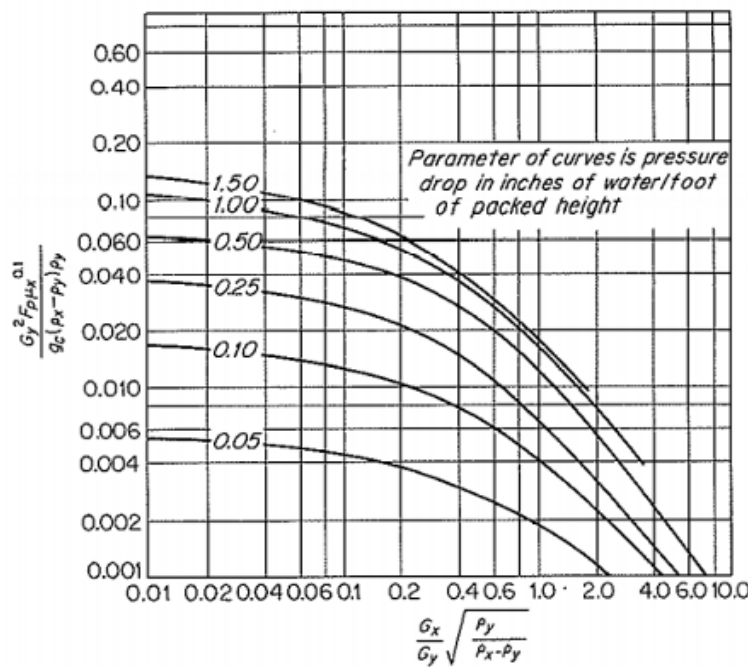


Figure 9.4. General correlation proposed by Eckert to predict pressure drop in a packed column (parameter curves). Reproduced from McCabe, Smith and Harriott (7th Edition).

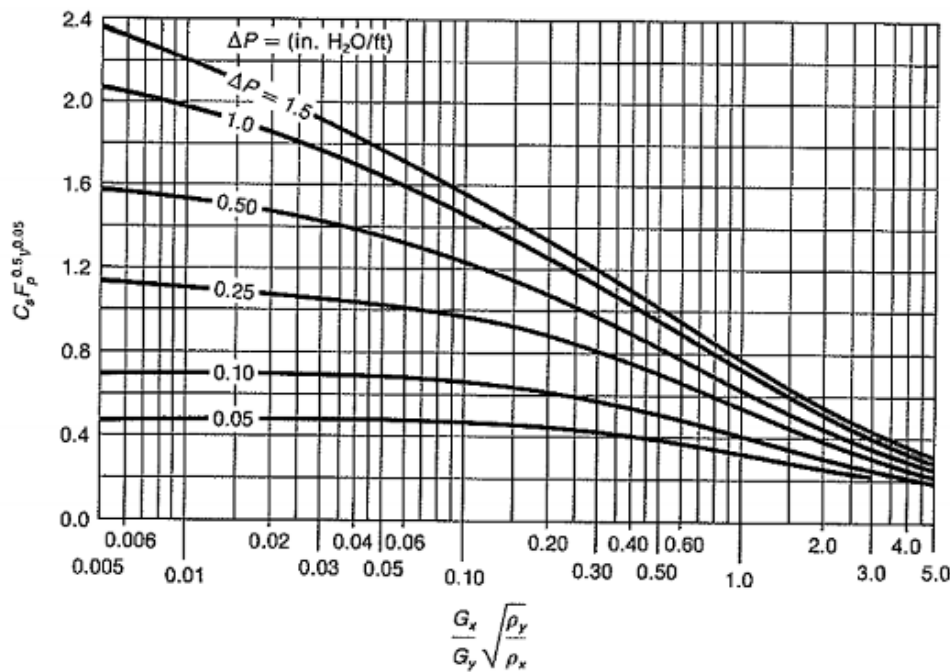


Figure 9.5. General correlation proposed by Strigle to predict pressure drop in a packed column (parameter curves). Reproduced from McCabe, Smith and Harriott (7th Edition).

9.2 Absorption Design Basis

As discussed in Section 8, the design of mass transfer operations necessitates the use of the "equilibrium curve" on an xy plot, as captured through (i) experimentation, (ii) calculation by thermodynamic simulators, and/or (iii) the result of setting Raoult's Law equal to the condition y/x . As is the case throughout mass transfer operations, the equilibrium line is then contextualised by the use of an *operating line* (which, despite its name, is not linear). Figure 9.6 provides a generalised mass balance across an absorption column, in which the mole fractions are represented by Figure 9.7 in the xy plane. First considering Figure 9.6, the overall material balance for the liquid (L) and vapour (V) phases is given by $L_a + V_b = L_b + V_a$, where the subscript "a" is used to indicate a *position* at the top of the column (not the component) and the subscript "b" represents the bottom of the column. If a control surface is drawn (as in Figure 9.6) to bisect *some* position in the middle of the column, the overall material balance is given by $L_a + V = L + V_a$, where both L and V are initially unknown. Similarly, component material balances can further be written across the entire column ($L_a x_a + V_b y_b = L_b x_b + V_a y_a$) or across the bisecting control surface ($L_a x_a + V y = L x + V_a y_a$).

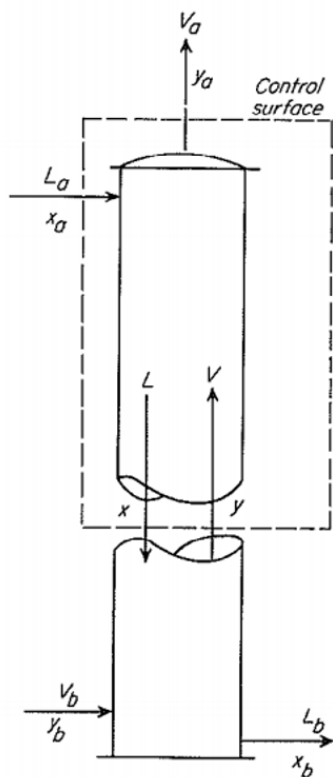


Figure 9.6. A component mass balance across an absorption column, where the identified control surface can be used to determine component mole fractions throughout the column interior. Reproduced from McCabe, Smith and Harriott (7th Edition).

In both the total and component material balances, the molar flowrates (L and V) represent a key operating parameter for the engineer, as informed by the discussion in Section 9.1 on the optimisation of contact area with respect to flooding velocity. As such, the component material balance across the *control surface* can be written in terms of the unknown y and x , as in Equation 9.2.

$$(Equation 9.2) \quad y = \frac{L}{V}x + \frac{V_a y_a - L_a x_a}{V}$$

This form of the component material balance allows it to be plotted in the same xy plane as the equilibrium curve, where the engineer is required to (i) know or assume the so-called "L/V ratio," and (ii) know or measure the flow rates and compositions of the streams entering and exiting the top of the column (that is, position "a"). The linear nature of Equation 9.2 is what gives rise to the monikor "operating line," where the curvature shown in Figure 9.7 emerges because *mass is transferred between the phases* (that is, minute variations to the L/V ratio within the column result in changes to the slope). To draw the operating line, the engineer nominates the position (in the xy plane) corresponding to the inlet/outlet mole fractions at the *top* of the column, and extends the operating line with a slope L/V (for a column operating at steady-state, this is the ratio of the *inlet liquid molar flowrate* on the *inlet vapour molar flowrate*) until the operating line bisects the molar fractions entering/exiting the bottom of the column (y_b and x_b , respectively, in Figure 9.7).

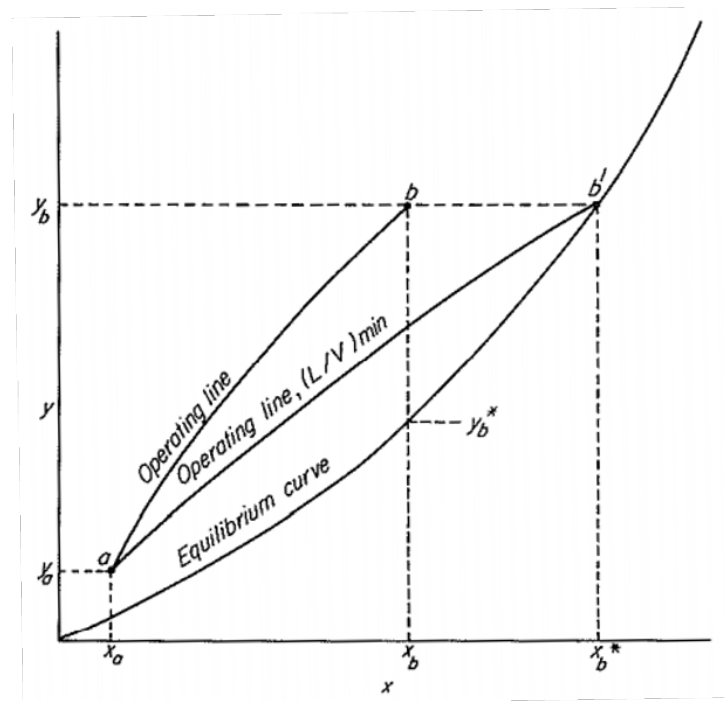


Figure 9.7. Representation of the absorption column in the xy plane, where the equilibrium curve is determined by thermodynamics, and the operating line is determined by the mole fractions of the component at the entry and exit to the column. Reproduced from McCabe, Smith and Harriott (7th Edition).

Critically, the ordinate distance (that is, the "y" axis) between the operating line and equilibrium curve indicate the magnitude of driving force for mass transfer throughout the column (that is, $y - y^*$): this is illustrated by the bisection of mass fraction x_b (the liquid mole fraction at the bottom of the column) with the equilibrium curve, yielding y_b^* . As drawn in Figure 9.7, weak liquor entering the top of the column (at point "a") has approximately one third of the driving force for mass transfer as the strong liquor exiting the bottom of the column (at point b). Such operating lines must always lie above the equilibrium line for an absorption process to occur (that is, transferring mass from the liquid to the vapour phase), and must always lie below for a desorption/stripping process. In analysing Figure 9.7, the engineer can further estimate the maximum possible extent of mass transfer for the operation, by decreasing the L/V ratio until the operating line bisects the equilibrium curve (illustrated in Figure 9.7 by "Operating line $(L/V)_{min}$ "): under this condition, there is no longer a driving force for mass transfer at the bottom of the column (that is, b' is on the equilibrium curve).

Together, the operating line and equilibrium curve fully characterise the absorption or stripping column, as the former contains information on the molar flow rate of material throughout the column. Equation 9.3 can be used to calculate the absorption or mass transfer rate (r) within the packed column (typically reported *per unit volume*), in terms of either local or overall mass transfer coefficients (respectively, k and K):

$$(Equation 9.3) \quad r = k_y a(y - y_i) = k_x a(x_i - x) = K_y a(y - y^*) = K_x a(x^* - x)$$

where a partial pressure difference ($p - p_i$), as may be given by Henry's Law, is proportional to ($y - y_i$). The phase and overall MTCs deployed in Equation 9.3 are related through the basis of Equation 8.16, which can be written with a consideration of contact area (a) for both the gas (Equation 9.4) and liquid (Equation 9.5) phases:

$$(Equation 9.4) \quad \frac{1}{K_y a} = \frac{1}{k_y a} + \frac{\mathbf{m}}{k_x a}$$

$$(Equation 9.5) \quad \frac{1}{K_x a} = \frac{1}{k_x a} + \frac{1}{\mathbf{m} k_y a}$$

where **m** (the driving force across the equilibrium line, illustrated in Figure 8.6) is identical in the definitions. Importantly, the engineer is *also* able to characterise the local mole fractions at the interface between gas and liquid phases (respectively, y_i and x_i):

$$(Equation 9.6) \quad \frac{y - y_i}{x_i - x} = \frac{k_x a}{k_y a}$$

These mole fractions, appropriate only at steady-state operation of the column, correspond to the general illustration in Figure 8.7. They can also be represented graphically in the xy plane, by considering an intermediate operating line position (x, y in Figure 9.8). Building upon the above understanding, the driving force for mass transfer from the liquid to the vapour is represented by ($y - y^*$) or the vertical dashed line in the diagram: similarly, the driving force is equally represented by the horizontal distance between the operating line and equilibrium curve (that is, $x^* - x$), as shown in Figure 9.8. The composition at the *interfaces* of the vapour and liquid phases are determined by a line perpendicular to *both* the operating line and equilibrium curve, the slope of which is $-k_x a / (k_y a)$ as rearranged from Equation 9.6. The coordinates of bisection with the equilibrium line represent the interface composition (x_i, y_i).

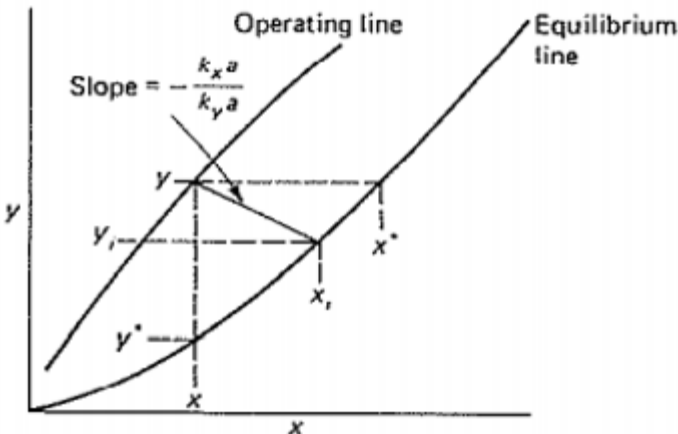


Figure 9.8. Representation of the absorption column in the xy plane, illustrating the role of local MTCs in determining the interface compositions for both phases. Reproduced from McCabe, Smith and Harriott (7th Edition).

9.3 Tower Design

As articulated in Section 6.4, the nature of considering "transfer units" is of limited value for heat transfer operation, but critically informs the design of mass transfer operations. That is, absorption or stripping columns are designed by considering the *number of transfer units* (N_{Oy}) required, alongside an understanding of the height of each transfer unit (H_{Oy}), where the total bed height (Z_T) is the product of both quantities: that is, $Z_T = H_{Oy}N_{Oy}$. The number of transfer units is defined in Equation 9.7 based on mole fractions in the gas phase, where "a" and "b" respectively represent the top and bottom of the absorption column.

$$(Equation\ 9.7)\ N_{Oy} = \frac{y_b - y_a}{\Delta y_L} = \frac{y_b - y_a}{\ln \left[\frac{y_b - y_b^*}{y_a - y_a^*} \right]}$$

The log-mean driving force is applied in the denominator of Equation 9.7, to appropriately capture the range of potential operating conditions and compositional extremes that may be considered. If the operation is considered to be *ideal*, Equation 9.7 simplifies to $N_{Oy} = (y_b - y_a)/(y - y^*)$. The number of transfer units only requires the engineer to perform a component material balance across the entirety of the column, and to deploy their knowledge of thermodynamics in order to assess the driving force for mass transfer. For a column of with vapour molar flowrate (V), cross-sectional area (S), overall vapour MTC (K_y), and interfacial/contact area (a), the height of *each* transfer unit is defined by:

$$(Equation\ 9.8)\ H_{Oy} = \frac{V}{(S \cdot K_y a)}$$

Both Equations 9.7 and 9.8 use the *overall gas MTCs*, but symmetric definitions can be used to return the *same* bed height (Z_T) by considering (i) the liquid film, where $H_x = \frac{L}{S \cdot k_x a}$ and $N_x = \int \frac{dx}{x_i - x}$; (ii) the overall liquid MTCs, where $H_{Ox} = \frac{L}{S \cdot K_x a}$ and $N_{Ox} = \int \frac{dx}{x^* - x}$; or (iii) the gas film, where $H_y = \frac{V}{S \cdot k_y a}$ and $N_y = \int \frac{dy}{y - y_i}$. Although the height of each transfer unit will change with the basis, and the number of transfer units will subsequently vary to maintain the same bed height, any basis may be used to design the column, enabling the engineer to nominate the basis that is best informed by reference data or empirical (e.g. Sherwood) correlations. Interestingly, there is only equality in the number and height of transfer units *when the operating and equilibrium lines are straight and parallel*. The consideration of transfer units allow the engineering to rapidly scale the operation, either toward the consideration of process upsets (e.g. a change in inlet composition) or for larger industrial operations.



[**Example 13 -- Absorption column design example \(video from Microsoft Stream\).**](#)

As mentioned above, the use of pressure is not common in absorption operations, which are typically designed around low-cost materials and operating requirements. However, if the engineer can access different pressure conditions, they are able to modify *both* the operating line and equilibrium curve, as shown in Figure 9.9 for a nominal system (dashed line) at twice the pressure of the original design (solid lines). Notably, increasing the pressure allows the engineer to increase the *capacity* of the operation (as illustrated in Figure 9.9) with inverse proportionality to pressure, as given by the definition of vapour phase mole fraction: $y_A = \frac{p_A}{P}$. For the two scenarios in Figure 9.9, and assuming equivalent liquid and gas flow rates between them, increasing the system pressure will subsequently increase the driving force for absorption, meaning the liquid rate can be decreased at higher pressures and the engineer can obtain a "richer" product stream. Importantly, the overall mass transfer coefficient *increases* with pressure, resulting in decreased resistance across the liquid film.

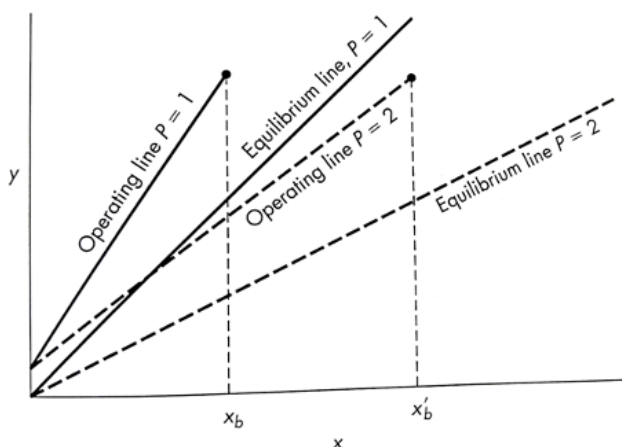


Figure 9.9. The manipulation of system pressure affects both the equilibrium curve and operating line in absorption columns. Reproduced from McCabe, Smith and Harriott (7th Edition).

While the use of packing material is useful across many applications, the availability of "structured" packing is increasingly of interest for columns at the industrial scale. An example of structured packing is shown in Figure 9.10. Having been in development for over a century, with early efforts focussed on wire gauze, perforated corrugated metal is now commonly used in the industry, with adjacent sheets to improve liquid spread across the surface (as per the example in Figure 9.10): vapour can then flow through the corrugation channels (right-hand illustration, Figure 9.10), where the thickness of each layer is typically between 1 and 2" with, critically, between 93 and 97% porosity. This results in a highly controllable pressure drop for the engineer, with a typical maximum (flooding) capacity of 1.22" H₂O/ft. (997 Pa/m). In offering the advantage of lower differential pressure, structured packing decreases the propensity of foam formation, which is a critical risk in the dehydration of raw (unprocessed) natural gas -- a common application for structured packing.

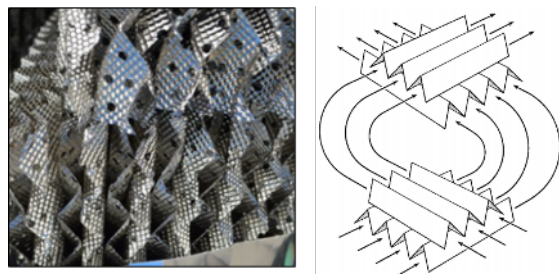


Figure 9.10.(left) Industrial example of structured packing, from MACH Engineering. (right) Illustration of how fluids flow through generic structured packing, reproduced from McCabe, Smith and Harriott (7th Edition).

[Example 14 -- Acetone absorption column \(video from Microsoft Stream\).](#)

Although not treated above in detail, stripping columns are equally common throughout the industry: their design basis is *identical* to that of an absorption column, with the exception that target components are transferred *from* the liquid phase to the vapour phase. As such, an example stripping column design, with a typical operating line (now with slope L/V) and equilibrium curve is shown in Figure 9.11. Stripping columns are typically used to regenerate liquid solutions, where multiple stripping columns (in series) may be required depending on the final purity requirements of

the solution. As they operate conversely to absorption, the performance of stripping columns can be improved with increased temperature and/or decreased pressure conditions.

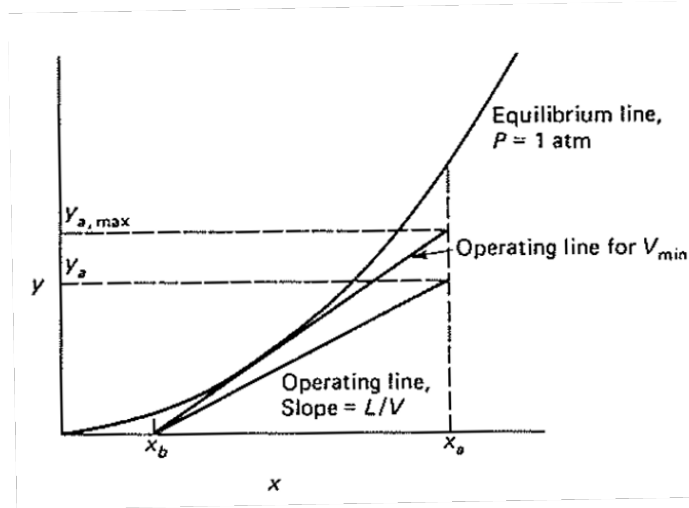


Figure 9.11. Example characterisation of a stripping column, where the operating line is placed below the equilibrium curve, enabling transfer of mass from the liquid to the vapour phase. Reproduced from McCabe, Smith and Harriott (7th Edition).

In the example of Figure 9.11, the curvature of the equilibrium curve is such that the operating line *cannot* intersect with the equilibrium at its terminal point (x_a , y_a): when the gas molar flowrate is set to V_{\min} , the *middle* of the operating line intersects with the equilibrium curve, indicating a "pinch point" in the system. Of critical importance, *pinch points represent a condition with an infinitesimally small driving force for mass transfer*: if operated under a pinch point, fluids are no longer able to exchange mass at concentrations beyond the pinch point. Throughout steady-state mass transfer operations, engineers must take every effort to identify and avoid pinch points: a similar approach applies to distillation (Section 10).



[Example 15 -- SO₂ absorption column \(video from Microsoft Stream\).](#)

Classically, distillation is one of the most important operations that the chemical engineer will consider, as it represents the primary method through which a complex, N-component feedstock can be separated for use throughout industrial applications. To appreciate the importance of distillation, consider that the absorption column treated in Section 9 represents a single vessel, in which two fluids are mixed to achieve equilibrium (necessitating the transfer of mass between both phases). Such an operation is similar to the single-stage thermodynamic "flash vessel" illustrated in Figure 1.2, where a new equilibrium condition (i.e. at the pressure and temperature within the vessel) requires components within the feed to split in to vapour or liquid outlets depending on their vapour pressure and degree of non-ideal interactions. As such, this single-stage flash can be considered as the simplest theoretical distillation operation, the purpose of which is to vaporise a finite amount of molecules from the feed. A basic single-stage flash model is shown in Figure 10.1, which is functionally comprised of a basic heat exchanger (such as a shell-and-tube discussed in Section 6), an expansion valve (typically treated as isenthalpic, as discussed in thermodynamics), and a single flash vessel (as per Figure 1.2). The extent of heating and subsequent pressure increase delivered by the shell-and-tube exchanger, alongside the extent of isenthalpic expansion (i.e. rapid pressure decrease) set by the valve, allow the engineer to control the pressure and temperature conditions of the flash vessel: Raoult's Law determines the equilibrium distribution of components in the vapour (y_D , referred to as the "distillate" product) and liquid (x_B , referred to as the "bottoms" product) exit streams.

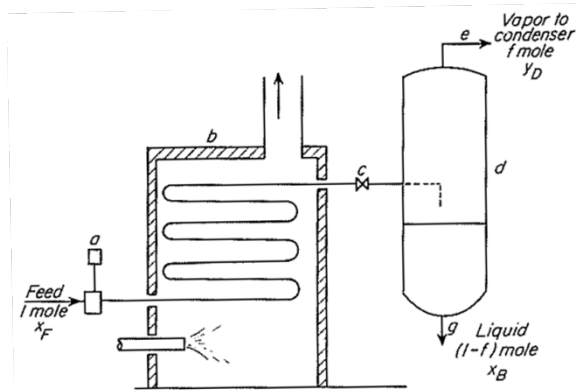


Figure 10.1 Illustration of a single-stage distillation, where the feed ("a") first passes through a basic heat exchanger ("b") before undergoing expansion across a valve ("c") at the inlet to the single-stage distillation column ("d"). Reproduced from McCabe, Smith and Harriott (7th Edition).

In designing a single-stage distillation unit, the feed composition is assumed to be well-known, where the distillate and bottoms product compositions are both unknown: as the solution basis is informed by Raoult's Law, which itself does not require knowledge of the molar flow rates involved, the engineer is able to first design the column on a nominal basis (for example, by considering 1 mole of feed). For the simplest application of a binary feed mixture (i.e. containing components "A" and "B"), the behaviour of each component in the flash vessel is characterised by its *relative volatility* (α), the definition of which can be expanded through Raoult's Law:

$$(Equation 10.1) \quad \alpha_{AB} = \frac{y_{Ae}/x_{Ae}}{y_{Be}/x_{Be}} = \frac{P_A^{sat} \gamma_A \phi_B}{P_B^{sat} \gamma_B \phi_A}$$

Relative volatility determines the extent to which the "lighter" component (A) will preferentially vaporise in the distillate product. For a binary mixture, the column performance can be

characterised with a balance on one component, where the lighter component is typically nominated. As shown in Figure 10.1, the distillate (i.e. vapour) molar flow rate can be presented as the "fraction vaporised" or f , which ranges from 0 to 100%: conversely, the bottoms (i.e. liquid) molar flow rate can then be represented by the quantity $(1 - f)$. With these definitions, the component material balance can be solved for the vapour mole fraction y :

$$(Equation 10.2) \quad y = \frac{\alpha x}{1 + (\alpha - 1)x}$$

which invokes the definition of relative volatility, as above. The enthalpy of feed, distillate, and bottom streams across the unit can also be balanced:

$$(Equation 10.3) \quad H_F = fH_y + (1 - f)H_x$$

In the example of a binary mixture, as shown in the $P - xy$ plane with Figure 10.2, the intersection of the nominated feed composition (vertical dashed blue line) and nominated flash pressure (horizontal dashed blue line) indicate the position of the feed in the two-phase region: this intersection *must* lie between the bubble and dew curves for a two-phase mixture to exist in the column, enabling components to separate according to their relative volatility (as per Equation 10.1). The solid red line in Figure 10.2 allows the engineer to determine the distillate and bottoms composition, based on the point of intersection with the dew curve (to obtain y_1) and bubble curve (to obtain x_1). For the example shown in Figure 10.2, the distillate product will be enriched in the lighter component (that is, "1") by around 7 mol%, while the bottoms product will be denuded in the lighter component by around 30 mol%.

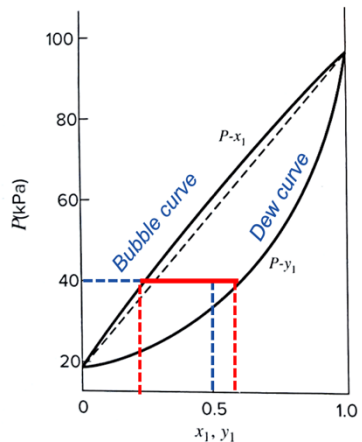


Figure 10.2 Representation of a single-stage flash operation in the $P - xy$ plane: a flash at 40 kPa with an equimolar feedstock will produce . Adapted from Smith, Van Ness, Abbott, and Swihart (8th Edition).

10.1 Multi-Stage Distillation

The illustration of a single equilibrium stage in Figure 10.2 explains a key limitation: if the engineer is seeking to generate a high purity of the lighter component (for example, $y_1 = 0.99$, as may be required in pharmaceutical manufacturing), a single feed position with less than 97 mol% of component "1" will not achieve this outcome. As the thermodynamic basis for the $P - xy$ diagram is immutable, the engineer who is presented with a dilute feedstock (e.g. 50 mol% component "1") is forced to consider how multiple flash stages in sequence might perform: similar to the conceptual framework of Figure 1.3, if the distillate product of the first equilibrium stage becomes the feedstock

to the next equilibrium stage, and so forth, the engineer can then consider N equilibrium stages in sequence to obtain the required outcome of $y_1 = 0.99$. Such is the basis for multi-stage distillation, within the example column shown in Figure 10.3. Critically, each "stage" of the column represents an equilibrium flash condition (thereby taking the independent flash tank from Figure 10.1 and collapsing it within a *stage*, which can be stacked atop any number of stages).

As vapour exits the top stage of the column (traditionally assigned the number "1," with stage numbers increasing downward), it is cooled in a condenser (as discussed in Section 7, using cold water or similar) and the resulting saturated liquid is collected in an accumulator. While Figure 10.3 includes a second cooling unit (labelled "E"), such an inclusion may only be required to satisfy downstream processing or unit operations. At the exit of the accumulator, a portion of the liquid is drawn off as the **distillate product** (also referred to as the "tops product" or "overhead product" as shown in Figure 10.3): critically, the engineer must nominate the fraction of the liquid that is *returned* to the column through the pump (labelled "F"), where this returned liquid stream is called the **reflux**. The ratio of the reflux on distillate product molar flowrates (that is, moles returned to the column on moles removed from the process) is called the **reflux ratio** (R_D). If the condenser removes *too much heat*, generating a subcooled liquid, the additional sensible heat removal must be considered in defining the reflux ratio: in this atypical design condition, $R_D = [L_c + \Delta L]/D$ where $\Delta L = [L_c C_p (T_{top,stage} - T_{reflux})]/\lambda$, which follows the basic definition from thermodynamics. As the reflux ratio decreases, the number of stages required to achieve the same degree of separation will increase. The placement of the feed stage controls the maximum enrichment of lighter components in the distillate product (that is, across stages within the *rectifying section*) and the maximum denuding of lighter components in the bottoms product (that is, across stages within the *stripping section*).

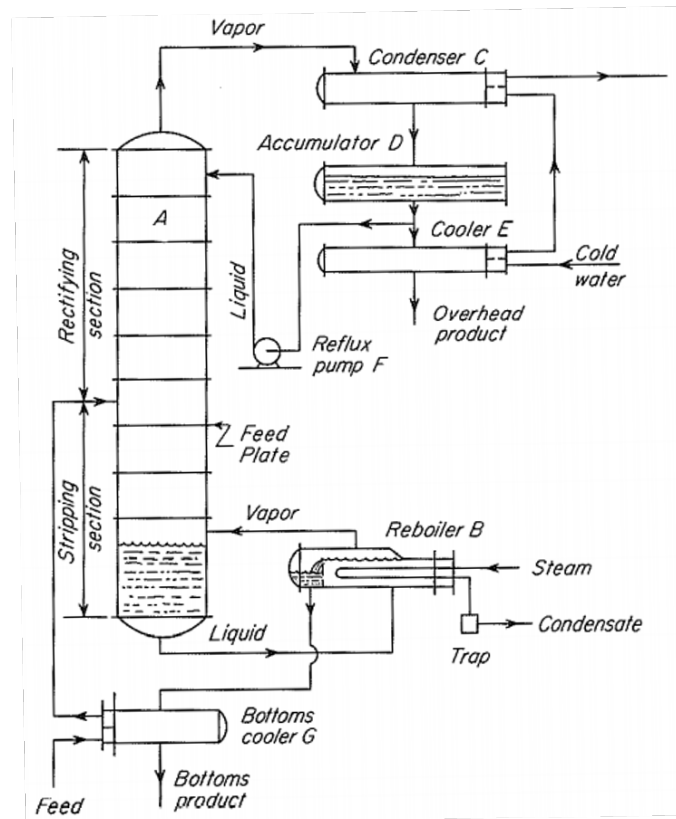


Figure 10.3 Illustration of a basic distillation column, configured for material feed in the middle stage of the column.
Reproduced from McCabe, Smith and Harriott (7th Edition).

In the bottom equilibrium stage of the column, liquid is drawn off and fed through a reboiler unit (labelled "B" in Figure 10.3), which can be heated with steam at various conditions (or alternative fluids) as discussed in Section 7. Critically, the engineer *can configure the reboiler in one of two ways*. A **full reboiler** is designed to completely vaporise the incoming liquid, returning all of it to the bottom equilibrium stage as vapour: in this configuration, the reboiler is *not* considered to operate as an equilibrium stage. Alternatively, a **partial reboiler** (which is pictured in Figure 10.3) requires a lower heating duty from steam or an alternative, because a portion of the stream is vaporised and returned to the column with the remaining portion taken drawn off as liquid to become the "bottoms product." In this second configuration, the reboiler *acts as a final equilibrium stage*. Notably, the final shell-and-tube heat exchanger improves the efficiency of the column, by using the warm bottoms product to heat the incoming feed: as the flowrates of both the incoming feed and bottoms product are set by the column design, the engineer must vary the surface area within the shell-and-tube exchanger to ensure the feed is preheated to the same (or very close) temperature as the stage on which the feed is to be injected.

Within the distillation column (labelled "A" in Figure 10.3), new material is fed first through a pre-heating stage (at the bottom of the diagram) where waste heat is exchanged from the warm, bottoms product of the column. After being warmed, the feed is then injected in any *one* of the column stages: Figure 10.3 shows the example of the "feed stage" placed in the centre of the column. Upon entering the column the feed experiences its first equilibrium flash, where lighter components are preferentially vapourised and heavier components *preferentially* (but not entirely) remain in the liquid phase. As each stage contains a weir, liquid remaining on the stage will spill down to the lower stage: conversely, the vapour exiting the equilibrium stage is permitted to flow upward to the next stage through the use of bubble caps (or similar). This process of liquid flow is illustrated in Figure 10.4, where the left-hand inset illustrates the industrial scale of such multi-stage columns (typically, between two and five stories in height).

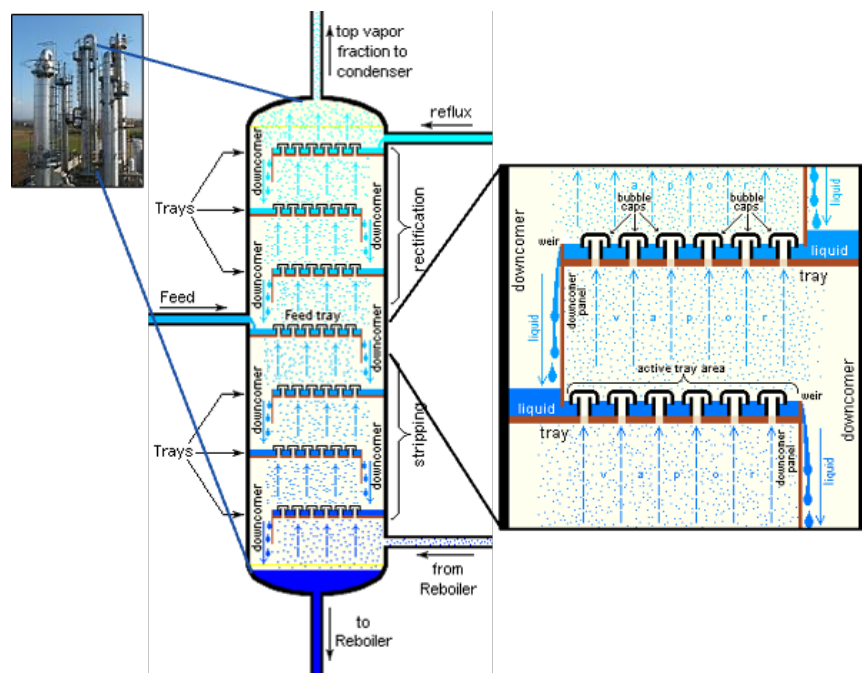


Figure 10.4 Illustration of internal column behaviour, including liquid and vapour behaviour for individual trays (right-hand inset), with an industry-scale distillation column pictured to the left. Adapted from Wikimedia Commons.

As each column stage is at a *different pressure and temperature condition*, this flow behaviour allows the vapour to be continually enriched in light components: the operation therefore empowers the engineer to take the feedstock with a dilute amount of the desired component (e.g. a few mol% of a pharmaceutical product), and reach the desired level of high purity (e.g. $y_1 = 0.99$) by gradually "stepping" the vapour product toward higher purity in the target component within each equilibrium stage. While there is typically a mild pressure distribution across the column, with higher pressures at the bottom due to the liquid inventory, *multi-stage distillation columns function by exploiting T-xy curves*, as shown in the example of Figure 10.5. In steady-state operation, the condenser at the top enforces the lower-temperature boundary by introducing the cold reflux stream to the top stage, while the reboiler enforces the higher-temperature boundary with hot vapour introduced on the bottom stage.

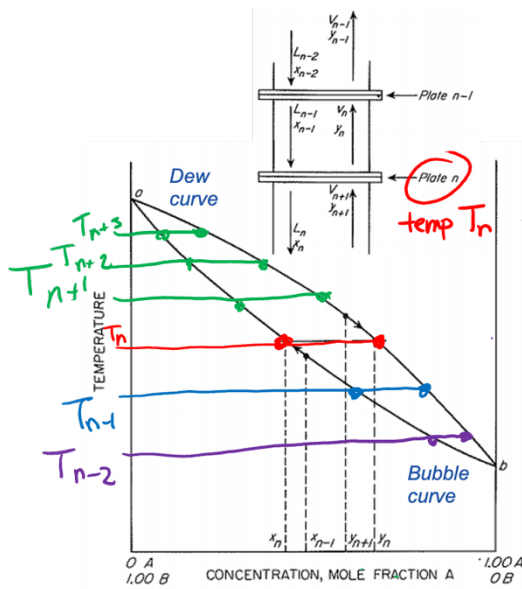


Figure 10.5 Representation of multiple distillation column stages in the $T - xy$ plane, where stages below the (red) feed stage are progressively warmer (denoted in green) while stages above the feed stage are progressively cooler (denoted in blue and purple). Adapted from McCabe, Smith and Harriott (7th Edition).

As illustrated in Figure 10.5, the nominal n^{th} stage, at a temperature of T_n , receives vapour from the stage below (at composition y_{n+1}) and liquid from the stage above (at composition x_{n-1}), respectively represented by the bottom-right green point and left-hand blue point in Figure 10.5. As the stage is operating at a different temperature to either T_{n+1} or T_{n-1} , the novel temperature of the stage (T_n) brings the fluids to a new equilibrium condition, where vapour and liquid compositions are y_n and x_n , respectively.

10.2 Column Design Parameters

For the engineer seeking to design a distillation column, with a knowledge of both the feedstock available and target product requirements, there are four key decisions that must be taken: (i) the number of stages in the column, including whether a partial or full reboiler should be used; (ii) the

location and *steady-state* flowrate of the feed; (ii) the reboiler duty and, consequently, set-point temperature; and (iv) the reflux ratio, which dictates the steady-state flow rate that can be expected in the overhead product. There are two methods available to design a multi-stage column: the use of steady-state simulation tools with integrated thermodynamic solvers, such as Aspen's HYSYS; and the manual McCabe-Thiele method. Importantly, these methods are not mutually exclusive, and should be used together to ensure the proposed column design -- itself representing one of the most expensive unit operations within industry -- is robust.

To deploy the McCabe-Thiele method, both overall and component material balances must be performed across the entire column, the rectifying section, and the stripping section. Following the nomenclature shown in Figure 10.6, the distillate molar flow rate is D (at composition x_D), the reflux molar flow rate is L_a (at composition $x_a = x_D$), the bottoms molar flow rate is B (at composition x_B), and vapour returns from the reboiler at molar flow rate V_b (with composition y_b). For each of the control surfaces shown in Figure 10.6, which are drawn across the rectifying and stripping sections, the component material balance must consider the in-flowing and out-flowing streams from the column itself: the control surfaces (or "system boundaries") can arbitrarily bisect column stages for the purpose of constructing component material balances, so long as the feed is not included in the treatment of either.

For the overall material balance across the entire unit operation (that is, $F = D + B$), for which the component material balance follows ($Fx_F = Dx_D + Bx_B$). Building upon this, Equations 10.4 and 10.5 respectively provide the component material balances for the rectifying and stripping control surfaces drawn in Figure 10.6:

$$(Equation 10.4) \quad Dx_D = V_a y_a - L_a x_a = V_{n+1} y_{n+1} - L_n x_n$$

$$(Equation 10.5) \quad Bx_B = L_b x_b - V_b y_b = L_m x_m - V_{m+1} y_{m+1}$$

with parallel overall balances for the rectifying ($D = V_a - L_a = V_{n+1} - L_n$) and stripping ($B = L_b - V_b = L_m - V_{m+1}$) sections.

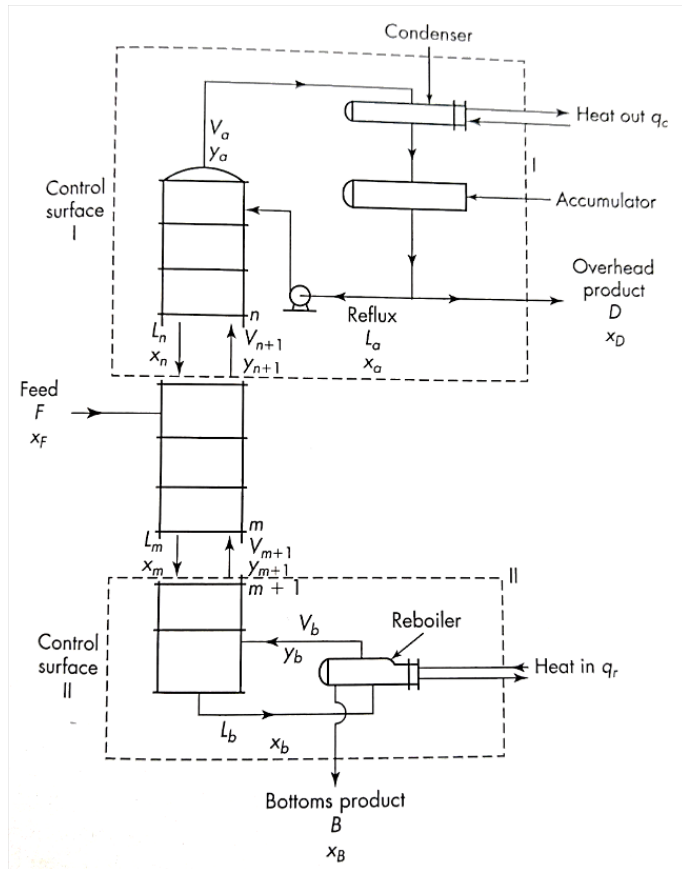


Figure 10.6 Basis for material balances in a multi-stage distillation column, where the top control surface (or "system") defines the rectifying operating line and the bottom control surface defines the stripping operating line. Reproduced from McCabe, Smith and Harriott (7th Edition).

Recalling the engineer's strategy for designing absorption columns -- in comparing thermodynamically-informed equilibrium curves with design-based operating line(s) -- the component material balance required rearrangement to the form $y = f(x)$ for reconciliation within the xy plane. The same treatment can be taken for Equations 10.4 and 10.5, where Equations 10.6 and 10.7 respectively represent the rectifying and stripping sections of the column:

$$(Equation 10.6) \quad y_{n+1} = \frac{L_n}{V_{n+1}} x_n + \frac{V_a y_a - L_a x_a}{V_{n+1}} = \frac{L_n}{L_n + D} x_n + \frac{D x_D}{L_n + D} = \frac{R_D}{R_D + 1} x_n + \frac{x_D}{R_D + 1}$$

$$(Equation 10.7) \quad y_{m+1} = \frac{L_m}{V_{m+1}} x_m - \frac{B x_m}{V_{m+1}} = \frac{L_m}{L_m - B} x_m - \frac{B x_b}{L_m - B} = \frac{\bar{L}}{\bar{L} - B} x_b - \frac{B x_b}{\bar{L} - B}$$

While the absorption column had *one* operating line, this treatment reveals that multi-stage distillation columns are characterised by having *two* operating lines. Equation 10.6 represents the *rectifying operating line*, for which the slope is always less than unity in the xy plane (analogous to the absorption operating line); conversely, Equation 10.7 represents the *stripping operating line*, for which the slope is always greater than unity in the xy plane. Critically, the boldface equalities in Equations 10.6 and 10.7 invoke the assumption of *constant molar overflow*: that is, the molar flowrates throughout the column are operating at *steady-state*. This assumption allows the engineer to simplify the form of the component material balances, but it is important to note that the assumption is *not* valid when (i) the column is being started up or shut down; or (ii) if the column is operated in batch mode, which will be discussed below.

In considering the **rectifying operating line**, the assumption of constant molal overflow allows for the substitution of the reflux ratio (R_D): as will be shown with the McCabe-Thiele method below, this introduction allows the engineer to conveniently consider how changes to the reflux ratio will affect the design parameters and performance of the column. This representation of the rectifying operating line further assumes the use of a total condenser (as has been drawn in Figures 10.3 and 10.6): as per Section 7, a "total" condenser will liquify the entirety of the incoming stream, while a "partial" condenser -- which is uncommon -- will function as another equilibrium stage, as the composition of the reflux (liquid) is different to that of the tops/distillate product. Similarly, the assumption of constant molal overflow simplifies the **stripping operating line** to consider the average liquid and vapor flow rates (\bar{L} and \bar{V} , respectively) in the stripping section: this treatment similarly assumes the tradition of a *partial reboiler* in the system, which functions as a single, ideal equilibrium stage. Only in very limited circumstances would a total reboiler be considered, as this would preclude taking a bottoms product from the column, thereby changing the liquid concentration in the bottoms over time and violating the assumption of constant molal overflow throughout the column.

Joining these two operating lines is one final consideration around how the feed (and its local equilibrium stage) should be handled. The so-called "feed line" (equivalent to an operating line) is given by Equation 10.8, which similarly follows the form $y = f(x)$ for representation in the xy plane, and requires knowledge of the feed composition (x_F) and *quality* (q , which must be determined from the options listed in Table 10.1).

$$(Equation 10.8) \quad y = -\frac{q}{1-q}x + \frac{x_F}{1-q}$$

Table 10.1. Characterisation of the feed quality in multi-stage distillation, reproduced from McCabe, Smith and Harriott (7th Edition).

Feed Condition	Consequence	Quality (q)
Subcooled Liquid ("cold feed")	Entire feed flows down, cooling liquid on stage	$q = 1 + \frac{C_p(T_{bub} - F)}{\lambda}$
Saturated Liquid (most common)	$\bar{V} = V$ and $\bar{L} = F + L$	$q = 1$
Partially Vaporised (two-phase)	Feed splits on entry stage (with vapour rising)	$q = \frac{H_{feed} - H_{liquid}}{H_{vapor} - H_{liquid}}$
Saturated Vapor	$V = \bar{V} + F$ and $L = \bar{L}$	$q = 0$
Superheated Vapor	Portion of liquid on stage vaporised to cool incoming feed	$q = \frac{-C_v(T_F - T_{Dew})}{\lambda}$

If the feed is between a saturated liquid and vapor, inclusive, quality follows a straight-forward definition from thermodynamics: note that the quality definition provided in Table 10.1 for two-phase feeds can equivalently be considered as the amount of mass in the vapor phase relative to the total mass of the feed mixture. For subcooled or superheated feeds, the quality is modified from the saturation boundary by approximating the energy of subcooling/superheating (that is, the product of heat capacity and differential temperature) relative to the enthalpy of vaporisation (λ). In general, subcooled or superheated feeds should be avoided in column design, but are important in column safety analyses where the feed may be off-specification for an unknown reason. As identified, saturated liquids are the most common feed condition. Once the feed quality is determined, the

molar flow rate in the rectifying and stripping sections is given by Equations 10.9 and 10.10, respectively:

$$(Equation 10.9) \quad V = \bar{V} + (1 - q)F$$

$$(Equation 10.10) \quad L = \bar{L} - qF$$

where \bar{V} and \bar{L} respectively represent the average molar flow rates in the rectifying and stripping columns in the absence of the feed, wherein the feed contributes qF to the molar flow rate of liquid and $(1 - q)F$ to the molar flow rate of vapour.

10.3 The McCabe-Thiele Method

The consideration of design parameters above functions to generate three coordinates in the xy plane: the rectifying operating line, the stripping operating line, and the feed line. The McCabe-Thiele method deploys these lines, alongside the equilibrium curve (similar to absorption) in the xy plane, as demonstrated by Figure 10.7. So-called McCabe-Thiele plots *also* include a manual line drawn on a 45-degree angle (that is, $y = x$ in the xy plane): as the method was originally drawn by hand, a square plot boundary is optimal.

There are five sequential steps to completing a McCabe-Thiele plot:

1. With the equilibrium curve and $y = x$ line drawn, identify the feed composition (that is x_F , representing the lighter component) *on* the $y = x$ line, and **draw the feed line toward** the equilibrium curve: the slope of this feed line is $-q/(1 - q)$, as dictated by Equation 10.8 and informed by Table 10.1.
2. **Draw the rectifying operating line** by identifying the ordinate (y-axis) intercept -- that is, $x_D/(R_D + 1)$ -- and connecting this point to the distillate composition required at coordinates (x_D, x_D) on the $y = x$ line.
3. **Draw the stripping operating line** by identifying the required bottoms product coordinates (x_B, x_B) on the $y = x$ line, and connecting this point to the existing intersection between the feed line and rectifying operating line.
4. If the **component material balances have not yet been solved**, the slopes of the rectifying and/or stripping operating lines can now be used to complete both: the slope of this line is equivalently defined by $R_D/(R_D + 1)$ or L/V , as shown in Equation 10.6; and the slope of this operating line is $\bar{L}/[\bar{L} - B]$ or equivalently \bar{L}/\bar{V} , as shown by Equation 10.7.
5. **Stair-step** from the distillate point (x_D, x_D) to the bottoms point (x_B, x_B) along the $y = x$ line, staying bounded between the equilibrium curve and the relevant operating line. First draw a horizontal line left from (x_D, x_D) to the equilibrium curve, followed by a vertical line downward to the rectifying operating line, followed by a horizontal line left to the equilibrium curve, and so forth. After crossing through the feed line, the stair-stepping continues, but obeys the stripping line. An example of this behaviour is shown in Figure 10.8.

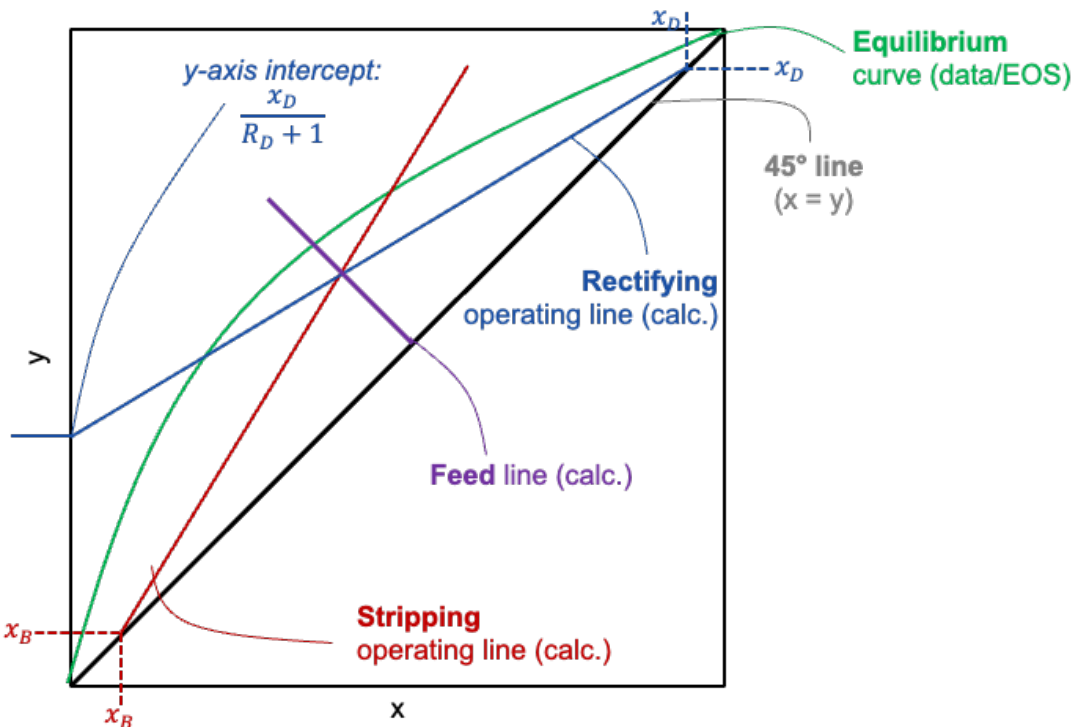


Figure 10.7 Example of the graphical McCabe-Thiele method setup for distillation column design.

The resultant McCabe-Thiele plot, as exemplified in Figure 10.8, is useful for two main purposes. It first informs the engineer *how many equilibrium stages are required in the column*, which would traditionally include the partial reboiler (noting the above discussion). As the example is drawn, six "stair-steps" are required before the bottoms composition has been reached by the last downward step: that is, *six equilibrium stages are required in the distillation column*. As equilibrium stages are constructed on an integer basis (one cannot have a "third of a stage" in a column), the integer number *after* crossing the bottoms composition is determined to be the correct number of stages. If there is a meaningful excess (e.g. half the stage is not necessary), the engineer may elect to modify the column conditions to generate an optimised solution. As the example in Figure 10.8 is drawn, the reflux ratio may be *decreased*, which would decrease the slope of the rectifying operating line and, critically, increase the distillate product molar flow rate (traditionally the product of value) in order to align the sixth stage precisely with the bottoms composition. Alternatively, a cheaper (or non-traditional) feedstock may be employed with *less* than 50 mol% of the light component, which would generate the same outcome. However, the engineer must remember that the McCabe-Thiele method returns the *ideal* number of stages: although a recently-fabricated column may operate near the ideal limit, the engineer should anticipate degraded performance in the primary unit operations over time (e.g. fouling in condensers or heat exchangers, as discussed in Section 7, or degradation/failure of bubble caps pictured in Figure 10.4). For this reason, the engineer may wish to acknowledge an "engineering margin" in the design of the column (that is, setting conditions such that only a portion of the final stage is required initially), thereby reducing the frequency with which maintenance operations would be required for the unit operations involved. Considerations of column efficiency are discussed below.

Second, the McCabe-Thiele plot indicates to the engineer the stage on which the feed should be placed for optimal performance, based on the "stair step" that encapsulates the intersection of the feed line and operating lines: the example in Figure 10.8 would indicate the feed should be placed

on the third stage (or tray) from the top of the column. Particularly in the case that an *existing* distillation column is being re-purposed, with limited-or-no ability to change the feed position, the McCabe-Thiele method allows the engineer to quickly assess those changes to the feed and operating conditions that will be required to match the column's physical construction.

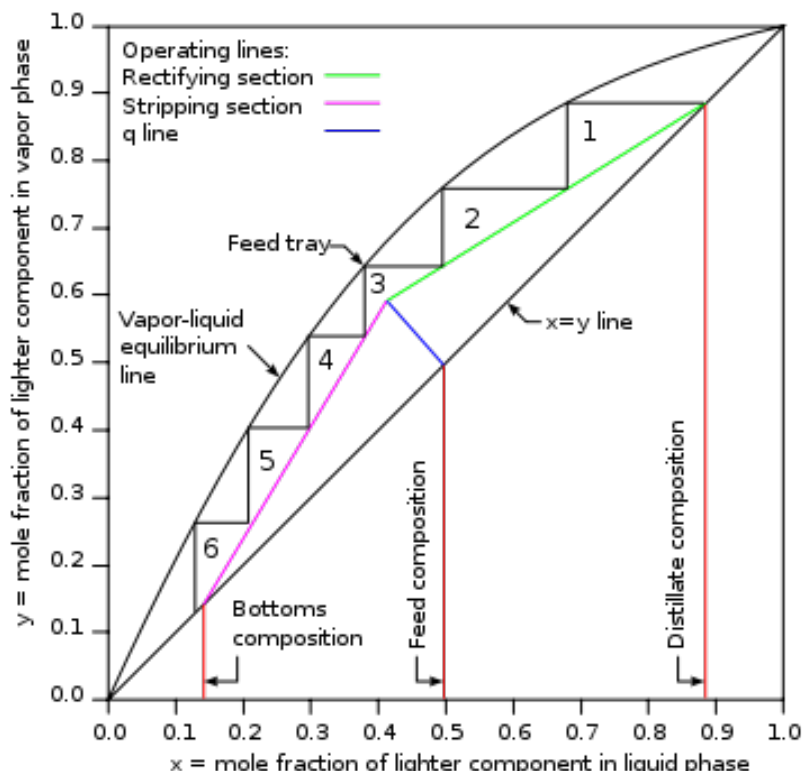
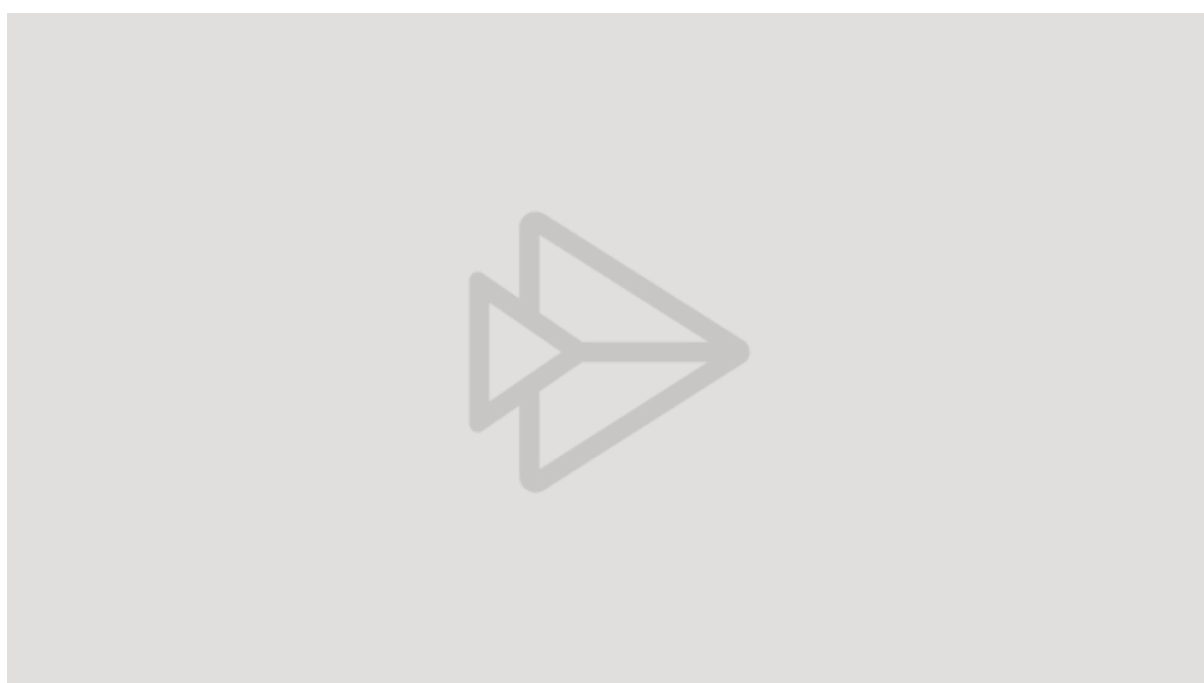


Figure 10.8 Example of a completed McCabe-Thiele analysis for a distillation column. Reproduced from Wikimedia Commons.



[Example 16 -- Deploying the McCabe-Thiele method \(video from Microsoft Stream\).](#)

In summary, the design of a new distillation system requires the engineer to consider two key questions:

1. **Feedstock:** the available supply (controlling overall size) and its composition (controlling the number of stages) should be established at the outset. Of course, the focus on recycling and reusing materials and feedstocks, alongside the growing research effort around the generation of biofuels (all of which *must* be purified by distillation) introduce new considerations as to whether existing or new processes may deliver lower overall environmental impact through the selection of alternative feedstocks.
2. **Objective:** while the discussion above has largely focussed on the distillate product out of tradition (as "heavy" components can occasionally be more easily purified through simple boiling processes), the engineer must establish the target (i) product quality and (ii) molar flowrate, which is of particular importance if the column outputs will act as a feedstock to other major processes.

If the column is already in operation, the engineer can also modify the McCabe-Thiele plot to account for the *actual* performance of the column relative to the ideal prediction. To achieve this, typically the individual stage/plate compositions are measured (termed y_n for efficiency analysis) and compared with the theoretical vapour composition at complete equilibrium (termed y_n^*). From this, the Murphree efficiency (η_M) can be determined through Equation 10.11:

$$(Equation 10.11) \quad \eta_M = \frac{y_n - y_{n+1}}{y_n^* - y_{n+1}}$$

where both real and theoretical compositions for the n^{th} stage are compared with the one below it. The Murphree efficiency is therefore bounded between 0 and 100%. It can be applied to the McCabe-Thiele diagram by introducing a *buffer* to the equilibrium curve (Figure 10.9): that is, each horizontal "step" ends prematurely and the vertical step is taken. That is, the length of each horizontal step (relative to the ideal step) is equal to the Murphree efficiency: for the example of a 90% Murphree efficiency on average in the column, each horizontal step would be 90% of the original length.

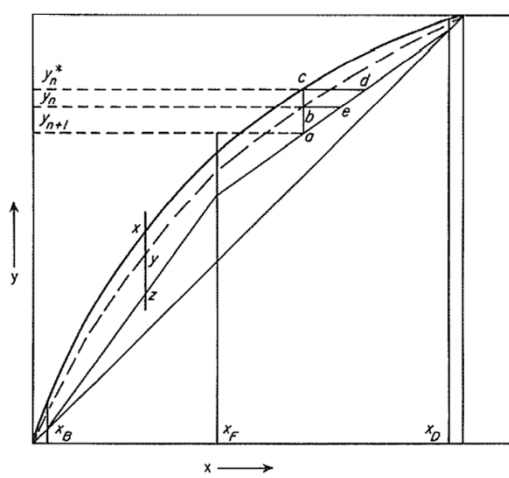


Figure 10.9 Basis for deploying Murphree efficiency in the McCabe-Thiele plot, where the equilibrium curve is drawn "inward" toward the $y = x$ line proportional to the departure from 100% efficiency. Reproduced from McCabe, Smith and Harriott (7th Edition).

10.4 Managing Reflux

After a distillation column has been fabricated, the engineer has a limited number of tools available with which to modify its operation: (i) changing condenser duty; (ii) changing reboiler duty; (iii) changing the feedstock; and (iv) modifying the reflux ratio. The former two options can significantly change the energy and operating cost requirements for the column, potentially rendering the operation economically unviable. The third option can be beneficial if the engineer identifies a better overall feedstock, but extreme changes can easily render the column unsuitable to the operation. In contrast, changing the reflux ratio allows the engineer the best degree of flexibility, both due to its relation to the McCabe-Thiele plot (i.e. the impact of proposed changes can quickly be assessed) and its natural requirement to change during start-up operations.

When a column started from rest, a **total reflux** condition is required, whereby *no distillate product outflow is taken* resulting in a reflux ratio of, by definition, infinity. Setting total reflux for column start-up minimises the time required to reach steady-state: while this may only take a few hours for a small column, large industrial columns can require weeks to reach steady-state operation. When total reflux is employed, the column should receive *no feed*, otherwise the total mass of material in the column would be increasing with time and again delay the time required to reach steady-state. In theory, a column operated at total reflux requires *the minimal number of equilibrium stages*: this condition forces both operating lines in Figure 10.7 to align with the $y = x$ line, where the McCabe-Thiele method can be used to assess the minimum number of stages required. If the species behave ideally, the Fenske equation can also be used to determine the minimum number of stages:

$$(Equation 10.12) \quad N_{min} = \frac{\ln[x_D(1-x_B)/x_B(1-x_D)]}{\ln \alpha_{AB}}$$

With these two conditions met, the engineer must then ensure that the reboiler is *filled* with liquid, as the reboiler will begin losing material after it reaches the boiling point of the liquid: as a note, reboilers should be equipped with a liquid level indicator (either visual or analytical), allowing the engineer to ensure heating tubes are fully submerged in liquid at all times (thereby avoiding safety hazards associated with locally superheating vapour). The reboiler duty should be increased to the point that nucleate boiling is observed on the first stage of the column: as discussed in Section 7.4, this represents a maximum efficiency condition for boiling, and wastes minimal energy in the reboiler. As liquid boils through to the bottom few stages of the column, the condenser can be started (typically at maximum duty, decreasing only after the full column has reached its final steady-state condition), so as to cool the metal housing and connected pipework in anticipation of the arriving (warm) vapour. During start-up, reboiler duty should be conservatively managed: as the lighter components vaporise, less material will be present in the reboiler and the effectiveness of the duty will increase (that is, for the same duty, a smaller amount of fluid will boil more aggressively than a larger amount of fluid).

As condensate begins to form in the condensation stage, and is fully directed back to the column by the total reflux condition, the remaining stages will begin to warm toward their steady-state condition (noting the physical plates, caps, and walls must themselves heat to the steady-state temperature). As steady-state behaviour is detected, both through constancy in the individual stage/plate temperatures and with minimal required adjustments to the reboiler duty, the feed flow rate in to the column can slowly be increased from zero. **Critically, the engineer should seek to maintain total mass within the column as feed is introduced during start-up**: this is accomplished through proportional increases in the feed and product flow rates (either only the distillate product flowrate for a total reboiler, or the distillate and bottoms product flowrates if a partial reboiler is used). The engineer will note column temperatures fluctuating away from their previous steady-

state condition as the feed and product flowrates are increased, indicating the successful distribution of new mass through the column. As the column was previously at steady-state with only internal recirculation, each increase in the feed flowrate introduces a process change to *each* stage in the column: thus, the column will require roughly the same amount of time to return to a steady-state condition following *each* change in feed flowrate (and subsequent decrease in the reflux ratio). Once the feed and product flowrates have reached their design specification, and steady-state has been re-established, the start-up operation has achieved **continuous distillation**.

Occasionally, the engineer may be required to consider **batch distillation**, where a finite volume of material will be heated in the reboiler until the maximum (practical) reboiler duty is unable to achieve boiling. Batch operations do not require a multi-stage column, which can be replaced with a single pipe connecting the reboiler vapour with the condenser inlet (in this scenario, the reboiler acts as the sole equilibrium stage). Batch operations typically require a very high relative volatility to be effective. If reflux is employed on a batch operation, the reflux ratio will also be required to *increase* with time to account for the denuding of the light component from the reboiler: otherwise, the engineer must account for the fact that the composition of the distillate product will change with time. For this reason, the assumption of constant molal overflow is not appropriate when a continuous distillation column is operated in batch mode, and the McCabe-Thiele diagram (Figure 10.7) is no longer applicable. While systems *designed* for batch distillation are much less expensive, as-designed continuous distillation columns should *never* be operated in a batch mode (unless absolutely required): as one heuristic, the cost of each industrial distillation column tray (equilibrium stage) is around that of a new luxury car. Considering an industrial column may require 15 or 20 stages for maximum performance, the purchase cost of the column itself can readily exceed multiple millions of dollars.

Minimum reflux represents the second bounding condition, alongside total reflux. At a minimum, the reflux ratio is decreased until the intersection of the feed and operating lines in Figure 10.7 takes place *on the equilibrium curve*. If the McCabe-Thiele method is attempted, the engineer will quickly find it is nearly impossible to determine the number of stages as there is insufficient space to "step" between the operating lines and equilibrium curve: in fact, an *infinite* number of equilibrium stages are required at minimum reflux. The minimum reflux ratio can be determined through Equation 10.13, where x' and y' represent the liquid and vapour mole fractions *at the point of intersection* between the operating/feed lines and the equilibrium curve:

$$(Equation 10.13) \quad R_{D,min} = \frac{x_D - y'}{y' - x'}$$

Appreciating the practical importance of total reflux for column start-up, calculating the minimum reflux ratio provides the engineer with bounding conditions for the reflux ratio during practical operation. In practice, the optimal reflux ratio is chosen based on the economics of the column operation, as shown in Figure 10.10. As the reflux ratio, fixed costs (e.g. capital purchases of equipment) decrease, while operating costs (such as condenser and reboiler duty) increase: the optimal reflux ratio lies at the minimum total of both cost curves, so long as this is above the minimum reflux ratio identified in Equation 10.13.

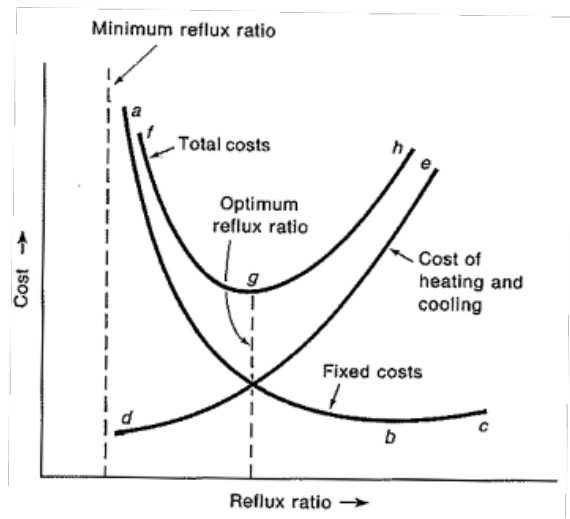


Figure 10.10 Theoretical basis for identifying the optimum reflux ratio in continuous distillation, by considering both fixed and variable costs of operation. Reproduced from McCabe, Smith and Harriott (7th Edition).

10.5 Multicomponent Distillation

In most instances, the chemical engineer will be presented with a diverse, multicomponent feedstock, where one or more components is of critical interest for a down-stream operation (e.g. as a pharmaceutical feedstock, where high purity is essential). Alternatively, the engineer may be seeking to purify a chemical of general interest (e.g. ethylene), with multiple feedstock options available: naturally, the fewer the components in the feedstock, the more expensive it will be. Thus, engineers often must consider how to manage the distillation with a large number of component, in order to deliver products of necessary purity at the lowest practical cost. As one extreme example, the distillation of crude oil to produce automotive petrol, jet fuel (kerosene), petrochemical feedstocks, bitumen, and so forth, typically requires on the order of 30 large (multi-storey height) distillation columns connected in series: the initial crude oil contains on the order of 10,000 individual components (beyond the current ability to characterise through advanced chemistry), exemplifying the approach to multicomponent distillation.

For any multicomponent system, the components (or component classes, for the example of crude oil) are arranged in order of vapour pressure. The engineer then determines the vapour pressure that will separate "light" components from "heavy" components: that is, components with higher vapour pressures will be progressively enriched in the distillate product (the higher the vapour pressure, the greater the enrichment), and will be progressively denuded in the bottoms product. When arranged in order of vapour pressure, the component *immediately lighter* than the as-decided vapour pressure is deemed the "light key," while the component *immediately heavier* is deemed the "heavy key." In the first instance, these two "keys" can be treated as a binary mixture for the purpose of deploying the McCabe-Thiele method, where the method will require a substantial engineering margin to account for the diversity of components and any unique fouling behaviour they may engender (e.g. bitumen-class components can readily precipitate and foul reboilers, if the temperature is off-specification). Simulation tools, such as Aspen's HYSYS, are ideal for such situations, as they enable the engineer to incorporate per-component (or per-component class) thermophysical properties, ultimately reducing the engineering margin associated with the design.

If a multi-component system is to be handled manually, the engineer must determine the "K-factor" for each component (also referred to as a "distribution coefficient" in some thermodynamic literature):

$$(Equation\ 10.14)\ K_i = \frac{y_{i,e}}{x_{i,e}} = \frac{\gamma_i P_i^{sat}}{\phi_i P}$$

where the definition of the factor is expanded on the right-hand side using the gamma-phi formulation of Raoult's Law. Of course, Raoult's Law may be simplified to enable tractable calculations, in the limit that activity and/or fugacity coefficient calculations are unable to be resolved. However, the historical use of K-factors has provided for a number of studies in the peer-reviewed and reference literature, to the point that component classes (e.g. the C₂₀-C₂₅ fraction of a traditional crude oil) have reference K-factors as a function of temperature and pressure. Interestingly, comparing the definition of the K-factor with that of relative volatility (Equation 10.1) reveals that, in a *binary* system, the relative volatility is the ratio of the light-on-heavy component K-factors.

Once K-factors are calculated with any necessary assumptions, they can be incorporated in bubble-point (Equation 10.15) or dew-point (Equation 10.16) calculations by manipulating the left-hand two equalities in Equation 10.14:

$$(Equation\ 10.15)\ \sum_{i=1}^{N_c} y_i = \sum_{i=1}^{N_c} K_i x_i = 1$$

$$(Equation\ 10.16)\ \sum_{i=1}^{N_c} x_i = \sum_{i=1}^{N_c} \frac{y_i}{K_i} = 1$$

As with binary systems, both bubble point and dew point calculations that incorporate K-factors must sum to unity. In both cases, the K-factors are themselves direct functions of pressure and temperature: as such, operating conditions can be varied to maintain unity in the summation (i.e. solving temperature for set pressure, or vice versa).



[**Example 17 -- Calculating dew and bubble points in multi-component systems \(video from Microsoft Stream\).**](#)

As defined in the context of Raoult's Law (Equation 10.14), K-factors can also be incorporated in single- or multi-stage flash calculations for multi-component systems. For a single-stage flash

discussed at the beginning of this section, the relationship between distillate and bottoms composition (that is, y_{Di} and x_{Bi}) is provided in Equation 10.17 as a function of the fraction (on a molar basis) of the feed vaporised, f :

$$(Equation 10.17) \quad y_{Di} = \frac{x_{Fi}}{f} - \left(\frac{1-f}{f} \right) x_{Bi}$$

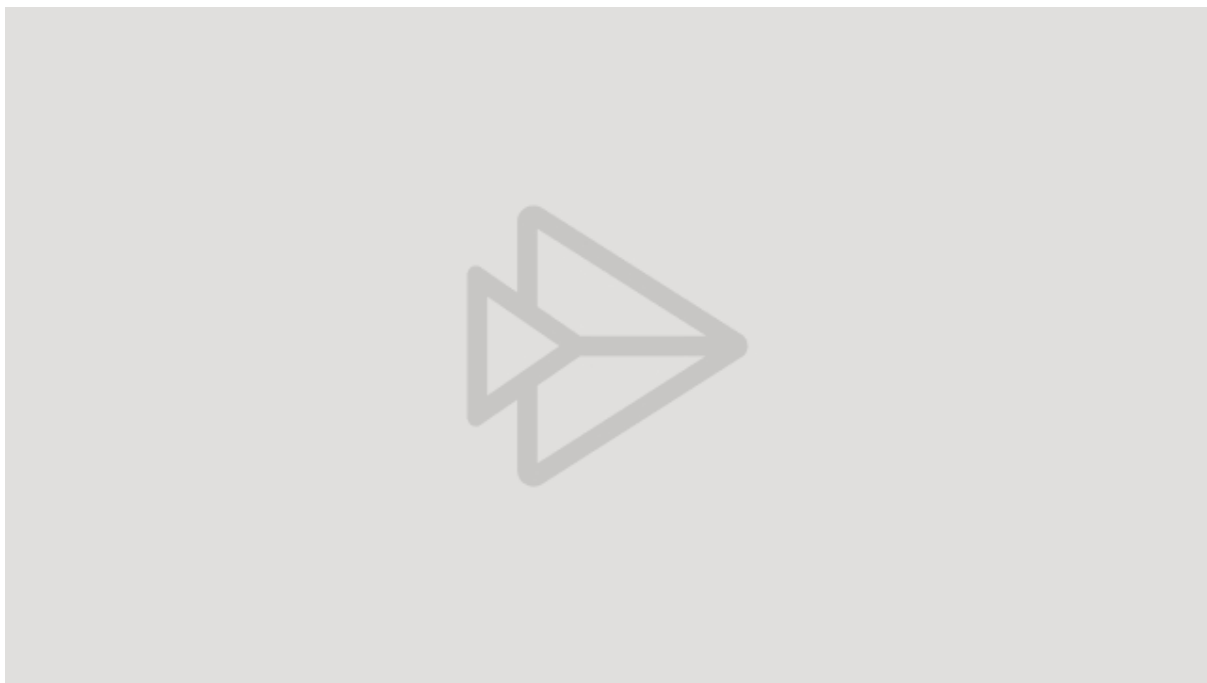
which can also be re-written in terms of the K-factor for the i^{th} component:

$$(Equation 10.18) \quad \frac{y_{Di}}{x_{Bi}} \equiv K_i = \frac{1}{f} \left(\frac{x_{Fi}}{x_{Bi}} + f - 1 \right)$$

Within a single flash stage, the amount of material vaporised (f) must first be solved to complete the overall material balance, enabling solution of the component material balances. Therefore, Equation 10.18 can be re-arranged to solve for the bottoms composition, which can then be *summed* to equal unity (by definition):

$$(Equation 10.19). \quad \sum_{i=1}^{N_c} x_{Bi} = \mathbf{1} = \sum_{i=1}^{N_c} \frac{x_{Fi}}{1+f(K_i-1)}$$

where the boldface portion of the expression is referred to as the Rachford-Rice equation. To use Equation 10.19, the engineer must only know the composition of components in the feed, pressure, and temperature, which enable calculation of the K-factors (with or without assumptions) to *iteratively* solve for the singular unknown (f) present in each term of the summation. Once this term is resolved, the component material balances can be solved for the unknowns (in order, x_{Bi} in Equation 10.18, and y_{Di} in Equation 10.17). Although beyond the scope of this discussion, the same K-factor approach can be deployed in multi-stage flash calculations, with the appreciation that the rectifying and stripping operating lines emerge by rearranging component mass balances (previously devoid of the K-factor).



Example 18 -- Multi-component single-stage flash (video from Microsoft Stream).

The unit operations discussed heretofore have all deployed an equilibrium design basis, whereby engineers must often invoke the assumption that steady-state operations are at equilibrium: although imperfect, such an assumption tends to hold true, as systems without variation in time are (more fundamentally) assumed to be absent of unresolved driving forces within the Gibbs energy landscape. Conversely, adsorption processes *cannot* be considered to be a steady-state process, as the adsorbing phase involved undergoes a physical change and subsequently regenerated before it is available for further adsorption. An exemplar adsorption process is in Figure 11.1, wherein mobile molecules in a fluid phase (in this case, CO₂) interact with and ultimately *bind to* (that is, "adsorb") to a physical solid: after adsorption, the molecules generally remain immobile until they are removed by chemical, physical, or thermodynamic (i.e. varying pressure or temperature) means.

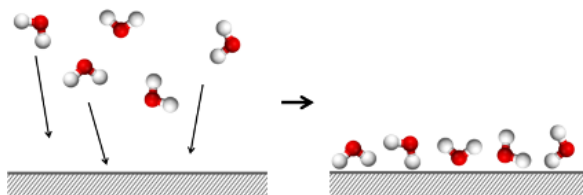


Figure 11.1 (left) Mobile molecules in the fluid phase adsorb by (right) binding to specific sites on the adsorbent material. Reproduced from Wikimedia Commons.

The extent of material that *can* adsorb in a given system is therefore dictated by the availability of adsorption *sites* that are appropriate for the fluid-phase molecules available: the example of Figure 11.1 illustrates five adsorption sites that become occupied. At the highest level, the subdiscipline of adsorption considers two fundamental types: chemisorption, where mobile molecules form chemical bonds with available sites on the adsorbent material; and physisorption, where mobile molecules remain bound through van der Waals-type interactions with the adsorbent material. Chemisorption is generally an irreversible process where only one molecule can interact per site (forming a so-called "monolayer" on the surface), making it ill-suited for unit operations. Conversely, physisorption is a reversible process, with (typically) minimal activation energy that makes it ideal for unit operations wherein significant numbers of molecules require separation. Fundamentally, both chemisorption and physisorption are informed by a minimum in Gibbs free energy for a molecule whose interaction is maintained at some nominal position from the surface of interest: as chemisorption relies on bond formation, the "depth" of the Gibbs energy well is much larger than that of physisorption, and the potential well typically occurs at much smaller distances. Fundamentally, the nature of a "lower Gibbs Energy" (where $\Delta G = \Delta H + T\Delta S$) means that the *change in enthalpy due to adsorption must be negative, as the change in entropy must be positive*: further, the appreciation of a negative differential Gibbs energy (that is, due to the adsorption process) indicates the process will occur *spontaneously*.

While the discussion below focusses on typical adsorption processes, such as capturing CO₂ from air, it is worth noting that adsorption processes play a critical role throughout chemical engineering and the broader industry. For example, the protection of metals from corrosion (oxidation) can be accomplished through electrochemistry with a sacrificial anode, and can be accomplished through the use of film-forming corrosion inhibitors (FFCIs), which are small surfactant molecules designed with dual affinity for both the metallic surface and the fluid in which they are immersed: specifically, FFCIs *adsorb* to available sites on the metal through the same conceptual mechanism in Figure 11.1, thereby introducing a barrier through which oxygen molecules cannot pass to facilitate further corrosion. Similarly, household soaps (e.g. dish soap) are surfactants -- where one half of the molecule prefers to engage with organic matter, including dirt, and the other half prefers to engage with water -- that *adsorb* to organic particles on the same basis as Figure 11.1, allowing the (dirt)

particle to migrate through the water phase with minimal inhibition. While the design and performance of surfactants is not within the remit of this curriculum, they highlight an important (and fully distinct) application of adsorption science that is found in most industrial processes.

In most applications of chemical engineering, adsorption is used to remove toxic or unwanted components from a process stream: for example, these may include organic (i.e. hydrocarbon) solvents used to generate paints, inks solutions, or fabrics; environmental pollutants such as CO₂ and H₂S; or ecotoxic components that must be removed from drinking water. Historically, such adsorbent materials, perhaps quite appropriately, are referred to as "molecular sieves" for their ability to separate nitrogen from oxygen. One such example is the removal of methane -- a greenhouse gas with *extreme* global warming potential, when compared to CO₂ -- from vent gasses, wherein the methane is not in sufficient concentration so as to be useful. Through a team led by UWA, a new class of zeolite (one such absorbent material) was discovered, which enabled the removal of methane from the vent gas stream with such an unusually high selectivity, that regenerating the zeolite bed produces a high-purity methane stream (e.g. as may be required in power plants). Such a recent discovery illustrates the role of adsorption as a high-activity research domain, when compared with earlier mass transfer techniques (such as absorption). Similar zeolites are commonly used to remove water content from natural gas, enabling its liquefaction.

11.1 Adsorption Columns

Distinguishable from other mass transfer operations, the fact that adsorption processes are inherently operated in a transient (that is, time-varying) manner requires any steady-state deployment to have two adsorption units: one that is actively adsorbing material, with a second that is being regenerated (through desorption of the adsorbed material). The basic design of an adsorption column is shown in Figure 11.2, wherein the feed (gas) is connected to both adsorption units, and the operator or control system must nominate the adsorption unit to which the feed should flow. As packed, these materials are supported by a perforated plate that allows vapour flow in to, or out from, the bed: during the adsorption process, the downward flow of gas is typically preferred, as this eliminates any concern of bed fluidisation (as discussed in Sections 4 and 9). If the adsorption material is selected, and the system proportioned, correctly, the target molecule(s) will be fully removed from the feed gas, such that it leaves the adsorption units as "clean gas" on the bottom, left-hand side of Figure 11.2.

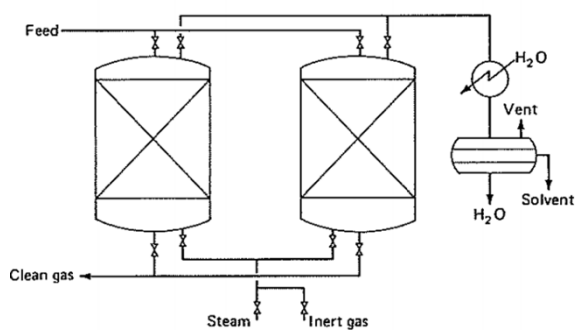


Figure 11.2 Illustration of a basic adsorption system, with the example of using warm steam for the regeneration of saturated adsorbate material. Reproduced from McCabe, Smith and Harriott (7th Edition).

In most cases, adsorption materials (that fill the beds) are regenerated at high temperature. From a chemical perspective, one might imagine that the relatively weak (when compared to covalent bonds) van der Waals forces binding the adsorbed molecule to the surface can easily be

overwhelmed by the kinetic energy of the adsorbed molecule itself. As such, increasing the temperature of the entire system results naturally in energy being distributed through translational, rotational (as available), and vibrational energy levels within the adsorbed molecules, where only a minor increase in the translational energy is required to overwhelm the van der Waals interaction that binds the adsorbed molecule to the adsorbate material (as in the right-hand side of Figure 11.1). To this end, steam is commonly used to regenerate adsorption units that operate at ambient (room) temperature: this configuration is referred to as **temperature swing adsorption (TSA)**, indicating the temperature of the column is varied to initiate the desorption (bed "regeneration") process. For adsorption beds typically between 0.3 and 1.0 m in length, the **cycle time** -- that is, the amount of time required to fully saturate and regenerate the bed -- is between 2 and 24 hours, depending on the material selected and concentration of target component in the vapour phase. One alternative to TSA is **pressure swing adsorption (PSA)**, where beds are operated at relatively constant temperature and system pressure is varied to control whether molecules adsorb (i.e. at high pressure) or desorb from the material: in the above research example of a methane capture zeolite, PSA was used as a basis for the column design, as this yielded much greater capture efficiencies than the alternative (TSA).

Figure 11.2 is based on TSA, where steam exiting the top of the adsorption units (containing the adsorbed material in dilute quantities) is arbitrarily passed through a water-cooled condenser and collection unit, where the adsorbed material exits (labelled "solvent," although it may well be any material) separate to the liquid water. Of course, if the adsorbed material is fully soluble in the aqueous phase, only one liquid would exit the post-condenser collection unit. In select applications, such as the novel methane-selective adsorbate described above, pressurised adsorbate beds may be used to control the adsorbing and desorbing processes. For example, the adsorption of methane may take place at a moderate pressure (e.g. 5 bar), after which the bed is depressurised (to any pressure condition, including vacuum) in order to initiate desorption.

Each adsorption unit (as pictured in Figure 11.2) is filled with some *adsorbate material*, typically in the form of small (1 mm or less) particles that are randomly packed to a height of at least 1 m (although industrial applications may deploy much larger systems). If the feed stream is assumed to contain an inert (that is, non-adsorbing) fluid containing at least one **dilute** species *capable* of adsorbing to the solid phase, the contact of the feed and adsorbate will result in rapid adsorption of the dilute species within the first layer of particles in the column. As the finite adsorption sites within this first layer become saturated (transitioning from the left- to right-hand panels of Figure 11.1), their *capacity* to adsorb more of the dilute species goes to zero: with the continued flow of fresh feed gas, the dilute species will next adsorb in the second layer of particles, and so forth. Thus, the adsorbing bed will become *saturated* over time, wherein the final layer of particles no longer retains available adsorption sites. This process is represented separately in space (i.e. as a function of the adsorbate bed length, L) and time in Figure 11.3, where the left-hand panel is traditionally referred to as a "profile plot" (with each curve representing different time points) and the right-hand panel is referred to as a "trend plot" (representing the temporal evolution of a single point in space). In both plots, the ordinate is the local (that is, in space and time) concentration of the target component(s) in the gas phase, normalised by the concentration of the component in the feedstock: thus, if the adsorbate is intended to remove 5 mol% of CO₂ from a flue gas, an absolute measurement of 2.5 mol% CO₂ corresponds to an ordinate value of $c/c_0 = 0.5$.

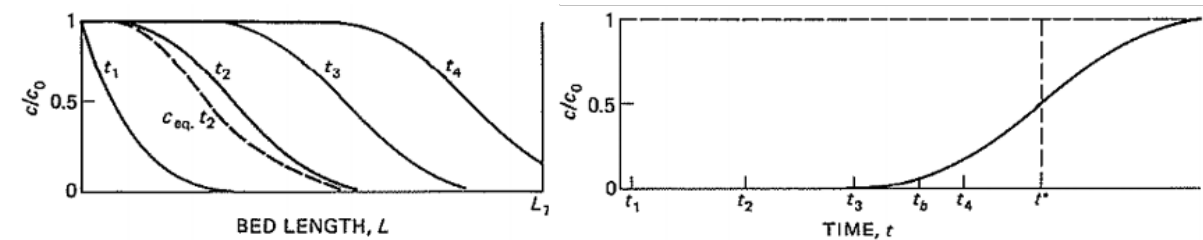


Figure 11.3 (left panel) Illustration of the adsorbate bed capacity evolving with flow over time. (right panel) Observation of the "breakthrough" of the target component in the end of the bed, indicating the adsorbate is fully saturated at time t^* . Reproduced from McCabe, Smith and Harriott (7th Edition).

The left-hand panel of Figure 11.3 illustrates that, at the time flow is initiated (t_1), the target will rapidly be depleted in the initial portion of the bed. However, the adsorbate material that contacts feed at the location $c/c_0 = 1.0$ will quickly become saturated (perhaps corresponding to the first 0.1% of the bed length, as pictured): at the next time point (t_2), the initial part of the bed is unable to remove any target component, so its concentration remains unchanged through that portion (that is, $c/c_0 = 1.0$). The target component is only denuded from the gas phase as it contacts fresh adsorbate material, approximately 15% through the bed length at t_2 . This process continues until the *end* of the bed (where $L = L_1$) is exposed to a non-zero concentration of the target component (corresponding to time t_3 in the right-hand panel of Figure 11.3). If the bed continues to operate, the target component concentration at the end of the bed will continue to increase monotonically until the outflowing gas is identical to the feed gas (that is, $c/c_0 = 1.0$). While the engineer may choose to cease flow in the adsorption bed at any point after break-through (that is, t_3), a traditional approach would maintain flow until time t^* , at which point $c/c_0 = 0.5$: it is worth noting that this condition may be unacceptable for highly toxic components, such as H_2S , that cannot be exposed to the environment in any concentration.

In considering time t_3 in left-hand panel of Figure 11.3, the bed length *between* which the component concentration diverges from unity and remains non-zero is considered to be the **mass transfer zone** (MTZ): in practice, uncertainty in both measurement and the surface area of randomly-packed particles necessitate a MTZ boundary of between 5 and 95% in concentration. In considering this definition ($0.05 < c/c_0 < 0.95$), the left-hand panel of Figure 11.3 further illustrates that the MTZ migrates from the top to the bottom of the bed through time (that is, from t_1 to t_4). For each combination of adsorbate material and target component, the *width* of the MTZ can change: this comparison is illustrated in Figure 11.4, where a wide MTZ will both reach the breakthrough time (t_b) sooner and require a longer time to reach saturation (t^*). For highly sensitive materials, flow may be diverted to the "fresh" (i.e. regenerated) adsorbate bed at the breakthrough time: however, the engineer may choose to only divert flow later in the process (e.g. at t^*) if the target material is not environmentally sensitive. As such, the selection of materials with a *narrow* MTZ is preferred, as they both increase the efficiency, and decrease the costs, of the overall process.

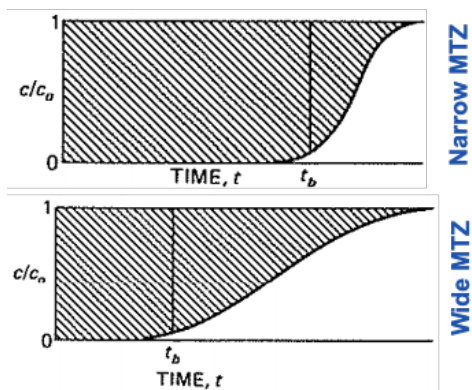


Figure 11.4 Illustration of the breakthrough curve for an adsorbing system with (top) a narrow MTZ and (bottom) a wide MTZ.

Reproduced from McCabe, Smith and Harriott (7th Edition).

As the breakthrough curve maintains an "S-shape," integration of the curve can be considered through the rectangle between $t = 0$ and $t = t^*$, which represents the **total solute adsorbed** in the process. While the characterisation of adsorbate materials most often requires laboratory or pilot-scale data, the idealised breakthrough curve is given by Equation 11.1:

$$(Equation 11.1) \quad t^* = \frac{L\rho_b(W_{sat} - W_0)}{u_0 c_0}$$

where ρ_b is the bulk density of the bed, W_{sat} and W_0 represent the respective loadings of material *in situ* and initially, u_0 is the inlet fluid velocity, and c_0 is the concentration of target (loading) material in the fluid feed. For a fully regenerated adsorbate material, W_0 is equal to zero: thus, only the *saturation* capacity is required to inform Equation 11.1, as may be accessed through integration of the shaded regions in Figure 11.4.

In some industrial applications, the complication of a time-dependent mass transfer process can be overcome by designing a mechanical system that conveys "saturated" adsorbate from the adsorption bed to the desorption bed. Such an arrangement is shown in Figure 11.5, with the relevant operating and equilibrium lines shown in the right-hand panel. Although reliant on additional considerations of the mechanical conveyer, this allows the engineer to design the beds for continuous flow: such a basis may be critical if the process is intended to purify gas for, or from, a second unit operation. In Figure 11.5, the migration of regenerated adsorbate (i.e. at the bottom of the desorber) would physically migrate via gravity to the top of the adsorber column, where it is contacted with the feed gas in a counter-flow arrangement. In this arrangement, the McCabe-Thiele visual design basis can be used to determine the "ideal" number of stages (or, more precisely, "transfer units" of packed material) in the system.

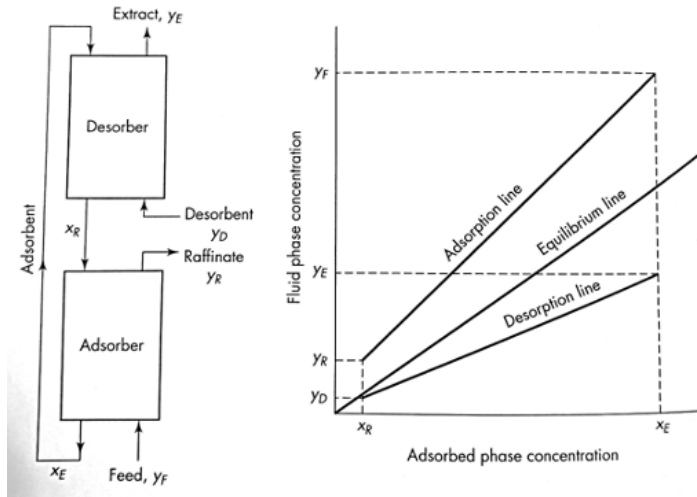


Figure 11.5. (left) Simple process diagram for a continuous adsorption system, where saturated adsorbate is physically moved on a conveyor to the desorption bed. (Right) Combinatorial adsorption, desorption, and equilibrium "lines" in the xy plane, as an adaptation of the absorption process treatment. Reproduced from McCabe, Smith and Harriott (7th Edition).

11.2 Adsorption Isotherms

With knowledge of the target component to be adsorbed, the engineer must only determine the appropriate adsorbate material and the dimensions of the bed in which it is used, where the maximum material loading (W_{sat}) is related to both the bed dimensions and residence time required for saturation. As such, characterisation of the adsorbate material is the primary focus of the selection process: the **adsorption isotherm** relates the mass of target material that can be captured (per mass of adsorbate) relative to the *concentration* of the target material in the fluid phase. Example isotherms are provided in Figure 11.6, wherein a "linear" isotherm indicates the effectiveness of the adsorption process increases directly with the concentration of the target component, and "irreversible" adsorption indicates the capacity of the material is *independent* of the target component concentration. Generally, engineers will choose to focus on materials with favourable or strongly favourable adsorption characteristics, which can adsorb a meaningful amount of material even when it is present at highly dilute concentrations: conversely, *unfavourable* isotherms are to be avoided, as increasing concentrations of the target material have a minimal effect on the adsorption process.

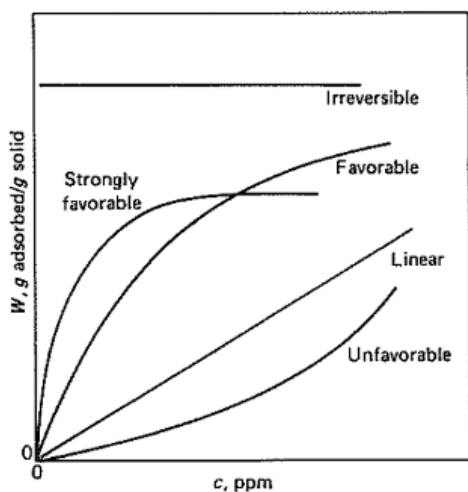


Figure 11.6 Illustration of theoretical adsorption isotherm types. Reproduced from McCabe, Smith and Harriott (7th Edition).

The *favourable* curve modelled in Figure 11.5 is traditionally represented by the **Langmuir isotherm**:

$$(Equation 11.2) \quad W = W_{max} \left(\frac{K \cdot c}{1 + K \cdot c} \right)$$

where W is the expected adsorption capacity (in *g adsorbed per g of adsorbent solid*), W_{max} is the maximum adsorbate loading as the component concentration approaches infinity, c is the expected concentration of target species in the system, and K is the adsorption constant (typically called the "Langmuir constant") of the material. As such, the engineer typically requires only two pieces of information to consider how an adsorbate material will perform: its maximum loading and the Langmuir constant. For the rare solids that demonstrate *strongly favourable* adsorption, the Freundlich equation may be used:

$$(Equation 11.3) \quad W = b \cdot c^m$$

where two adsorption constants (b and m) are required for the material characterisation. Examples of solid dessicants are shown in Figure 11.7, as adsorbent materials designed to remove water (i.e. humidity) from air: as practical implementations, these illustrate that the adsorbent may not follow a precise model isotherm as shown in Figure 11.6, but may rather follow different isotherm behaviours within different concentration ranges. For example, the performance of silica gel in Figure 11.7 is linear with water concentration through approximately 50% relative humidity, but follows a "favorable" model isotherm behaviour thereafter. Conversely, the "molecular sieve" is a close representation of irreversible adsorption, wherein the engineer would require significant effort to desorb the water: this behaviour occurs due to the extremely low pore volume (and resultant capacity) of molecular sieves, which are only deployed in select (e.g. high-temperature) industrial processes.

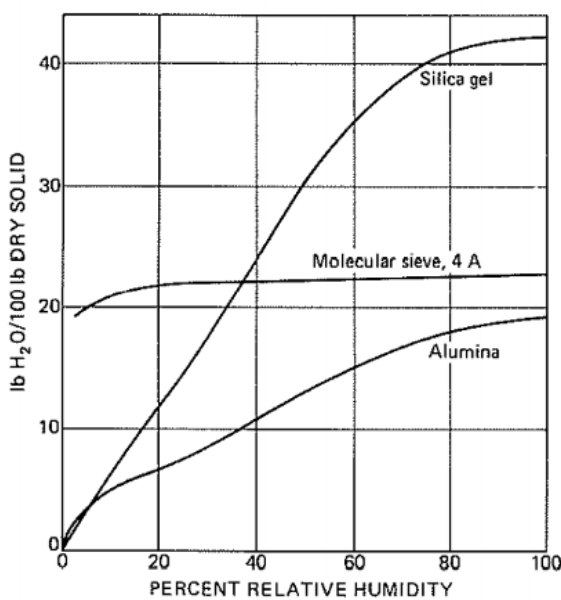


Figure 11.7 Example performance of three water adsorbates as a function of relative humidity. Reproduced from McCabe, Smith and Harriott (7th Edition).

11.3 Transient Mass Transfer Rates

As adsorption cannot be brought to steady state, it limits the application of traditional rate equations. As discussed in Section 8, the mathematical treatment of transient rates is typically complex, as the required solutions must describe both spatial and temporal conditions. In the case of adsorption, an infinitesimal cross-section (of length dL) of the bed is considered, as pictured in Figure 11.8.

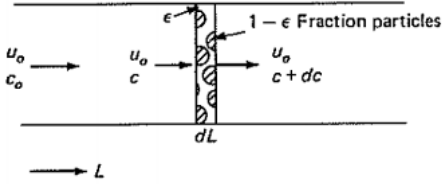


Figure 11.8 Model framework for considering transient mass transfer in adsorption. Reproduced from McCabe, Smith and Harriott (7th Edition).

For the highlighted cross-section in Figure 11.7, with void fraction ϵ (and particle fraction $1 - \epsilon$), the overall material balance may be written:

$$(Equation 11.4) \quad \epsilon \frac{\partial c}{\partial t} + (1 - \epsilon) \rho_p \frac{\partial w}{\partial t} = -u_0 \frac{\partial c}{\partial L}$$

where concentration changes with time and space, *and* capacity changes with time. As is typical in partial differential equations, one such approach is to approximate the *driving force* for mass transfer (that is, the terms $\frac{\partial c}{\partial t}$ and $\frac{\partial c}{\partial L}$) with an *overall* driving force (given by $c - c^*$, where c is the local concentration of the component and c^* is the concentration after the local adsorption process reaches saturation):

$$(Equation 11.5) \quad \rho_b (1 - \epsilon) \frac{\partial w}{\partial t} = K_c a (c - c^*)$$

This approximation used within Equation 11.5 allows for a simplification to only one partial differential term -- how the capacity of the bed changes with time (or, in other words, the full solution to the right-hand panel of Figure 11.3). To solve equation 11.5, the engineer can deduce the local concentration at saturation (c^*) through experimentation with breakthrough (similar to Figure 11.4), and may approximate the overall mass transfer resistance (K_c) as:

$$(Equation 11.6) \quad \frac{1}{K_c} \approx \frac{1}{k_{c,ext}} + \frac{1}{k_{c,int}} \approx \frac{1}{k_{c,ext}} + \frac{D_p}{10 D_e}$$

where the Sherwood relation for external spheres (given in Equation 8.27) can be used to inform $k_{c,ext}$, D_p represents the adsorbate particle size, and D_e is the effective diffusion coefficient through the bed (varying with porosity and pore diameter). While Equations 11.5 and 11.6 can be used in concert to provide an *approximate* solution to Equation 11.4, the formal solution -- as is an established practice to solve partial differential equations -- requires the invocation of new dimensionless quantities:

$$(Equation 11.7) \quad \tau \equiv \frac{t}{t^*} \equiv \frac{u_0 c_0 \left[\frac{t - L \epsilon}{u_0} \right]}{\rho_p (1 - \epsilon) L (W_{sat} - W_0)}$$

$$(Equation 11.8) \quad N \equiv \frac{K_c a L}{u_0}$$

where a dimensionless time (τ) to reach bed saturation is proposed in Equation 11.7 and the number of mass transfer units (N) in the bed is defined by Equation 11.8. Together, these analytical solutions require the engineer to specify bed length (L), void fraction (ε , which can be estimated based on particle geometry), bulk density (ρ_b), alongside inlet fluid velocity (u_0) and concentration (c_0) with initial and saturation adsorbent loading (W_0 and W_{sat} , respectively).

As within the subdiscipline of **reaction kinetics**, such transient processes are often represented through a semi-empirical framework so as to simplify the mathematics. In the special case of *irreversible* adsorption, the deployment of Equation 11.5 within Equation 11.4 can be used to simplify the solution, as the time-derivatives can be taken as zero: that is, $-u_0(\partial c/\partial L) = K_c ac$, which can be integrated to reveal the concentration profile in the bed ($\ln c/c_0 = -K_c aL/u_0$). When framed in terms of the bed concentration, Equation 11.9 exemplifies the solution to a so-called **zeroth order kinetic** rate, which is named for the fact that the kinetic solution *depends on time to the 0th power* (that is, it *doesn't* depend on time in the case of irreversible adsorption):

$$(Equation 11.9) \quad c = c_0 \cdot e^{-N} = c_0 \cdot e^{-\frac{K_c aL}{u_0}}$$

If the adsorption process varies with time, then Equations 11.10 or 11.11 (respectively) can be used to approximate local concentration:

$$(Equation 11.10) \quad \frac{dq}{dt} = k_1(q_\infty - q)$$

$$(Equation 11.11) \quad \frac{dc}{dt} = k_2 C^2$$

where the term k_1 is the **first order rate constant** with units of inverse time (e.g. s^{-1}), q represents the local material capacity (which changes with time), and q_∞ is the equilibrium capacity of the material (with units of mass per mass, as shown in Figure 11.6). Within Equation 11.11, k_2 is the **second order rate constant**, with units of volume (adsorbed) per mass (of adsorbate) per time and C denotes the local concentration of the target component. It should be emphasised that, while the framework for Equations 11.9 through 11.11 is adopted from the subdiscipline of reaction kinetics, the rate equations themselves does *not* include the additional considerations of a reacting, chemical system.

11.4 Chromatography

One such application of adsorption commonly deployed by chemists and engineers is through chromatography, which has become common in recent decades as the preferred method of characterising complex fluids (e.g. crude oil or biofuels, which may contain thousands or tens of thousands of components). In this way, chromatography provides a process for separating individual components within a solid (adsorbate) bed, where an inert, non-adsorbing carrier gas is used to move feed material through the bed. The distribution coefficients (referred to as K-factors in Section 10.5) of each component ensure that components will adsorb at different points in the column, based on the local pressure and temperature conditions. *Chromatograms* are generated from analysing the column's effluent gas, where individual components are initially adsorbed -- saturating sites at a certain temperature -- before eventually being transmitted through the saturated sites and carried to the analyser (at the end of the bed) by the carrier gas. An example chromatograph is shown in Figure 11.9, where the ordinate represents the *amount* of a component in the system (in arbitrary units) as a function of the component's "retention time" in the column: specifically, heavier components have longer retention times. The example of Figure 11.9 illustrates five peaks (or five components): in this example, components 1 and 2 have "saturated" the signal (thereby

necessitating a different column or faster flowrate of gas to be applied. Similarly, the illustration of components 4 and 5 indicates a similar relative concentration (based on similar integrated areas in the chromatograph), where peaks at longer retention times are naturally broader.

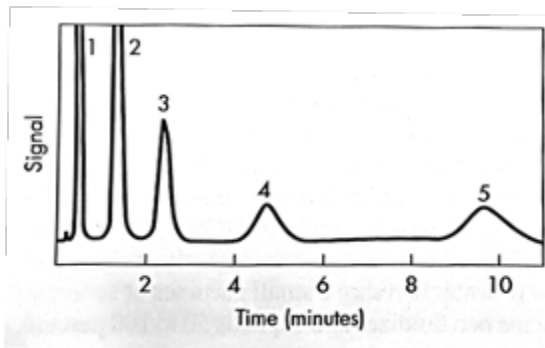


Figure 11.9 Example chromatograph, where the signal (in arbitrary units) varies as a function of "retention time" in the column. Reproduced from McCabe, Smith and Harriott (7th Edition).

In most gas chromatography (GC) systems, helium is the most common inert carrier, with options of nitrogen or hydrogen also available. Feed is injected in the column, vaporised, and swept through the adsorbate (itself either being solid, or liquid held in porous media): the "analyser" at the end of the column then analyses components based on either thermal conductivity (simplest), density (standard), or -- in highly complex systems -- through a flame ionization detector (FID) that is commonly used in the energy industry given its high sensitivity for organic molecules. The "pulse" of feed material injected in the column is typically quite small, so as to maintain dilute (or ideal) gas conditions. Further, the GC system can be combined with a mass spectrometer for parallel analysis, allowing the engineer to reconstruct individual components from the chemical fragmentations recorded (in combination, the system is referred to as a GC-MS). As the vapour phase is typically designed to maintain near-ideal conditions, Raoult's Law may be simplified to omit the fugacity coefficient: of note, the activity coefficient *must* be maintained when chromatography systems with liquid in the porous media (so-called gas-liquid chromatography, or GLC). As such, the simplified Raoult's Law can be re-written on the basis of concentration (of greatest interest to chemists), where the concentration of a component in the liquid phase ($c_{A,L}$) can be related to what is measured in the vapour phase ($c_{A,g}$) and any liquid activity considerations of interest (through γ_A):

$$(Equation 11.12) \quad c_{A,L} = \frac{P}{\gamma_A P_A^{vap}} \left(\frac{\rho_{M,l}}{\rho_{M,g}} \right) c_{A,g}$$

where the densities of the components in the vapour and liquid phases ($\rho_{M,g}$ and $\rho_{M,l}$, respectively), and the vapour pressure of each component (P_A^{vap}), are -- as thermophysical properties -- typically available from a local database, so long as the component(s) are known. Without this knowledge, the engineer must either deploy a GC-MS system to reconstruct the components (as may be possible for a relatively *simple* multi-component mixture) or group components based on retention time and assign each "grouping" a pseudo-component class (that is, giving a collection of N components with similar retention times an averaged molecular weight, molar volume, and activity).

In GLC systems, the mass of solvent (in the pore space of the adsorbate solid) per unit volume is defined by $w = \rho_b s$, informed by the density of the bed (ρ_b) and solvent loading in the porous media (s). In such systems, vaporised components reach equilibrium with the liquid in the pore

space, where the mass of a nominal component ("A") *per unit volume* of the column is given by the amount *within* the pore volume (of liquid) and that dissolved/adsorbed in the stationary phase:

$$(Equation 11.13) \quad m_A = \varepsilon \cdot c_{A,g} + \left[\rho_b s \cdot \frac{P}{\gamma_A P_A^{vap}} \cdot \frac{\rho_{M,l}}{\rho_{M,g}} \right] c_{A,g} = c_{A,g}(\varepsilon + K_A)$$

which employs Equation 11.12 in the middle term and where carrier gas is passed through the column with a superficial velocity given by u_0/ε . Importantly, Equation 11.13 can be simplified (as on the right-hand side) to combine the bracketed terms as K_A , the **partition coefficient** (analogous to K-factors used in Section 10.5). As the time for the feed "pulse" to leave the column can be directly calculated ($t = L\varepsilon/u_0$), the *retention time of an individual component* (t_A^*) can be directly related to the partition coefficient:

$$(Equation 11.14) \quad t_A^* = L(\varepsilon + K_A)/u_0$$

where, in GLC systems, the partition coefficient is typically much larger than amount of material in the pore volume (ε). This reveals the insight that **retention time is directly proportional to the partition coefficient of the component**. Where the amount of material in the pore volume is sufficiently small that it can be neglected, the ratio of retention times can be ascribed to the ratio of partition coefficients and, subsequently, activity coefficients and vapour pressures (as per Raoult's Law):

$$(Equation 11.15) \quad \frac{t_A^*}{t_B^*} = \frac{K_A}{K_B} = \frac{\gamma_B P_B^{vap}}{\gamma_A P_A^{vap}}$$

In practice, the employment of GCs to characterise complex hydrocarbon mixtures -- including crude oil or biofuels -- requires high temperatures of up to 600 K in order to vaporise heavy components and the use of a FID for analysis: such applications are labelled high-temperature (HT) GC, based on the operating temperatures. One such example is shown in Figure 11.10, where such a HTGC was deployed alongside a mass spectrometer to characterise a complex liquid hydrocarbon fuel. In considering the necessary difficulty in applying the full form of Raoult's Law for either thermodynamic or unit operations applications, such HTGC and HTGC-MS (where required) tools are a critical application of adsorption technologies.

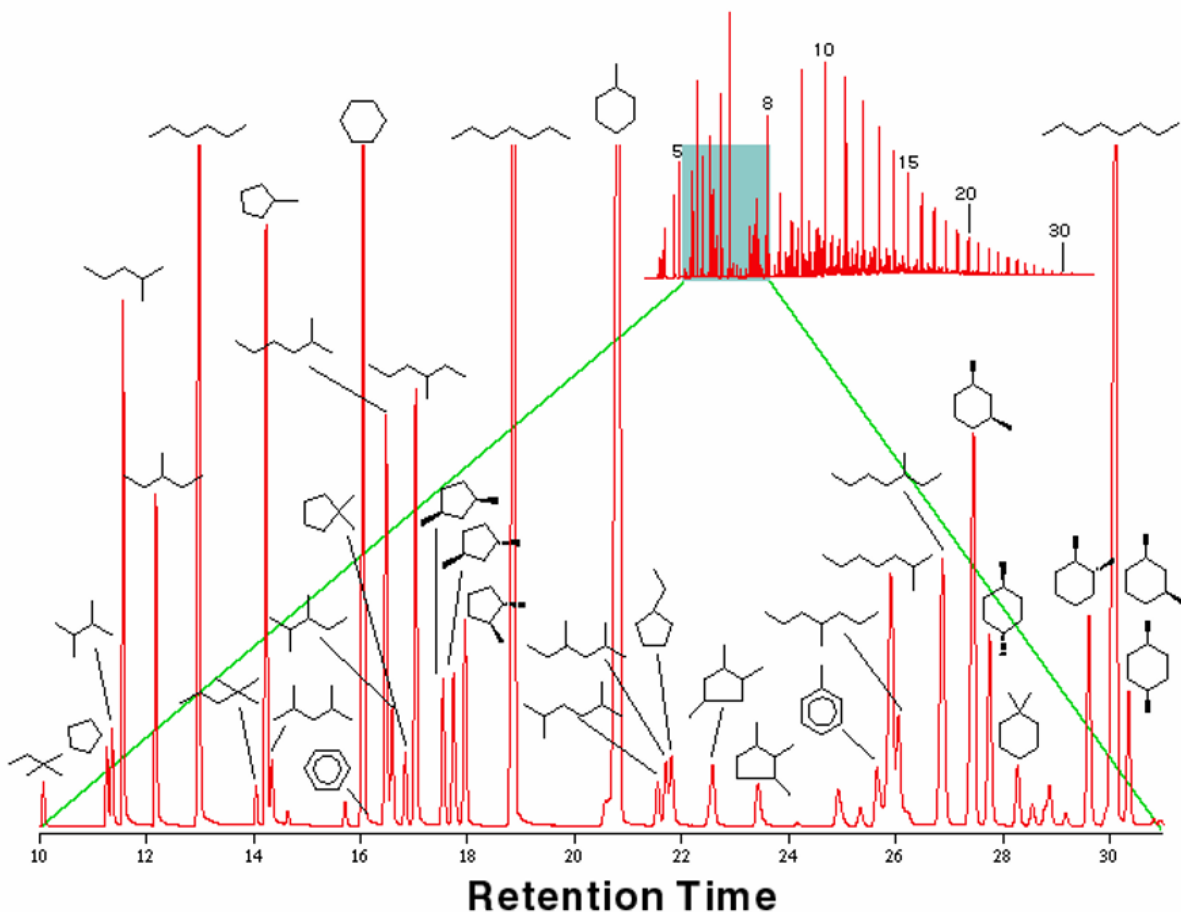


Figure 11.10 Example HTGC result (inset graph at top), where MS analysis enables labelling of individual components (main plot).

Reproduced from Dr Jeff Creek (Chevron ETC), 2018.

Previous sections concerning mass transfer are based on the concept of exploiting changes in the Gibbs free energy landscape -- constituted by modifying pressure, temperature, and/or chemical potential -- to separate components on a molecular level. While effective, these methods are distinguishable from the use of membranes, through which fluid components can only transmit with sufficiently small molecular diameters. This section summarises the treatment of membrane separation in the context of designing a unit operation: it is intended to complement membrane theory and basic operation, as discussed in Process Synthesis.

A theoretical membrane is shown in Figure 12.1, illustrating a feedstock containing three component (A, B, and C) across a membrane of thickness z . As the membrane is comprised of a porous material, the diameter of the pores illustrated in Figure 12.1 may be selected so as to only allow components with similar (average) molecular diameters, or smaller, through the membrane: as drawn, the molecular diameter of component "C" is sufficiently large as to prevent migration through the membrane, where component "B" diameter is very close to that of the average pore diameter (only a small amount of "B" is recognised in the product stream). Conversely, component "A" is able to readily transmit through the porous network to the product stream: the result is a product mole fraction of component "A" (labelled C_{A2} in Figure 12.1) that is substantially higher than its mole fraction in the feed stream (C_{A1}). This basic description has historically been deployed in both medical dialysis and water desalination.

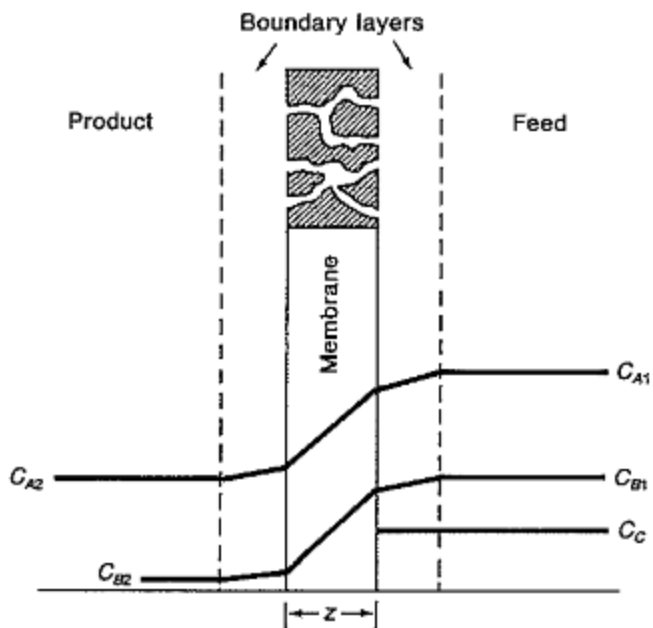


Figure 12.1. Theoretical membrane behaviour seeking to purify component "A" in the product stream, where component "A" is more readily able to transit through the membrane than component "B," and component "C" is unable to transmit through the membrane. Reproduced from McCabe, Smith and Harriott (7th Edition).

Considering the perspective of a single molecule of component "A," in the context of *fluid flow* (in to the page) in both the product and feed streams, the experience of mass transfer must deductively consider three main contributions: (i) diffusion through the boundary layer on the *feed* side, (ii) diffusion through the membrane pores, and (iii) diffusion through the boundary layer on the *product* side. Within this context and with a focus on component "A," the general mass flux and associated resistance can be written:

$$(Equation 12.1) \quad J_A = K_A(c_{A1} - c_{A2})$$

$$(Equation 12.2) \quad \frac{1}{K_A} = \frac{1}{k_{1A}} + \frac{1}{k_{mA}} + \frac{1}{k_{2A}}$$

where c_{A1} and c_{A2} respectively represent the feed and product concentrations of component "A," k_{1A} and k_{2A} respectively represent the mass transfer coefficients for flow through the feed and product boundary layers, and k_{mA} represents the mass transfer coefficient *through* the membrane material (as discussed in Section 8.2, relevant to equations 8.7 through 8.11) as defined by the *effective diffusivity* (D_e) through, and thickness of, the membrane:

$$(Equation 12.3) \quad k_{mA} = \frac{D_e}{z}$$

Considering an idealised case with two fluids that are highly similar (e.g. both are > 98 mol% water) and where a target component begins diffusing through a membrane separating them, the "dilute" nature of the component allows the chemical engineer to assume the chemical potential changes *nearly linearly* with the "activity" of the chemical in solution, which scales inversely with concentration for dilute solutions (giving rise to its applicability in Equation 12.1). As with the heat transfer analogy, the effective diffusivity through the membrane material is commonly the

controlling factor, where fluid turbulence in both boundary layers contributes a minority -- if not negligible -- resistance to mass transfer. With knowledge of the fluid components for consideration, and through selecting a porous media with an appropriate pore size distribution, Equations 8.7 through 8.11 provide a basis to calculate effective diffusivity and, through Equation 12.3, the primary contributor to mass transfer resistance (K_A) can be calculated for deployment in determining the overall flux (J_A) of component(s) through the membrane.

12.1 Reverse Osmosis

As an appropriate membrane should be selected such that the target component (solute) can permeate the material, while being nearly impermeable to the solvent, basic membranes take advantage of the osmotic gradient: that is, the difference in concentration of the "feed" and "product" sides of the membrane. Functionally, this can be observed through the definition of Gibbs free energy (Equation 1.2): for two fluids at equal pressure and temperature (respectively neutralising the mechanical and thermal driving forces), a difference in the *number* of molecules (qualified by their chemical potential: that is, $dG = \sum_i \mu_i dn_i$) enables a free energy gradient that is resolved by mass transfer. Appreciating the *activity* of a component in solution decreases as the solution becomes more concentrated in that component, the transfer of molecules to the less concentrated solution decreases the activity (and chemical potential, μ_i) of *all* components in that phase: in other words, increasing dn_i for a phase decreases μ_i for that phase, and vice versa. Therefore, when two fluids are contacted at constant temperature and pressure, the global minimum in Gibbs free energy will be achieved through molecular diffusion (modifying the quantity $\mu_i dn_i$ for both phases contacting the membrane). As before, the definition of Gibbs energy provides an elegant explanation for the origin of the osmotic gradient, while the practical engineering solution employs a generalised mass transfer resistance (as per Section 8.2) that represents this complex molecular behaviour.

Where an osmotic gradient exists between two fluids, both the temperature and pressure of the phases can be modified by the engineer who wishes to modify the Gibbs energy landscape: that is, by modifying either dP or dT in Equation 1.2, the engineer can control the relative "importance" of the mass transfer driving force ($\mu_i dn_i$). As temperature is assessed on an absolute scale, modifying temperature by an integer factor is required before the thermal driving force achieves the same order of magnitude as that of the mass transfer driving force. However, pressure can more easily be modified to such extents (e.g. adding a fluid "head" to increase the hydrostatic pressure on one fluid, as per Section 2.1) that it balances against the mass transfer (i.e. osmotic) driving force, such that the overall Gibbs energy driving force (dG) is neutralised. Specifically, the **osmotic pressure** (π) for a component represents the *exact* pressure required to suspend osmosis within that system. If the system is operated *above* the osmotic pressure, so that the fluid must go *against* its natural osmotic gradient to maintain balance in dG , the component(s) of interest will migrate *toward* the more concentrated solution. This process is known as **reverse osmosis**, wherein the solvent(s) will diffuse from high to low concentration (or, identically, the solute will diffuse from low to high concentration). For this reason, reverse osmosis is a powerful demonstration to the chemical engineer of how the Gibbs energy landscape can be manipulated to achieve a difficult outcome. Example of both traditional osmosis, osmotic equilibrium (achieved by increasing the fluid head of the saltwater solution to $P = \pi$), and reverse osmosis (where $P > \pi$) are shown in Figure 12.2.

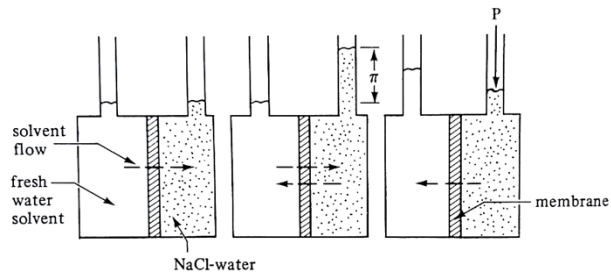
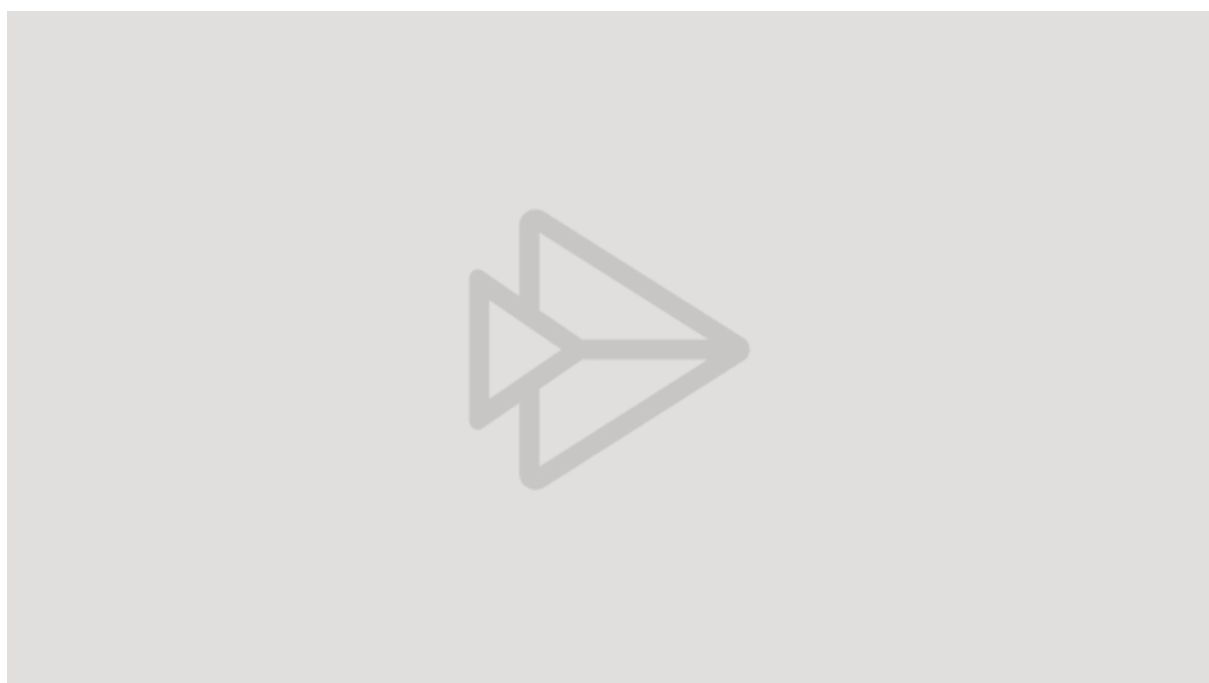


Figure 12.2. Example of membrane separation at different pressures (achieved by varying fluid head). Reproduced from McCabe, Smith and Harriott (7th Edition).



[Example 19 -- Calculating osmotic pressure \(video from Microsoft Stream\).](#)

In reverse osmosis systems, the product ("permeate") extracts fresh solvent (pure water in the case of Figure 12.2) from a phase containing additional components (such as dissolved salt). A generalised example of this process is shown in Figure 12.3, which also includes the effect of a fouling layer (called the "skin") that contributes an additional resistance to mass transfer per Equation 12.2. The activity and concentration of water in the permeate (a_{wP} and C_{wP} , respectively) are approximately equal on the permeate side and throughout the membrane ("porous support"), but both increase (distinguishably) on the feed side due to the presence of dilute salt components (subscript "s" in Figure 12.3).

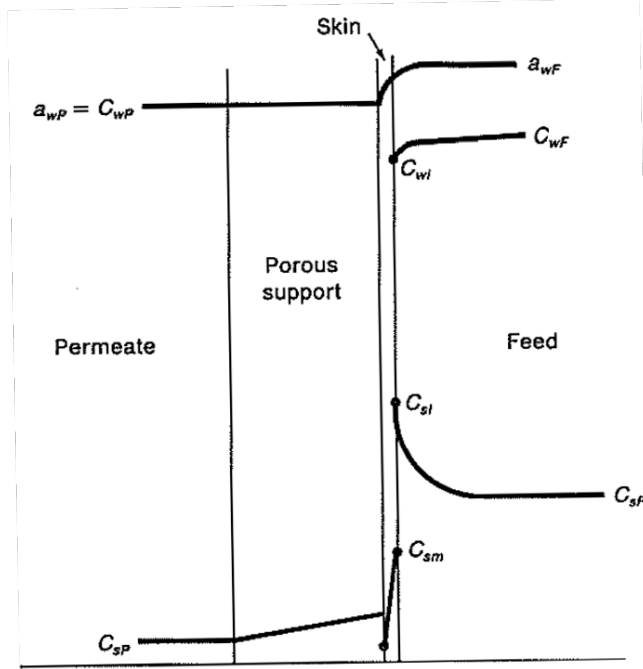


Figure 12.3. Component concentration profiles (vertical axis) for a membrane system operating under reverse osmosis, where a "skin" represents a fouling layer (not dissimilar to metallic corrosion) that contributes toward mass transfer resistance. Reproduced from McCabe, Smith and Harriott (7th Edition).

On the low-pressure side of the reverse osmosis membrane (that is, the fresh water in Figure 12.2) is typically maintained at ambient (i.e. 1 atm) for ease of operation, where the activity of the low-pressure side is nearly equal to unity. Complex applications may certainly consider the viability of a partial vacuum environment, in the example of materials or components that may react or change in conformation at excessive pressure. For a typical reverse osmosis membrane designed to extract fresh water from salt water (represented through Figures 12.2 and 12.3), the high-pressure side is typically maintained between 20 and 50 atm (that is, 20 to 50 times the pressure of the permeate side): the activity of the high-pressure side increases above unity, as the pressure increases beyond the osmotic pressure. With this application of reverse osmosis, the mass fluxes of water and salt are respectively given:

$$(Equation 12.4) J_w = \frac{c_w D_w \rho_{m,w}}{RT} \left(\frac{\Delta P - \Delta \pi}{z} \right)$$

$$(Equation 12.5) J_s = D_s S_s \left(\frac{\Delta c_s}{z} \right)$$

where the driving force is defined by the difference of the applied pressure (ΔP) and the osmotic pressure ($\Delta \pi$) for the feed and permeate sides of the membrane; z is the thickness of the membrane; c_w is the average water concentration across the volume; $\rho_{m,w}$ is the partial molar volume of the water (typically in cm^3/gmol); D_w and D_s are the diffusivities of water and salt (i.e. taken to be "through the membrane" as the primary resistance); S_s is the solubility of the salt component through the membrane (informed by its **distribution coefficient**); and Δc_s is the difference in salt concentration between the permeate and feed sides. In typical desalination applications, D_w is on the order of $10^{-6} \text{ cm}^2/\text{s}$, while D_s and S_s -- themselves varying with the membrane material and design -- are typically on the order of $10^{-9} \text{ cm}^2/\text{s}$ and 0.03.

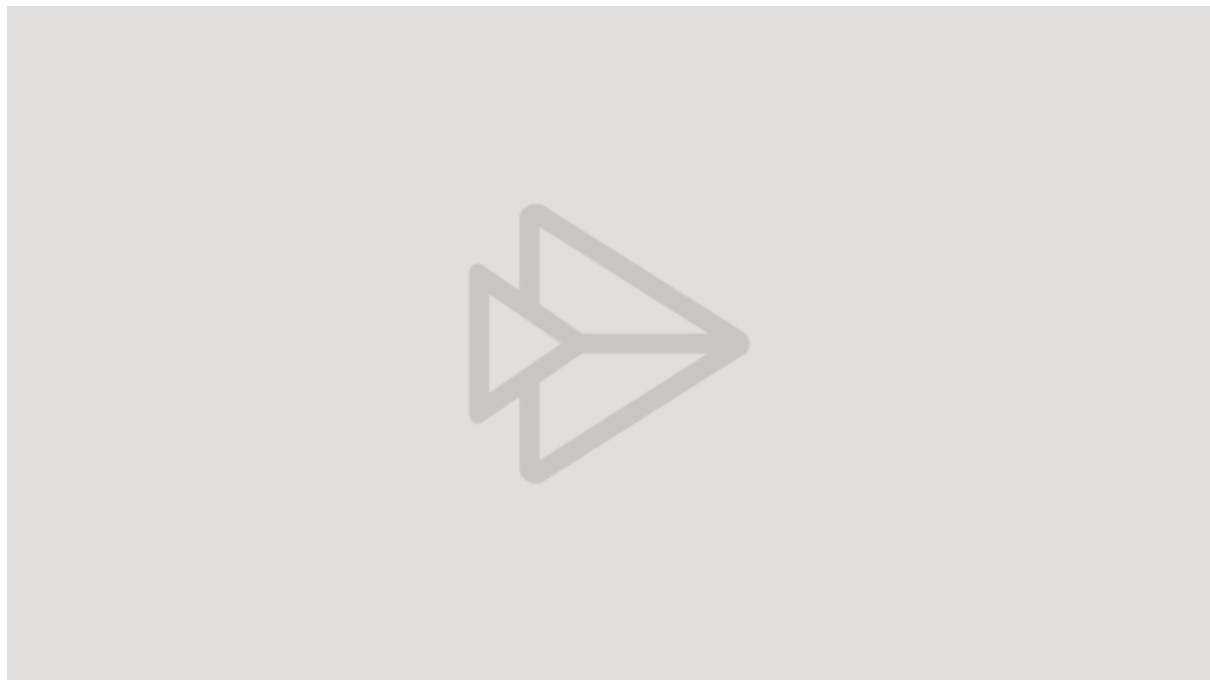
The dependencies of these flux equations illustrates several key messages. First, the chemical potential driving force is captured by the difference in osmotic pressures, and balanced against the physical pressure applied to the system: this allows the engineer to rapidly interrogate the effect of varying membrane material (affecting the effective diffusivity) on the required thickness for a maximum achievable pressure. Second, the flux of water through the membrane (J_w) increases *linearly* with the pressure difference (above the osmotic pressure) applied to the system, which gives the engineer a practical means to control product (fresh water) flowrate throughout the process. Finally, note that salt flux (J_s) does *not* vary with the applied pressure difference, although the presence of a fouled "skin" on the feed side of the membrane will naturally decrease the effective diffusivity.

12.2 Desalination

While sodium chloride (NaCl) is often used as a laboratory benchmark, "sea salt" contains a diversity of anions and cations of varying charges. Table 12.1 below provides an example of how NaCl and sea salt each affect the osmotic pressure (and density) in water, where data across alternative reverse osmosis applications can typically be found in the peer reviewed literature and in appropriate reference texts. As seawater is typically estimated to contain around 3.5 wt% salt, Table 12.1 illustrates that at least 25 atm of pressure will be required before reverse osmosis will take place.

Table 12.1. Effect of sodium chloride and sea salt on solution density and osmotic pressure. Reproduced from Geankoplis (4th Edition).

Sodium Chloride Solutions			Sea Salt Solutions	
gmol NaCl per kg H ₂ O	Density (kg/m ³)	Osmotic pressure (atm)	Salt (wt%)	Osmotic pressure (atm)
0	997.0	0	0	0
0.01	997.4	0.47	1.00	7.10
0.1	1001.1	4.56	3.45	25.02
0.5	1017.2	22.55	7.50	58.43
1.00	1036.2	45.80	10.00	82.12
2.00	1072.3	96.2		



Example 20 -- Characterizing a hollow-fibre membrane (video from Microsoft Stream).

For the common application of seawater desalination, the current generation of polymers can achieve up to a 99% rejection of salt, at which point the product *may* be eligible for use as potable water depending on jurisdictional requirements. It should be noted that, while water flux increases linearly with the pressure difference applied, higher pressure-difference conditions also produce a greater rejection of salt, primarily through modifying the distribution coefficient (S_s) as discussed in Section 10.5). Cellulose acetate polymers are one common asymmetric membrane design, which can produce water fluxes of between 10 and 20 gal/ ft^2/day with more than 95% of salt rejected.

Commercial vendors, such as du Pont, offer hollow-fibre membranes for use in desalination applications, which can support between 1 and 3 gal/ ft^2/day . An example illustration of a spiral-wound separator is shown in Figure 12.4, as a common deployment in reverse osmosis. The rolled "sandwich" typically contains an exterior covering, where thin layers of membrane material and spacers are stacked multiple times so as to generate cross flow between the feed (flowing through spacers) and permeate flows. Such designs typically produce mass transfer areas on the order of a 200 ft^2/ft^3 .

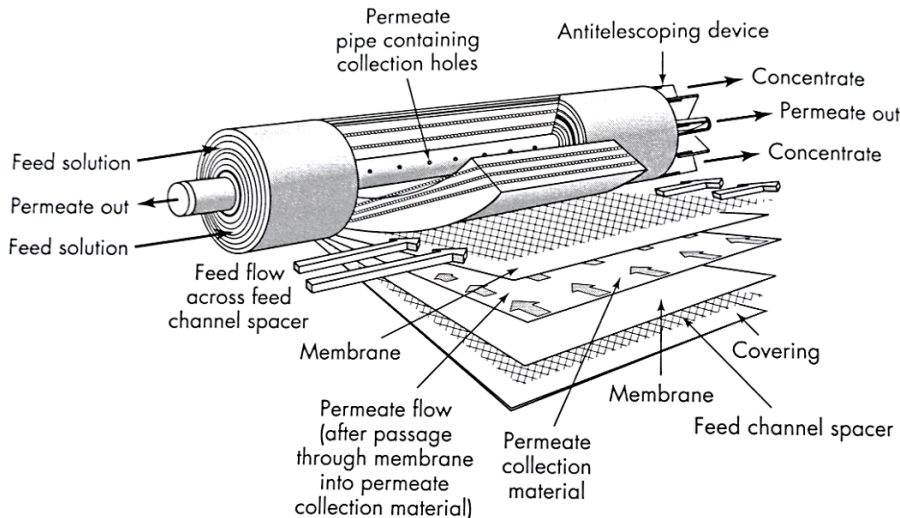


Figure 12.4. Example spiral-wound membrane separation system, where feed solution enters the face of the rolled membrane and diffuses through to a central pipe containing the permeate. Reproduced from McCabe, Smith and Harriott (7th Edition).

Where a single membrane unit operation may not produce water of consumption quality for a given jurisdiction, a multi-stage reverse osmosis system can be employed, as pictured in Figure 12.5. If not independently re-pressurised, the second stage of the system will naturally be less productive than the first stage, as it is (i) fed with a more concentrated salt solution and (ii) operates with a lower pressure due to the frictional loss through the flow network.

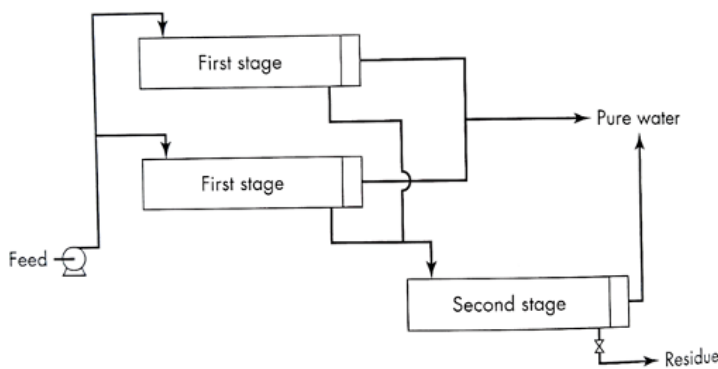


Figure 12.5. Illustration of two-stage reverse osmosis system for desalination. Reproduced from McCabe, Smith and Harriott (7th Edition).

To determine the pressure available for the second stage, Equation 12.6 provides an estimate of the pressure drop for a system operating at constant water flux (that is, volume flow per surface area per time):

$$(Equation 12.5) \frac{dp_s}{dL} = \frac{128 J_w \mu}{D^3} \cdot \frac{L^2}{2}$$

where the viscosity of the water (μ) can be assumed to be invariant with salt content in desalination applications, L represents the length of the membrane, and D is the tube diameter.



Example 21 -- Designing a reverse-osmosis desalination system (video from [Microsoft Stream](#)).